REPORT DOCUMENTATION PAGE

Form Approved
OMB No. 0704-0188

1. AGENCY USE ONLY (Leave blank)	2. REPORT DATE	3. REPORT TYPE AND DATES COVERED
	2 February 1996	Final. 1 Jan. 1994 - 31 Dec. 1995

4. TITLE AND SUBTITLE

Control of structural vibrations by vorticity productio

AFOSR-TR-96
0258

6. AUTHOR(S)

Michael S. Howe

F49620-94-1-0093

7. PERFORMING ORGANIZATION NAME(S) AND ADDRESS(ES)

Boston University
College of Engineering
110 Cummington Street
Boston MA 02215

8. PERFORMING ORGANIZATION REPORT NUMBER

AM-96-006

9. SPONSORING/MONITORING AGENCY NAME(S) AND ADDRESS(ES)

AFOSR/NA
Bolling AFB DC 20332-6448

NA

10. SPONSORING/MONITORING AGENCY REPORT NUMBER

94-1-0093

11. SUPPLEMENTARY NOTES

12a. DISTRIBUTION/AVAILABILITY STATEMENT

Approved for public release,
distribution unlimited

12b. DISTRIBUTION CODE

19960617 112

13. ABSTRACT *(Maximum 200 words)*

Analytical models are investigated of the damping of sound and structural vibrations by vorticity production in the apertures of bias flow and grazing flow perforated elastic plates. A generalized bending wave equation is formulated for a plate perforated with an homogeneous distribution of small apertures, and is used to predict the attenuation of sound and resonant bending waves. The results depend on the Rayleigh conductivity of an aperture in a thin plate which is determined numerically in the presence of one and two-sided mean grazing flows. The Kutta condition is applied to model the generation of vorticity at the edges of the aperture by an applied time-varying pressure field. The influence of flow nonlinearity in the apertures is investigated by use of a model equation for the aperture flows. Preliminary validation tests are described, and recommendations made for future research.

14. SUBJECT TERMS

Damping, sound, structural vibrations, vorticity, bias flow and grazing flow perforated screen, bending waves, Rayleigh conductivity, Kutta condition, flow nonlinearity.

15. NUMBER OF PAGES

158 + iv

16. PRICE CODE

17. SECURITY CLASSIFICATION OF REPORT	18. SECURITY CLASSIFICATION OF THIS PAGE	19. SECURITY CLASSIFICATION OF ABSTRACT	20. LIMITATION OF ABSTRACT
Unclassified	Unclassified	Unclassified	

NSN 7540-01-280-5500

Standard Form 298 (Rev. 2-89)
Prescribed by ANSI Std. 239-18
298-102

TABLE OF CONTENTS

TABLE OF CONTENTS (continued)

PREFACE

The research reported here was sponsored by the Air Force Office of Scientific Research under Grant No. F49620-94-1-0093, administered by Dr. Spencer T. Wu and Captain Brian Sanders.

Part of the work described in Chapter 3 was conducted in collaboration with Professor S. R. Sipcic (formerly of Boston University), and formed the basis of the MS thesis of Mr. M. I. Scott. Mr. Scott was supported jointly by the present research grant and by Grant No. N00014-93-1-0111 from the Office of Naval Research, administered by James A. Fein.

The following articles document research performed under the present grant:

1. Howe, M. S. *The damping of flexural waves by vorticity production*. pp 303-308, ASME Publication DE-Vol. 75: Active Control of Vibration and Noise, 1994.
2. Howe, M. S. *The damping of flexural and acoustic waves by a bias-flow perforated elastic plate*. European Journal of Applied Mathematics 6, 307 - 328, 1995.
3. Howe, M. S. *Damping of sound and vibration by flow nonlinearity in the apertures of a perforated elastic screen*. Institute of Mathematics and its Applications, Journal of Applied Mathematics 55, 221 - 242, 1995.
4. Howe, M. S. *Energy conservation and the damping of flexural waves by vorticity production*. Journal of Sound and Vibration (in press) 1996.
5. Howe, M. S., Scott, M. I. and Sipcic, S. R. *The influence of tangential mean flow on the Rayleigh conductivity of an aperture*. Proceedings of the Royal Society of London (in press) 1996.

CHAPTER 1

THE DAMPING OF FLEXURAL AND ACOUSTIC WAVES BY A BIAS-FLOW PERFORATED ELASTIC PLATE

SUMMARY

An analysis is made of the damping of sound and structural vibrations by vorticity production in the apertures of a bias flow, perforated elastic plate. Unsteady motion causes vorticity to be generated at the aperture edges; the vorticity and its energy are swept away by the bias flow and result in a net loss of acoustic and vibrational energy. In this paper we investigate the interaction of an arbitrary fluid-structure disturbance with a small circular aperture in the presence of a high Reynolds number, low Mach number bias flow. By considering the limit in which the aperture is small compared to the length scale of the impinging disturbance, it is shown that the effect of the interaction can be represented by a concentrated source in the plate bending wave equation consisting of a delta function and two of its axisymmetric derivatives. A generalized bending wave equation is then formulated for a plate perforated with an homogeneous distribution of small, bias flow circular apertures. This equation is used to predict the attenuation of sound and resonant bending waves by vorticity production. Acoustic damping is found to be significant provided the fluid loading is sufficiently small for the plate to be regarded as rigid (e.g., for an aluminium plate in air when the frequency is not too small). On the other hand, a bending wave is effectively damped only when the fluid loading is large enough for the wave to produce a substantial pressure drop across the plate; when this occurs the predicted attenuations are comparable with those usually achieved by the application of elastomeric damping materials. Numerical predictions are presented for steel and aluminium plates in air and water.

1. INTRODUCTION

Aerodynamic sound and vibrations are generated by turbulence and other unsteady distributions of vorticity, and by their interactions with adjacent elastic bodies [1 - 11]. Acoustic energy can also be dissipated by vorticity *production*, however, when a sound wave impinges on a solid surface or fluid region of nonuniform mean density. For example, sound incident on the sharp trailing edge of an airfoil in a mean flow will cause vorticity to be shed into a wake in accordance with the unsteady Kutta condition; at low Mach numbers this leads to an increase in the kinetic energy of the mean flow and wake at the expense of the sound [12, 13]. Similarly, one or more perforated plates aligned with the mean flow through the tube banks of a heat exchanger cavity can be used to suppress flow-induced, cavity acoustic resonances by the production of vorticity in the perforates; the kinetic energy of the vorticity is extracted from the sound, convected away by the mean flow, and ultimately dissipated by viscous and thermal processes [14, 15]. The same mechanism is responsible for the greatly improved attenuation of "screech" tones in the jet pipe of a jet engine when a bias flow is maintained through the perforated heat shield normally used to protect the wall liner from contact with hot combustion products [16, 17].

The effectiveness of the acoustic attenuation in these cases is critically dependent on the presence of mean flow [18 - 21]. Analytical predictions for rigid perforated screens indicate that the attenuation is linearly proportional to the acoustic amplitude [16, 17, 20 - 24], which is in broad agreement with experiment [17 - 19, 24, 25]. In the absence of flow the attenuation is either a nonlinear function of the acoustic amplitude (and therefore weak) or is dominated by the less efficient action of viscous dissipation in the apertures [26 - 30].

Theoretical analyses of sound absorption by vorticity production have hitherto assumed the screen, plate, etc (where the vorticity is generated) to be *rigid*. However, in most practical configurations high acoustic intensities are accompanied by structural vibrations, and a substantial part of the noise energy is actually contained in vibratory modes of the structure. These modes would also be expected to be damped by vorticity production, and the primary

practical objective may be the suppression of potentially harmful structural vibrations rather than the sound. The simplest model problem that exhibits structural damping by this means (and which is analogous to the acoustic-trailing edge problem mentioned above [12, 13]) is that in which a *bending wave* on a thin elastic plate is reflected at a trailing edge in a parallel mean flow (see [31]). Incident bending wave energy is dissipated at the edge by scattering into sound, and by a transfer to the kinetic energy of the mean flow and wake. Below the *coincidence* frequency of the plate (conventionally defined as the frequency above which the phase velocity of bending waves on the plate *in vacuo* exceeds the speed of sound in the fluid) the efficiency with which sound is generated is usually very small, but much larger net losses are predicted in [31] owing to the generation of wake vorticity.

In this paper we investigate the efficiency with which both sound and thin plate bending waves are attenuated when the plate is drilled with an homogeneous array of small circular apertures through which is maintained a steady bias flow. Damping is caused by vorticity generation at the aperture edges triggered by the fluctuating pressure drop across the plate produced by the incident disturbance. The attenuation of *sound* by a *rigid* bias flow screen was considered in [21]; it will be concluded from the present analysis that the rigid plate approximation is applicable only for *small* fluid loading, for a steel plate in air, say. A sound wave incident on the same plate in water generally induces a negligible pressure differential across the plate, and the acoustic attenuation is also negligible. For heavy fluid loading, bending waves are predicted to be significantly damped over an intermediate range of low frequencies, centred around an aperture Strouhal number $\omega R/U \sim O(1)$, where ω denotes radian frequency, R aperture radius, and U is the mean velocity in the aperture. The strength of this damping will be compared with that normally achieved by coating the plate with an elastomeric material [32], whose use frequently entails substantial and undesirable increases in the structural mass, especially in applications at low frequencies. It is predicted that comparably large attenuations are possible by perforating the plate (say, with 5% "open area") and maintaining a bias flow through the apertures. In principle the bias flow velocity and aperture radius can be chosen to yield optimal attenuation over a prescribed frequency range, and a

practical damping system might be "tuned" within certain limits by varying the bias flow pressure to accommodate varying frequency characteristics of a particular noise source.

The scattering theory for an arbitrary flexural disturbance incident on a single, small aperture in the presence of a bias flow is developed in §2. The result is used (§3) to formulate a generalized bending wave equation for a plate perforated with a uniform (but sparse) distribution of apertures. Numerical results are given in §3 for the attenuation of sound and bending waves, and a comparison made with damping produced by an elastomeric coating.

2. SCATTERING BY AN APERTURE IN THE PRESENCE OF A BIAS FLOW

2.1 The governing equations

A thin infinite plate of thickness h, mass m per unit area and bending stiffness B is immersed in fluid of mean density ρ_o and sound speed c_o. In the undisturbed state the plate occupies the plane $x_2 = 0$ of the rectangular coordinate system (x_1, x_2, x_3) and is pierced by a small circular aperture of radius R whose center coincides with the coordinate origin (see Figure 1). A mean pressure differential is maintained across the plate which produces a nominally steady, low Mach number, high Reynolds number "jet" of fluid through the aperture from the "upper" ($x_2 > 0$) to the "lower" ($x_2 < 0$) side.

Consider small amplitude, time harmonic motions of frequency ω (> 0) proportional to $e^{-i\omega t}$. The exponential time factor is henceforth suppressed, and the flexural displacement of the plate (in the positive x_2-direction) and perturbation pressure are respectively denoted by $\zeta_+(x_1, x_3)$ and $p(x)$. On $x_2 = 0$, $(x_1^2+x_3^2)^{1/2} > R$, ζ_+ and p satisfy the bending wave equation [33]

$$(B\nabla_2^4 - m\omega^2)\zeta_+ + [p] = 0, \qquad (x_1^2+x_3^2)^{1/2} > R, \tag{2.1}$$

where,

$$[p] = p(x_1, +0, x_3) - p(x_1, -0, x_3). \tag{2.2}$$

and $\nabla_2^4 \equiv (\partial^2/\partial x_1^2 + \partial^2/\partial x_3^2)^2$ is the biharmonic operator. Except in the immediate vicinity of the aperture, where the influence of the jet becomes important, the small amplitude pressure fluctuations may be assumed to satisfy the acoustic equation

$$\{\nabla^2 + \kappa_o^2\}p = 0, \quad x_2 \gtrless 0, \tag{2.3}$$

where $\kappa_o = \omega/c_o$ is the acoustic wavenumber. This equation ignores the influence of convection by the residual effects of mean flow at large distances from the aperture, but this is negligible when the Mach number is small.

As $x_2 \to \pm 0$, $(x_1^2+x_3^2)^{1/2} > R$, the x_2-component of the fluid velocity becomes equal to $-i\omega\zeta_+$, so that for small amplitude flexural motions of the plate the pressure p and ζ_+ are related by the linearized, x_2-component of the momentum equation of the fluid:

$$\zeta_+ = \frac{1}{\rho_o \omega^2} \frac{\partial p}{\partial x_2}, \quad x_2 \to \pm 0, \quad (x_1^2+x_3^2)^{1/2} > R. \tag{2.4}$$

For an aperture whose radius R is much smaller than the length scales of the flexural and fluid motions, the motion in the immediate vicinity of the aperture may be regarded as axisymmetric. The boundary conditions that no force and moment are applied at the edge can therefore be taken in the form [34]

$$\left.\begin{aligned} \nabla_2^2 \zeta_+ - \frac{(1-\sigma)}{r} \frac{\partial \zeta_+}{\partial r} &= 0 \\ \frac{\partial}{\partial r} \nabla_2^2 \zeta_+ &= 0 \end{aligned}\right\} \quad r \equiv (x_1^2+x_3^2)^{1/2} \to R+0, \tag{2.5}$$

where $\nabla_2^2 \equiv \partial^2/\partial x_1^2 + \partial^2/\partial x_3^2$, and σ is Poisson's ratio of the material of the plate.

2.2 The composite bending wave equation

The domain of validity of the bending wave equation can formally be extended to include the region occupied by the aperture by first introducing the indicator function

$$f(x_1, x_3) \equiv r(x_1, x_3) - R, \tag{2.6}$$

and defining a composite fluid-structure displacement ζ on $x_2 = 0$ by

$$\zeta(x_1, x_3) = \zeta_+ H(f-\varepsilon) + \zeta_- H(-f-\varepsilon), \quad \varepsilon \to +0, \tag{2.7}$$

where H(x) is the Heaviside step function (= 1, 0 according as $x \gtrless 1$), and ζ_- denotes the *perturbation* of the x_2-component of the fluid displacement within the aperture. Equation (2.1) is then multiplied by $H(f-\varepsilon)$ and rearranged to yield, as $\varepsilon \to +0$,

$$\{B\nabla_2^4 - m\omega^2\}\{H(f)\zeta_+\} + H(f)[p] = B\nabla_2^2\{\nabla\bullet\{\zeta_+ \nabla H(f)\}\} + B\nabla_2^2\{\nabla H(f)\bullet\nabla\zeta_+\} + B\nabla\bullet\{(\nabla_2^2\zeta_+)\nabla H(f)\} + B\nabla H(f)\bullet\nabla(\nabla_2^2\zeta_+), \tag{2.8}$$

where $\nabla H(f) \equiv \delta(f)\nabla f$, and $\delta(f)$ is the Dirac delta function, which vanishes except at the rim r = R of the aperture; ζ_+ and its derivatives on the right

hand side are evaluated at r = R+0.

Continuity of pressure within the aperture implies, for a plate of infinitesimal thickness (more precisely for h ≪ R), that [p] = 0 within the aperture, and therefore (as $\varepsilon \to +0$)

$$\{B\nabla_2^4 - m\omega^2\}\{H(-f)\zeta_-\} + H(-f)[p] = \{B\nabla_2^4 - m\omega^2\}\{H(-f)\zeta_-\}. \qquad (2.9)$$

When this is combined with equation (2.8) the composite displacement ζ is seen to satisfy

$$\{B\nabla_2^4 - m\omega^2\}\zeta + [p] = B\nabla_2^2\{\nabla\bullet\{\zeta_+\nabla H(f)\}\} + B\nabla_2^2\{\nabla H(f)\bullet\nabla\zeta_+\} + B\nabla\bullet\{(\nabla_2^2\zeta_+)\nabla H(f)\}$$
$$+ B\nabla H(f)\bullet\nabla(\nabla_2^2\zeta_+) + \{B\nabla_2^4 - m\omega^2\}\{H(-f)\zeta_-\}, \qquad (2.10)$$

where the "source" terms on the right hand side depend only on conditions at the edge of the aperture and on the perturbation flux through the aperture. This equation is applicable everywhere on $x_2 = 0$, including the region occupied by the aperture.

Consider the limiting form of this equation when R becomes small compared to the dominant length scales of the fluid and structural motions, i.e., for $\kappa_o R$, $K_o R \ll 1$, where $K_o = (m\omega^2/B)^{1/4}$ is the *in vacuo* bending wavenumber. In this limit the dominant components of the scattered fields, and therefore of the source terms in (2.10), must be axisymmetric. As R → 0 the sources vanish everywhere except at r = 0, and must ultimately reduce to combinations of the surface delta function $\delta(\mathbf{x}) \equiv \delta(x_1)\delta(x_3)$ and its axisymmetric derivatives [35], where, however, the highest order derivatives in the limiting forms of the first four source terms in (2.10) must be restricted to ensure that the displacement of the plate remains finite as r → R+0. In the final source $\{H(-f)\zeta_-\} \to q\delta(\mathbf{x})$ as R → 0, where q denotes the perturbation *volume* displacement through the aperture. Thus, in the leading order of approximation, equation (2.10) becomes,

$$\{B\nabla_2^4 - m\omega^2\}\zeta + [p] = a_0\delta(\mathbf{x}) + a_2\nabla_2^2\delta(\mathbf{x}) + q\{B\nabla_2^4 - m\omega^2\}\delta(\mathbf{x}), \quad R \to 0, \qquad (2.11)$$

where the values of the coefficients a_0, a_2, q remain to be determined; they represent the strengths of the various source terms to which the aperture is equivalent as R → 0.

2.3 The scattering problem

Let the flexural disturbance

$$\zeta_+ \equiv \zeta_I = \zeta_o e^{i\kappa x_1} , \qquad \kappa R \ll 1, \tag{2.12}$$

propagating parallel to the x_1-axis be incident on the aperture, where ζ_o is constant. ζ_I and the accompanying pressure jump across the plate $[p_I]$, say, satisfy the homogeneous form of equation (2.11) (no source terms).

Denote the scattered flexural displacement and pressure by $\zeta_s(x_1,x_3)$ and $p_s(\mathbf{x})$, respectively. Equation (2.11) determines the functional forms of ζ_s and p_s in an "outer region" at distances $|\mathbf{x}| \gg R$ from the aperture in terms of the coefficients a_0, a_2, q. Write

$$\left.\begin{aligned} \zeta_s(x_1,x_3) &= \int_{-\infty}^{\infty} \hat{\zeta}_s(\mathbf{k}) e^{i\mathbf{k}\bullet\mathbf{x}}\, dk_1 dk_3, \quad \mathbf{k} = (k_1,0,k_3) \\ p_s(\mathbf{x}) &= -i\rho_o\omega^2 \operatorname{sgn}(x_2) \int_{-\infty}^{\infty} \frac{\hat{\zeta}_s(\mathbf{k})}{\gamma(k)} e^{i\{\mathbf{k}\bullet\mathbf{x}+\gamma(k)|x_2|\}} dk_1 dk_3, \quad x_2 \gtrless 0, \end{aligned}\right\} \tag{2.13a, b}$$

where $\hat{\zeta}_s(\mathbf{k})$ is the Fourier space transform of ζ_s with respect to the planar coordinates x_1, x_3, and $\gamma(k) \equiv (\kappa_o^2 - k^2)^{1/2}$ $(k = |\mathbf{k}|)$ is positive for real $k < \kappa_o$, and positive imaginary for $k > \kappa_o$. The integral representation of the scattered pressure is a solution with "outgoing" wave behavior of the acoustic equation (2.3), and is applicable in the outer region where convection by the bias flow jet can be ignored; the integrand is chosen to ensure that ζ_s and p_s satisfy condition (2.4).

The Fourier amplitude $\hat{\zeta}_s(\mathbf{k})$ is determined by substituting from (2.13) into the left hand side of (2.11). The net displacement on $x_2 = 0$ can then be cast in the form:

$$\zeta(x_1,x_3) = \frac{1}{(2\pi)^2} \int_{-\infty}^{\infty} \frac{\{a_0 - a_2 k^2 + q(Bk^4 - m\omega^2)\} e^{i\mathbf{k}\bullet\mathbf{x}}}{D(k,\omega)}\, dk_1 dk_3 \; + \zeta_o e^{i\kappa x_1} , \tag{2.14}$$

where

$$D(k,\omega) \equiv Bk^4 - m\omega^2 - 2i\rho_o\omega^2/\gamma(k) \tag{2.15}$$

is the bending wave dispersion function [33]. In the absence of dissipation $D(k,\omega)$ has two real zeros that determine the wavenumbers k of undamped flexural motions of the homogeneous plate, and the integration contours in (2.14) must be indented to pass around the corresponding poles of the integrand in directions that are consistent with the radiation condition. This can de done by temporarily assigning to ω a small *positive* imaginary part, thereby displacing the poles off the real **k**-axes [36].

The values of the source strengths a_0, a_2, q are found from a consideration of conditions in the immediate vicinity of the aperture. This is facilitated by first re-casting (2.14) in the form

$$\zeta(x_1,x_3) = q\delta(\mathbf{x}) + \frac{1}{(2\pi)^2}\int_{-\infty}^{\infty} \frac{\{a_0 - a_2k^2 + 2iq\rho_o\omega^2/\gamma(k)\}e^{i\mathbf{k}\bullet\mathbf{x}}}{D(k,\omega)}\, dk_1\, dk_3 + \zeta_o e^{i\kappa x_1}. \tag{2.16}$$

In this "outer" formula for ζ, the first term on the right hand side is the singular component of ζ_- associated with the volume displacement through the aperture. The remaining terms (which are non-singular at $\mathbf{x} = 0$) make finite contributions to the *plate* displacement ζ_+, and two linear algebraic equations involving the coefficients a_0, a_2, q are obtained by substituting for ζ_+ into the edge conditions (2.5). Since only the axisymmetric part of the scattered field is being considered, it is necessary to retain only the axisymmetric component $\zeta_o J_0(\kappa r)$ of the incident wave Bessel function expansion [37]

$$\zeta_o e^{i\kappa x_1} \equiv \zeta_o e^{i\kappa r\cos\theta} = \zeta_o\left[J_0(\kappa r) + \sum_{n=1}^{\infty} i^n J_n(\kappa r)\cos(n\theta)\right],\quad x_1 = r\cos\theta.$$

Conditions (2.5) are then found to give, respectively,

$$\left.\begin{aligned} A_{01}\,a_0 + A_{21}\,a_2 + Q_1 q &= \{\kappa R J_0(\kappa R) - (1-\sigma)J_1(\kappa R)\}(\kappa\zeta_o/R) \\ A_{02}\,a_0 + A_{22}\,a_2 + Q_2 q &= -\kappa^3 J_1(\kappa R)\zeta_o\ , \end{aligned}\right\} \tag{2.17}$$

where A_{0j}, A_{2j}, Q_j (j = 1, 2) are defined in the appendix.

A third relation involving a_0, a_2, q is obtained by examining the motion in an "inner" neighborhood of the aperture. The pressure here can be written,

$$p(\mathbf{x}) \approx \rho_o\omega^2\zeta_o x_2 + p'(\mathbf{x}), \tag{2.18}$$

where the first term on the right is defined such that the corresponding component of $(-1/\rho_o)\partial p/\partial x_2$ at $x_2 = \pm 0$ is equal to the normal acceleration of the plate produced by the incident wave $\zeta_o e^{i\kappa x_1}$. When the characteristic bending wavelength is much larger than the aperture diameter ($K_o R \ll 1$), the motion of the plate at distances from the aperture smaller than the characteristic flexural wavelength will be identical with that of a *rigid* plane executing translational oscillations of amplitude ζ_o in the normal direction. Since also $\kappa_o R \ll 1$, the fluid motion may similarly be regarded as locally incompressible, and the additional pressure $p'(x)$ in (2.18) calculated as for an incompressible fluid subject to the rigid surface condition $\partial p'/\partial x_2 = 0$ on $x_2 = 0$.

The volume displacement through the aperture can then be expressed in the form,

$$q = K_R[p_\infty]/\rho_o\omega^2 . \tag{2.19}$$

In this expression K_R is the *Rayleigh conductivity* of an aperture in a *rigid* plate taking account of the mean bias flow [38]; it has the dimensions of length and typically $K_R \sim O(R)$. p_∞ denotes the pressure at distances $|x|$ from the aperture satisfying $R \ll |x| < 1/\kappa_o$, where the flow may still be regarded as incompressible. This interval in $|x|$ will exist provided the frequency is sufficiently small, and it then defines an "overlap" region in which both the incompressible representation (2.18) and the outer solution (2.13b) are both applicable. This implies that $[p_\infty]$ can be calculated by considering the limiting value of the integral in (2.13b) in the overlap region. This limiting value contains the term

$$-\rho_o\omega^2 q/2\pi|x| = -K_R[p_\infty]/2|x| \ll [p_\infty], \tag{2.20}$$

which is discarded, and we then obtain (including also the contribution $[p_I]$ of the incident disturbance),

$$[p_\infty] = [p_I] - \frac{i\rho_o\omega^2}{\pi}\left(\kappa_o q + \int_0^\infty \frac{[a_0 - a_2k^2 + 2i\rho_o\omega^2 q/\gamma(k)]kdk}{\gamma(k)D(k,\omega)}\right). \tag{2.21}$$

For consistency with the matching procedure the remaining terms in q on the right hand side should also be discarded, since they are easily shown to be at most $O(K_oK_R)[p_\infty]$, which is of smaller order than the term discarded in (2.20). We shall do this, but it should be noted that this is actually equivalent to neglecting a small effect of fluid compressibility responsible for energy

losses due to acoustic scattering. Then substituting into the right hand side of (2.19), we obtain the third equation for a_0, a_2, q:

$$A_{03}\, a_0 + A_{23}\, a_2 + q = K_R[p_I]/\rho_o\omega^2 \ , \tag{2.22}$$

where A_{03} and A_{23} are defined in the Appendix.

The solutions of equations (2.17), (2.22) are now expanded in powers of K_oR ($\ll 1$). Only the axisymmetric components of the scattered fields are being retained in the present approximation, and it can readily be verified that the expansion must therefore stop at terms of order $(K_oR)^2$. The expansion can be effected by first nondimensionalizing the expressions (A.1) - (A.3) for the coefficients A_{0j}, A_{2j}, Q_j. It is found that a_0 and a_2 are each $O\{(K_oR)^2\}$ and that $q \sim O(K_oR)$. To this order of approximation equations (2.17) and (2.22) yield

$$\left.\begin{aligned} a_0 &= -\pi R^2 B\kappa^4 \zeta_o - 2RK_R[p_I] \ , \\ a_2 &= -\frac{(1+\sigma)}{(1-\sigma)}\pi R^2 B\kappa^2 \zeta_o \ , \\ q &= \frac{K_R}{\rho_o\omega^2}[p_I] \ , \end{aligned}\right\} \tag{2.23}$$

In these expressions $\kappa^4\zeta_o = \nabla_2^4\zeta_I$, $\kappa^2\zeta_o = -\nabla_2^2\zeta_I$, so that (2.11) becomes

$$\{B\nabla_2^4 - m\omega^2\}\zeta + [p] = -\{\pi R^2 B\nabla_2^4\zeta_I + 2RK_R[p_I]\}\delta(x) + \frac{(1+\sigma)}{(1-\sigma)}\pi R^2 B\nabla_2^2\zeta_I . \nabla_2^2\delta(x)$$

$$+ \frac{K_R}{\rho_o\omega^2}[p_I]\{B\nabla_2^4 - m\omega^2\}\delta(x). \tag{2.24}$$

In this form, the equation describes the scattering of an *arbitrary* incident displacement ζ_I and pressure field p_I whose characteristic length scale is much larger than the aperture radius.

2.4 Scattering of a bending wave

The physical significance of the different source terms on the right of equation (2.24) can be exhibited by consideration of the problem in which the incident disturbance $\zeta_I = \zeta_o e^{i\kappa x_1}$ is a plane *bending wave*, for which,

$$p_I = - \frac{\mathrm{sgn}(x_2) i\rho_o \omega^2 \zeta_o}{\gamma(\kappa)} e^{i\{\kappa x_1 + \gamma(\kappa)|x_2|\}} \quad , \quad \gamma(\kappa) = i(\kappa^2 - \kappa_o^2)^{1/2} \quad , \qquad (2.25)$$

where the wavenumber $\kappa > \kappa_o$ may be taken to be the positive real zero of the dispersion function $D(k,\omega)$ defined by (2.15). This is an *evanescent* wave that propagates subsonically relative to the fluid; the accompanying fluid motion is confined to boundary layer regions of width $\sim 1/(\kappa^2 - \kappa_o^2)^{1/2}$ on either side of the plate within which the pressure p_I decays exponentially, although the decay may be slow when $\kappa \sim \kappa_o$ (i.e., when $\omega > \omega_c$).

The interaction at the aperture will result in an exchange of energy between the wave field and the bias flow jet, whose magnitude can be determined from a consideration of the energy equation. To do this, consider an homogeneous, time-dependent, fluid loaded plate, driven by a distribution $F(x_1, x_3, t)$ of normal stresses (taken to be positive in the x_2-direction). This equation is derived from (2.1) by first replacing ω by $i\partial/\partial t$, and inserting F on the right hand side. Multiplying by $\dot{\zeta} \equiv \partial\zeta/\partial t$ and rearranging, we find

$$\frac{\partial}{\partial t}\left(\tfrac{1}{2}m\dot{\zeta}^2 + \tfrac{1}{2}B(\nabla_2^2\zeta)^2\right) + \mathrm{div}\left(B\dot{\zeta}\nabla(\nabla_2^2\zeta) - B(\nabla_2^2\zeta)\nabla\dot{\zeta}\right) + \dot{\zeta}[p] = \dot{\zeta}F. \qquad (2.26)$$

The first term on the left is the time rate of change of the structural energy density; the divergence describes the flux of energy within the plate, and $\dot{\zeta}[p]$ is the energy flux from the plate into the fluid. The power supplied or dissipated by the stress field F is determined by their rate of working $\dot{\zeta}F$.

In equation (2.10) the role of the stress distribution F is taken by the limiting form of the sources as $\varepsilon \to 0$, where the composite displacement ζ is given by (2.7). To evaluate the mean energy flux from the aperture the time factor $e^{-i\omega t}$ is restored and the real parts taken of the resulting expressions for all perturbation quantities. The sources are then multiplied by

$$\partial\zeta/\partial t = \mathrm{Re}\{-i\omega\zeta(x_1, x_3)e^{-i\omega t}\} \equiv \mathrm{Re}\{-i\omega\zeta_I(x_1, x_3)e^{-i\omega t} - i\omega\zeta_s(x_1, x_3)e^{-i\omega t}\},$$

averaged over a wave period $2\pi/\omega$, and integrated with respect to (x_1, x_3). Note that the first four source terms on the right of (2.10) are multiplied by the component $\partial\zeta_+/\partial t$ of $\partial\zeta/\partial t$, and the final source by $\partial\zeta_-/\partial t$. As $\varepsilon \to +0$ this

is equivalent to multiplying the first two sources in (2.11) by $\partial\zeta_+/\partial t$ and the final source by $\partial\zeta_-/\partial t$. If Π_A denotes the incident bending wave power *dissipated* at the aperture, we then find

$$\Pi_A = - \frac{2\rho_o\omega^3|\zeta_o|^2}{(\kappa^2-\kappa_o^2)}[1 - R(\kappa^2-\kappa_o^2)^{1/2}]\mathrm{Im}\{K_R\}. \qquad (2.27)$$

Thus, flexural wave power is dissipated at the aperture provided the imaginary part of the conductivity K_R is negative (for $\kappa R \ll 1$). In the absence of the bias flow, and when viscous dissipation is ignored, K_R is real and equal to 2R for a plate of negligible thickness [38]. In this case, however, energy must actually be extracted from the bending wave by scattering into sound. This loss cannot appear in (2.27) because the left hand side of the energy equation already accounts for energy interchanges between the structural and acoustic fields.

The aperture conductivity K_R becomes complex when account is taken of the bias flow. For a high Reynolds number, low Mach number jet it can be expressed in terms of the aperture Strouhal number $S_t \equiv |\omega|R/U_c$ in the form

$$K_R = 2R\{\Gamma(S_t) - i\Delta(S_t)\}, \qquad (2.28)$$

where Γ and Δ are real valued, and U_c is the mean convection velocity of vorticity in the jet shear layer (approximately equal to one half of the jet velocity). The following expressions for Γ and Δ are derived in [21] and used in the following discussion:

$$\Gamma(S_t) = \frac{\pi^2[1+S_t]I_1(S_t)^2 + 4[S_t\cosh(S_t) - \sinh(S_t)]\cosh(S_t)K_1(S_t)^2e^{2S_t}}{S_t[\pi^2 I_1(S_t)^2 + 4\cosh^2(S_t)K_1(S_t)^2e^{2S_t}]},$$

$$\Delta(S_t) = \frac{2\pi I_1(S_t)K_1(S_t)e^{2S_t}}{S_t[\pi^2 I_1(S_t)^2 + 4\cosh^2(S_t)K_1(S_t)^2e^{2S_t}]}, \qquad (2.29)$$

where I_1 and K_1 are modified Bessel functions [37]. $\Gamma(S_t)$ and $\Delta(S_t)$ are both positive for $S_t > 0$, and their variations with S_t are illustrated in Figure 2. Predictions based on these formulae of the attenuation of sound by a *rigid* bias flow perforated screen have been found to be in good agreement with experiment [17].

The first term in the square brackets of (2.27) is supplied by the volume displacement (final) source in equation (2.24); it accounts for the absorption of energy by the mean flow. The second term, which is of opposite sign, comes from the first source on the right of (2.24) (i.e., from a_0), and describes the *production* of bending waves at the aperture by the extraction of energy from the mean jet flow. However, $\kappa R \ll 1$, and the net effect is always energy dissipation, at least for the range of wavenumbers and frequencies for which the present approximations are applicable.

The absorption cross-section of the aperture is equal to $\Pi_A/2R\Pi_I$, where Π_I is the power in the incident bending wave per unit distance parallel to the plate and wavefront. It can be expressed in the form [39]

$$\Pi_I = \frac{\omega}{4}|\zeta_o|^2 \frac{\partial D}{\partial \kappa}(\kappa,\omega), \tag{2.30}$$

where $D(k,\omega)$ is the bending wave dispersion function (2.15). The energy in the incident wave is shared between the kinetic and elastic energies of the plate and the energy of the evanescent fluid motions on either side of the plate [33]. Combining equations (2.27) and (2.30) we find

$$\frac{\Pi_A}{2R\Pi_I} = \frac{8(\epsilon\rho_o R/\rho_s h)^{1/2}}{(MS_t)^{1/2}} \frac{\Delta(S_t)[1 - R(\kappa^2-\kappa_o^2)^{1/2}]}{(\kappa/K_o)[5(\kappa/K_o)^4 - 4(\kappa\kappa_o/K_o^2)^2 - 1]}, \tag{2.31}$$

where $M = U_c/c_o$ is the convection Mach number of the bias flow jet, $\rho_s = m/h$ is the mass density of the material of the plate, and ϵ is a fluid loading parameter defined by

$$\epsilon = \frac{\rho_o}{\rho_s}\left(\frac{E}{12\rho_s c_o^2(1-\sigma^2)}\right)^{\frac{1}{2}}, \tag{2.32}$$

where E is Young's modulus for the plate.

The dependence of $\Pi_A/2R\Pi_I$ on Strouhal number $S_t = \omega R/U_c$ is illustrated in Figure 3 for an aperture in a steel plate in water ($\epsilon \approx 0.135$) when the bias flow convection Mach number $M = 0.003$ ($U_c \approx 4.5$ m/s). The absorption peaks near $S_t = 1$ where $\Delta(S_t) \equiv -\mathrm{Im}\{K_R\}$ assumes its maximum value. It may be remarked that the corresponding loss due to acoustic scattering (which has been neglected) is $O(\kappa_o R)$ relative to (2.31).

3. THE BIAS-FLOW PERFORATED ELASTIC PLATE

3.1 The generalized bending wave equation

Consider next the case of an elastic plate perforated with a distribution of small circular apertures. Let the apertures have equal radius R, and be distributed with their centers at the random points $\mathbf{x}_n \equiv (x_{n1}, 0, x_{n3})$ on the plate, with N per unit area. By setting

$$f_n = \{(x_1 - x_{n1})^2 + (x_3 - x_{n3})^2\}^{1/2} - R,$$

we can define the following analog of equation (2.7)

$$\zeta(x_1, x_3) = \zeta_+ \prod_n H(f_n - \varepsilon) + \zeta_- \sum_n H(-f_n - \varepsilon). \quad \varepsilon \to +0, \tag{3.1}$$

When the *open area ratio* $\alpha = N\pi R^2 \ll 1$, the distance ($\sim 1/\sqrt{N}$) between neighboring apertures is much greater than R. Then, provided $\kappa_o R$, $K_o R \ll 1$, the length scales of variation of all disturbances incident on an aperture (including those $\sim O(1/\sqrt{N})$ due to scattering by neighboring apertures) will be large relative to R, and the dominant component of the scattered acoustic and flexural waves will have radial symmetry with respect to that aperture. To the order of approximation considered in §2, it can then be deduced that

$$\{B\nabla_2^4 - m\omega^2\}\zeta + [p] = \sum_n \Big(-\{\pi R^2 B\nabla_2^4 \zeta_n + 2RK_R[p_n]\}\delta(\mathbf{x}-\mathbf{x}_n)$$

$$+ \frac{(1+\sigma)}{(1-\sigma)}\pi R^2 B\nabla_2^2\zeta_n . \nabla_2^2\delta(\mathbf{x}-\mathbf{x}_n) + \frac{K_R}{\rho_o\omega^2}[p_n]\{B\nabla_2^4 - m\omega^2\}\delta(\mathbf{x}-\mathbf{x}_n)\Big). \tag{3.2}$$

In this equation ζ_n and $[p_n]$ respectively denote the flexural displacement and pressure jump at $\mathbf{x}_n$ produced by any incident sound or flexural waves together with collective contributions caused by scattering by the remaining apertures.

When the characteristic wavelengths of the sound and structural motions are large compared to the distance between neighboring apertures it is convenient to simplify (3.2) by averaging with respect to aperture positions. This enables attention to be focussed on the overall effect of the apertures rather than local details at each aperture, and henceforth ζ and p will be taken to denote the averaged displacement and pressure respectively. This averaging procedure is equivalent to that used to study wave propagation in

dusty gases and bubbly media [40 - 45], and in the classical Lorentz-Lorenz theory of a dielectric [46]. To determine the average contribution from the sources in (3.2) at $\mathbf{x} = \mathbf{x}_m$, say, we first obtain appropriate expressions for ζ_m and $[p_m]$ by means of the following argument. For a large plate of area A the probability that $\mathbf{x}_n$ lies within the area element $dx_n \equiv dx_{n1}\, dx_{n3}$ is equal to dx_n/A, and there are NA apertures in all. In a first approximation, for $\alpha \ll 1$, the apertures may be regarded as independently distributed, and the average on the right of (3.2) can be evaluated by first averaging over all $\mathbf{x}_n \neq \mathbf{x}_m$. The quantities ζ_m and $[p_m]$ must then be set equal to the corresponding averaged incident fields, following which we can average with respect to $\mathbf{x}_m$. When the total number of apertures is large, these incident field averages cannot differ significantly from the overall average displacement and pressure jump, since the latter are hardly affected by the presence or absence of the aperture at $\mathbf{x}_m$ when NA $\to \infty$. Thus in the leading approximation the contribution from $\mathbf{x}_m$ as NA $\to \infty$ is given by writing

$$\zeta_m = \zeta(x_{m1}, x_{m3}) - NK_R[p_m]/\rho_o\omega^2 \text{ and } [p_m] = [p(x_{m1}, 0, x_{m3})], \text{ for } \alpha \ll 1.$$

Making this substitution in (3.2) and performing the average with respect to the $\mathbf{x}_n$, we obtain the *generalized* bending wave equation

$$\left(\left[1 - \frac{2\alpha\sigma}{(1-\sigma)}\right]B\nabla_2^4 - m\omega^2\right)\zeta + \left(1 + 2NRK_R\left[1 - \frac{1}{2R\rho_o\omega^2}\left(\left[1 - \frac{2\alpha\sigma}{(1-\sigma)}\right]B\nabla_2^4 - m\omega^2\right)\right]\right)[p] = 0. \tag{3.3}$$

In this equation the term in σ accounts for an effective decrease in the stiffness of the plate caused by the presence of the apertures: this is independent of fluid loading, and an identical term is obtained if the calculation is repeated for a plate *in vacuo*. The terms involving the conductivity K_R represent the influence of the fluid at the apertures. In the absence of bias flow all of the modified coefficients in the equation are real, and equation (3.3) then has undamped plane wave solutions that correspond to the undamped bending wave modes of an ideal, fluid loaded, homogeneous plate (the attenuation caused by acoustic scattering at the apertures is a higher order effect, and is not included at the present order of approximation).

3.2 Dissipation of sound

To illustrate the implications of equation (3.3) consider the absorption of sound incident on a bias flow elastic screen. For simplicity attention is confined to plane acoustic pressure waves of the form $e^{-i\kappa_o x_2}$ incident *normally* on the screen from $x_2 > 0$ (see Figure 4). The pressure can be taken in the form

$$\left.\begin{aligned} p &= e^{-i\kappa_o x_2} + \Re e^{i\kappa_o x_2}, \quad x_2 > 0, \\ &= \Im e^{-i\kappa_o x_2}, \quad x_2 < 0, \end{aligned}\right\} \tag{3.4}$$

where $\Re$ and $\Im$ are appropriate reflection and transmission coefficients, respectively. The (generalized) displacement ζ of the screen is related to p by $\zeta = (1/\rho_o\omega^2)\partial p/\partial x_2$ $(x_2 \to \pm 0)$. This relation and equation (3.3) supply two equations, from which $\Re$ and $\Im$ are found to be given by

$$\Re = 1 - \Im = \frac{m\kappa_o/\rho_o}{\frac{m\kappa_o}{\rho_o} + 2i\left(1 + \frac{4}{\pi}\alpha(\Gamma - i\Delta)\left[1 + \frac{m}{2\rho_o R}\right]\right)}. \tag{3.5}$$

Define an *absorption coefficient* $\delta\Pi_I/\Pi_I$, where Π_I denotes the acoustic power incident on the screen and $\delta\Pi_I$ is the dissipated power. Then

$$\begin{aligned} \delta\Pi_I/\Pi_I &= 1 - |\Re|^2 - |\Im|^2 \\ &\equiv \frac{\frac{8}{\pi}\alpha M S_t \Delta\left[1 + 2\frac{\rho_o R}{\rho_s h}\right]}{S_t^2\left(M + \frac{4\alpha\Delta}{\pi S_t}\left[1 + 2\frac{\rho_o R}{\rho_s h}\right]\right)^2 + 4\left(\frac{\rho_o R}{\rho_s h} + \frac{2\alpha\Gamma}{\pi}\left[1 + 2\frac{\rho_o R}{\rho_s h}\right]\right)^2}. \end{aligned} \tag{3.6}$$

The solid curves in Figure 5 depict the variation of $\delta\Pi_I/\Pi_I$ with aperture Strouhal number $S_t = \omega R/U_c$ for sound incident on a perforated aluminium plate in air, when the bias flow convection Mach number M = 0.05 and when R/h = 5. According to this figure the maximum possible attenuation of $\delta\Pi_I/\Pi_I$ just less than 0.5 (3 dB) occurs at an open area ratio α = M over a range of Strouhal numbers centered on $S_t \approx 0.4$. At very low frequencies the impedance

offered to the sound by the plate becomes negligible, the bias flow jet velocities are unmodulated by the sound, and there is no transfer of acoustic energy to hydrodynamic motions. In this low frequency limit ($S_t \ll 1$)

$$\Gamma - i\Delta \approx \tfrac{1}{3}S_t^2 - \tfrac{1}{4}i\pi S_t ,$$

and

$$\delta\Pi_I/\Pi_I \approx \frac{2\alpha M S_t^2\left[1 + 2\frac{\rho_o R}{\rho_s h}\right]}{S_t^2\left(M + \alpha\left[1 + 2\frac{\rho_o R}{\rho_s h}\right]\right)^2 + 4\left(\frac{\rho_o R}{\rho_s h}\right)^2} , \qquad (3.7)$$

which implies that significant damping can occur provided $\omega h/c_o > \rho_o/\rho_s$. The results shown in the figure are for R/h = 5. The present theory is applicable only when R is large enough to ensure that the Reynolds number of the bias flow jets is large. At smaller values of R/h the predicted absorption is similar to that shown in the figure, but the widths of the bell-shaped solid curves increase, and the maxima shift to slightly lower frequencies.

The corresponding attenuation produced by a bias flow *rigid* screen at arbitrary frequency is obtained by setting $\rho_o R/\rho_s h = 0$ in (3.6); the predictions in this case are depicted by the broken curves in Figure 5. At low frequencies the rigid screen absorption coefficient approaches the limiting value given by (3.7) when $\rho_o R/\rho_s h \to 0$ namely, $\delta\Pi_I/\Pi_I \approx 2\alpha M/(M+\alpha)^2$ ($S_t \ll 1$) [13], which takes its maximum value (of $\frac{1}{2}$) when $\alpha = M$, as for the elastic screen. The elastic screen predictions of Figure 5 differ from those for a rigid screen when the frequency is low enough that the screen may be regarded as acoustically transparent. This behavior is typical of situations in which the fluid mass loading of the plate is small (e.g., for metallic screens in air). For large mass loading (which in practice occurs when $\rho_o/\rho_s > 10^{-3}$, for steel in water, say) equation (3.6) predicts that the absorption of acoustic energy by the elastic screen is negligible at all frequencies, in contrast to the rigid screen predictions, which are similar to those illustrated by the broken curves in Figure 5.

3.3 Damping of flexural waves

The damping of a flexural wave can be examined similarly. Let the flexural wave be the plane bending wave $\zeta = \zeta_o e^{i\kappa x_1}$ with the associated pressure field defined as in equation (2.25) where now, however, the bending wavenumber κ is a zero of the generalized dispersion function

$$\bar{D}(\kappa,\omega)$$

$$\equiv \left[1 - \frac{2\alpha\sigma}{(1-\sigma)}\right]B\kappa^4 - m\omega^2 - \frac{2i\rho_o\omega^2}{\gamma(\kappa)}\left(1 + 2NRK_R\left[1 - \frac{1}{2R\rho_o\omega^2}\left(\left[1 - \frac{2\alpha\sigma}{(1-\sigma)}\right]B\kappa^4 - m\omega^2\right)\right]\right), \tag{3.8}$$

which is obtained by substituting for ζ and [p] in equation (3.3).

In the absence of the bias flow ($K_R \to 2R$), $\bar{D}(\kappa,\omega)$ has precisely two equal and opposite real zeros. They satisfy $|\kappa| > \kappa_o$ (where $\gamma(\kappa) = i(\kappa^2 - \kappa_o^2)^{1/2}$) and correspond to undamped flexural waves on the perforated plate; they are generally close to the corresponding zeros of the dispersion function $D(k,\omega)$ of the homogeneous plate (see (2.15)). To the present order of approximation there is no damping due to scattering of structural energy into sound. This is analogous to the corresponding approximation in the theory of surface-acoustic waves propagating over a nominally plane rigid wall with small surface irregularities, where the scattering by surface roughness elements of characteristic dimension R causes the wave to be damped only over very large propagation distances of order $1/\{R^4\kappa^5\}$ [47, 48].

The absorption of bending wave energy by the bias flow jets causes the formerly real bending wavenumber κ to acquire a small *positive* imaginary part that accounts for the progressive decay of the wave. The reduction in the flexural wave power over a propagation distance δx_1 is equal to $20\mathrm{Im}\{\kappa\}\delta x_1 \log_{10}(e)$ dB, and the power absorbed per wavelength of propagation is therefore $40\pi\log_{10}(e)\mathrm{Im}\{\kappa\}/\mathrm{Re}\{\kappa\} \approx 54.6\mathrm{Im}\{\kappa\}/\mathrm{Re}\{\kappa\}$ dB. The dependence of this absorption on the bias flow Strouhal number $S_t = \omega R/U_c$ is illustrated in Figures 6 and 7 for a perforated steel plate in water and several different open area ratios α for an aperture radius R = h, 3h respectively. In both cases the bias flow vorticity convection velocity U_c = 3 m/s (M = 0.002). Increasing the open area ratio increases the attenuation, whereas increasing the size of the apertures reduces the maximum possible attenuation. These

results have been obtained from a numerical solution of the dispersion equation $\bar{D}(\kappa,\omega) = 0$, by iterating about the real zero κ in the absence of the bias flow jets. The absorption may also be estimated from the absorption cross-section formula (2.31). The fraction of the incident power Π_I absorbed in a distance δx_1 in the direction of propagation is $N\Pi_A \delta x_1/\Pi_I \equiv 2\mathrm{Im}\{\kappa\}\delta x_1$; using (2.31) it follows that

$$\frac{\mathrm{Im}\{\kappa\}}{\mathrm{Re}\{\kappa\}} \approx \frac{8\alpha\epsilon\Delta(S_t)\{1 - R(\kappa^2-\kappa_o^2)^{1/2}\}}{\pi M S_t (\kappa/K_o)^2[5(\kappa/K_o)^4 - 4(\kappa\kappa_o/K_o^2)^2 - 1]}\ , \qquad (3.9)$$

where on the right hand side κ denotes the real value of the wavenumber in the absence of dissipation. This approximate formula tends to over predict the attenuation by several dB near the maxima of Figures 6 and 7. It shows, however, that the change in the attenuation with R/h (for fixed values of the remaining parameters) is caused by the consequent change in the real part of the bending wavenumber κ relative to the vacuum wavenumber K_o (c.f., Figure 8 below). Note also that, implicit in the present analysis is the requirement that $R \gg h$, and this might cast some doubt on the validity of the results shown for R/h = 1 in Figure 6. However, the damping is governed by the imaginary part ($-\Delta$) of the Rayleigh conductivity K_R, which is non-zero because of the production of vorticity in the apertures. The value of Δ given in (2.29) would be expected to be applicable provided the length scale U_c/ω of the vorticity is large compared to the plate thickness h, and the predictions of Figure 6 should therefore be valid at least for $S_t < 1$.

To assess the likely significance of the attenuations produced by a bias flow screen we plot in Figure 8 the corresponding absorption of bending waves on a coated steel plate in water. For the purpose of illustration the mass of the coating is neglected, but the coating is assumed to make the effective stiffness of the plate complex, such that the bending stiffness B of the uncoated plate is replaced by $B(1 - i\eta)$, where η (> 0) is a *loss factor* whose value is determined by the properties of the coating, and is typically of the same order as shown in the figure [32]. The abscissa $\omega/\omega_c \equiv \epsilon M(\rho_s h/R\rho_o)S_t$, where $\omega_c = c_o^2(m/B)^{1/2}$ is the *coincidence frequency*. As ω increases towards ω_c both the bending and acoustic wavelengths become comparable to the thickness of the plate and the thin plate equation (2.1), on which the present analysis

is based, ceases to be applicable. A comparison with figures 6 and 7 indicates that the attenuations achieved by the bias flow jets can be comparable with those predicted for the coated plate.

Much smaller attenuations are predicted for bending waves propagating on a bias flow screen in air. Figure 9 depicts typical predictions for an aluminium plate with three different open area ratios when R = 5h and the mean bias flow jet velocity $U \approx 2U_c = 3.4$ m/s. In possible applications the thickness h of the plate will usually be small (of the order of 0.01 cms), and the bias flow Reynolds number UD/ν (D = 2R being the aperture diameter, and ν the kinematic viscosity) must be large enough to ensure that motion in the apertures is not impeded by viscous action. For the cases illustrated in the figure $UD/\nu \approx 250$, which is probably close to the lower limit for which the theory is likely to be relevant. The Reynolds number could be raised by operating at a higher jet velocity, but this would degrade the absorption which, according to (3.9), is inversely proportional to the vorticity convection Mach number M.

4. CONCLUSION

Vorticity is produced by fluid motion relative to a solid surface, the rate of production being greatest in regions where the pressure and velocity in the primary flow change rapidly, such as at corners and sharp edges. The kinetic energy of the motion induced by this vorticity is derived from the primary flow, and vorticity generation accordingly transfers energy from that flow to generally smaller scale vortex motions. In this paper we have examined the production of vorticity at the sharp edges of circular apertures in a thin elastic plate by long wavelength sound and vibrational motions of the plate The vorticity is diffused from the edges by viscosity, resulting in the dissipation of the sound and structural motions. In the absence of mean flow through the apertures the dissipation is caused by the nonlinear convection of vorticity from the apertures and by viscous damping, both of which are weak because the growth of vorticity tends to be inhibited by periodic reversals in the primary motions, which produce vorticity of fluctuating sign. The damping is significantly increased, however, when a high Reynolds number mean flow is maintained through the apertures. Viscous effects are now important only in the immediate vicinity of the aperture edges, where vorticity is released into the flow; but the vorticity is swept away from the plate by the flow, and its kinetic energy is permanently lost to the incident acoustic and vibrational motions.

Our analysis of this mechanism for a bias flow, perforated elastic plate has confirmed that significant attenuations of sound and flexural vibrations are possible provided a sufficiently large fluctuating pressure gradient can be established across the screen to cause unsteady production of vorticity in the apertures. When the fluid loading is large (e.g., for metallic plates in water) an unrestrained elastic screen is effectively acoustically "transparent", and the damping of sound by vorticity production tends to be negligible. Significant acoustic attenuations can occur for a lightly loaded plate (in air, say) provided the frequency ω satisfies $\omega h/c_o > \rho_o/\rho_s$.

The damping of bending waves (i.e., of resonant structural waves that propagate subsonically relative to the fluid) increases with the fluid loading, since the surface pressure fluctuations produced by the passage of a

bending wave of given surface displacement tends to increase with fluid density. The damping is greatest for aperture Strouhal numbers $S_t = \omega R/U_c$ between about 0.03 and 3, and the attenuation experienced by bending waves on a perforated steel plate in water (of the order of 4 - 6 dB per wavelength of propagation) can then exceed or be comparable with that possible when motions of the plate are heavily damped by the application of surface coatings. In air the predicted attenuations are very much more modest, ranging between 0.5 - 1 dB per wavelength.

APPENDIX

The coefficients A_{0j} , A_{2j} , Q_j

$$A_{01} = \frac{-i}{8B}\left[H_0^{(1)}(K_oR) + H_0^{(1)}(iK_oR) - \frac{(1-\sigma)}{K_oR}H_1^{(1)}(K_oR) + \frac{i(1-\sigma)}{K_oR}H_1^{(1)}(iK_oR)\right]$$

$$- \frac{i\rho_o\omega^2}{\pi R}\int_0^\infty \frac{k^2\,[kRJ_0(kR)-(1-\sigma)J_1(kR)]\,dk}{\gamma(k)(Bk^4-m\omega^2)D(k,\omega)} ,$$

$$A_{21} = \frac{-iK_o^2}{8B}\left[H_0^{(1)}(K_oR) - H_0^{(1)}(iK_oR) - \frac{(1-\sigma)}{K_oR}H_1^{(1)}(K_oR) - \frac{i(1-\sigma)}{K_oR}H_1^{(1)}(iK_oR)\right]$$

$$+ \frac{i\rho_o\omega^2}{\pi R}\int_0^\infty \frac{k^4\,[kRJ_0(kR)-(1-\sigma)J_1(kR)]\,dk}{\gamma(k)(Bk^4-m\omega^2)D(k,\omega)} ,$$

$$Q_1 = \frac{i\rho_o\omega^2}{\pi R}\int_0^\infty \frac{k^2\,[(1-\sigma)J_1(kR)-kRJ_0(kR)]\,dk}{\gamma(k)D(k,\omega)} ; \qquad (A.1)$$

$$A_{02} = \frac{K_o}{8B}\left[iH_1^{(1)}(K_oR) - H_1^{(1)}(iK_oR)\right] + \frac{i\rho_o\omega^2}{\pi}\int_0^\infty \frac{k^4J_0(kR)\,dk}{\gamma(k)(Bk^4-m\omega^2)D(k,\omega)} ,$$

$$A_{22} = \frac{-iK_o^3}{8B}\left[H_1^{(1)}(K_oR) + iH_1^{(1)}(iK_oR)\right] - \frac{i\rho_o\omega^2}{\pi}\int_0^\infty \frac{k^6J_1(kR)\,dk}{\gamma(k)(Bk^4-m\omega^2)D(k,\omega)} ,$$

$$Q_2 = \frac{i\rho_o\omega^2}{\pi B}\left[\frac{1-e^{i\kappa_oR}}{\kappa_oR} + \omega^2\int_0^\infty \frac{[m+2i\rho_o/\gamma(k)]J_1(kR)\,dk}{\gamma(k)D(k,\omega)}\right]; \qquad (A.2)$$

$$A_{03} = \frac{iK_R}{\pi}\int_0^\infty \frac{k\,dk}{\gamma(k)D(k,\omega)} , \qquad A_{23} = \frac{-iK_R}{\pi}\int_0^\infty \frac{k^3\,dk}{\gamma(k)D(k,\omega)} . \qquad (A.3)$$

The integrals in these expressions are taken along the positive real axis indented to pass *below* real singularities of the integrands (equivalent to replacing ω by $\omega + i\varepsilon$ and taking the limit $\varepsilon \to +0$).

LIST OF PRINCIPAL SYMBOLS

a_j	source coefficients in equation (2.11) (j = 1, 2)
A_{ij}	see (2.17), (2.22) and appendix
B	bending stiffness
c_o	speed of sound
$D(k,\omega)$	uniform plate dispersion function (2.15)
$\bar{D}(k,\omega)$	perforated plate dispersion function (3.8)
E	Young's modulus
f	see equation (2.6)
h	plate thickness
H	Heaviside unit function
$\mathbf{k}$	$(k_1, 0, k_3)$, wavenumber in plane of plate
K_o	$(m\omega^2/B)^{1/2}$, vacuum bending wavenumber
K_R	$2R(\Gamma - i\Delta)$, Rayleigh conductivity of aperture, see (2.28)
m	$\rho_s h$, mass of plate per unit area
M	U_c/c_o, Mach number
N	number of apertures per unit area
p	pressure
p_I	incident bending wave pressure, (2.25)
p_s	scattered pressure
q	displacement flux through the aperture
Q_j	see (2.17) and appendix
r	$(x_1^2+x_3^2)^{1/2}$,
R	aperture radius
S_t	$\omega R/U_c$, Strouhal number
U_c	$\approx \frac{1}{2}U$, vorticity convection velocity
U	mean bias flow velocity
x_j	rectangular coordinate (j = 1, 2, 3)
$\mathbf{x}$	$(x_1, 0, x_3)$
α	$N\pi R^2$, open area ratio
$\gamma(k)$	$(\kappa_o^2 - k^2)^{1/2}$ $(k = \lvert\mathbf{k}\rvert)$
ϵ	fluid loading parameter, (2.32)

ζ	displacement
ζ_+	flexural displacement of plate
ζ_-	perturbation displacement in the aperture
ζ_o	flexural wave amplitude
ζ_s	scattered flexural disturbance
κ	flexural wavenumber
κ_o	ω/c_o, acoustic wavenumber
Π_A	power dissipated at the aperture, (2.27)
Π_I	incident bending wave power, (2.30)
ρ_o	fluid density
ρ_s	density of plate material
σ	Poisson's ratio
ω	radian frequency
$\mathfrak{R}$	reflection coefficient, (3.4)
$\mathfrak{T}$	transmission coefficient, (3.4)

REFERENCES

1. Lighthill, M. J. 1952 *Proc. Roy. Soc. Lond.* **A211**, 564 - 587. On sound generated aerodynamically. Part I: General theory.
2. Curle, N. 1955 *Proc. Roy. Soc. Lond.* **A231**, 505 - 514. The influence of solid boundaries upon aerodynamic sound.
3. Powell, A. 1963 *AGARD* Rept. 466. Mechanisms of aerodynamic sound production.
4. Ffowcs Williams, J. E. & Hawkings, D. L. 1969 *Phil. Trans. Roy. Soc.* **A264**, 321 - 342. Sound generation by turbulence and surfaces in arbitrary motion.
5. Howe, M. S. 1975 *J. Fluid Mech.* **71**, 625 - 673. Contributions to the theory of aerodynamic sound, with application to excess jet noise and the theory of the flute.
6. Crighton, D. G. 1981 *J. Fluid Mech.* **106**, 261 - 298. Acoustics as a branch of fluid mechanics.
7. Lilley, G. M. 1991 *Jet noise classical theory and experiments*. Chapter 4 of *Aeroacoustic of Flight Vehicles: Theory and Practice. Volume 1: Noise Sources*. NASA Ref. Publ. 1258 (edited by H. H. Hubbard).
8. Ffowcs Williams, J. E. 1965 *J. Fluid Mech.* **22**, 347 - 358. Sound radiation from turbulent boundary layers formed on compliant surfaces.
9. Chandiramani, K. L. 1977 *J. Acoust. Soc. Am.* **61**, 1460 -1470. Vibration response of fluid loaded structures to low speed flow noise.
10. Blake, W. K. 1986 *Mechanics of flow-induced sound and vibration, Vol. 2: Complex flow-structure interactions*. New York: Academic Press.
11. Howe, M. S. 1993 *Proc. Roy. Soc. Lond.*, **A442**, 533 - 554. Structural and acoustic noise produced by turbulent flow over an elastic trailing edge.
12. Rienstra, S. W. 1981 *J. Fluid Mech.* **108**, 443 - 460. Sound diffraction at a trailing edge.
13. Howe, M. S. 1984 *IMA J. Appl. Math.* **32**, 187 - 209. On the absorption of sound by turbulence and other hydrodynamic flows.
14. Ver, I. L. 1982 *Perforated baffles prevent flow-induced acoustic resonances in heat exchangers*. Paper presented at 1982 meeting of the Federation of the Acoustical Societies of Europe; Gttingen, September 1982.

15. Ver, I. L. 1990 *Noise Control Eng. J.* **35** (Nov/Dec issue) pp. 115 - 125. Practical examples of noise and vibration control: case history of consulting projects.
16. Bloxsidge, G. J., Dowling, A. P. & Langhorne, P. J. 1988 *J. Fluid Mech.* **193**, 445 - 473. Reheat buzz: an acoustically coupled combustion instability. Part 2. Theory.
17. Hughes, I. J. & Dowling, A. P. 1990 *J. Fluid Mech.* **218**, 299 - 336. The absorption of sound by perforated linings.
18. Bechert, D., Michel, U. & Pfizenmaier, E. 1977 *AIAA Paper 77-1278*. Experiments on the transmission of sound through jets.
19. Bechert, D. W. 1979 *AIAA Paper* 79-0575. Sound absorption caused by vorticity shedding, demonstrated with a jet flow.
20. Howe, M. S. 1980 *J. Sound Vib.* **70**, 407 - 411. The dissipation of sound at an edge.
21. Howe, M. S. 1979 *Proc. Roy. Soc. Lond.* **A366**, 205 - 233. On the theory of unsteady high Reynolds number flow through a circular aperture.
22. Howe, M. S. 1980 *Proc. Roy. Soc. Lond.* **A370**, 523 - 544. On the diffraction of sound by a screen with circular apertures in the presence of a low Mach number grazing flow.
23. Fukumoto, Y. & Takayama, M. 1991 *Phys. Fluids* **A3**, 3080 - 3082. Vorticity production at the edge of a slit by sound waves in the presence of a low Mach number bias flow.
24. Dowling A. P. & Hughes, I. J. 1992 *J. Sound Vib.* **156**, 387 - 405. Sound absorption by a screen with a regular array of slits.
25. Cargill, A. M. 1982 *J. Fluid Mech.* **121**, 59 - 105. Low frequency sound radiation and generation due to the interaction of unsteady flow with a jet pipe.
26. Blackman, A. W. 1960 *Am. J. Rocket Soc.* (November issue), 1022 - 1028. Effect of nonlinear losses on the design of absorbers for combustion instabilities.
27. Zinn, B. T. 1970 *J. Sound Vib.* **13**, 347 - 356. A theoretical study of nonlinear damping by Helmholtz resonators.
28. Melling, T. H. 1973 *J. Sound Vib.* **29**, 1 - 65. The acoustic impedance of perforates at medium and high sound pressure levels.

29. Cummings, A. 1983 *AIAA Paper 83-0739.* Acoustic nonlinearities and power losses at orifices.

30. Cummings, A. 1984 *AIAA Paper 84-2311.* Transient and multiple frequency sound transmission through perforated plates at high amplitude.

31. Howe, M. S. 1992 *J. d'Acoustique* 5, 603 - 620. On the damping of structural vibrations by vortex shedding.

32. Beranek, L. L. & Ver, I. L. 1992 *Noise and Vibration Control Engineering* New York: John Wiley.

33. Cremer, L., Heckl, M, & Ungar, E. E. 1988 *Structure-borne sound* (2nd ed). New York: Springer-Verlag.

34. Kraus, H. 1967 *Thin elastic shells.* New York: John Wiley & Sons.

35. Gel'fand, I. M. & Shilov, G. E. 1964 *Generalized Functions. Volume 2: Spaces of Fundamental and Generalized Functions.* New York: Academic Press.

36. Lighthill, M. J. 1960 *Phil. Trans. Roy. Soc.* A252, 397 - 430. Studies on magneto-hydrodynamic waves and other anisotropic wave motions.

37. Abramowitz, M. & Stegun, I. A. 1970 (eds.) *Handbook of Mathematical Functions* (Ninth corrected printing), US Dept. of Commerce, Nat. Bur. Stands. Appl. Math. Ser. No.55.

38. Rayleigh, Lord 1945 *Theory of Sound, Vol 2.* New York: Dover.

39. Howe, M. S. 1992 *Proc. Roy. Soc. Lond.* A436, 351 - 372. Sound produced by an aerodynamic source adjacent to a partly coated, finite elastic plate.

40. Williams, F. A. 1985 *Combustion theory* (2nd Ed.) Menlo Park, CA: Benjamin/Cummings Pub. Co.

41. Marble F. E. 1970 *Ann. Rev. Fluid Mech.* 2, 397 - 446. Dynamics of dusty gases.

42. Marble, F. E. & Wooton, D. C. 1970 *Phys. Fluids* 13, 2657 - 2664. Sound attenuation in condensing vapor.

43. Marble, F. E. 1975 *Acoustic attenuation by vaporization of liquid droplets - application to noise reduction in aircraft power plants.* Cal. Tech. Guggenheim Jet Propulsion Center Rept. AFOSR-TR 75-0511.

44. Wijngaarden, L. van 1979 *Sound and shock waves in bubbly liquids*, pp 127 - 140, in *Caviatation and Inhomogeneities in Underwater Acoustics* (ed. W. Lauterborn), Berlin: Springer.

45. Wijngaarden, L. van & Kapteyn, C. 1990 *J. Fluid Mech.* 212, 111 - 138. Concentration waves in dilute bubble/liquid mixtures.

46. Brillouin, L. 1960 *Wave propagation and Group Velocity*. New York: Academic Press.

47. Tolstoy, I. 1983 *J. Acoust. Soc. Am.* 73, 1192 - 1199. Coherent modes and boundary waves in a rough-walled acoustic waveguide.

48. Tolstoy, I. 1985 *J. Acoust. Soc. Am.* 77, 482 - 488. Rough surface boundary wave attenuation due to incoherent scatter.

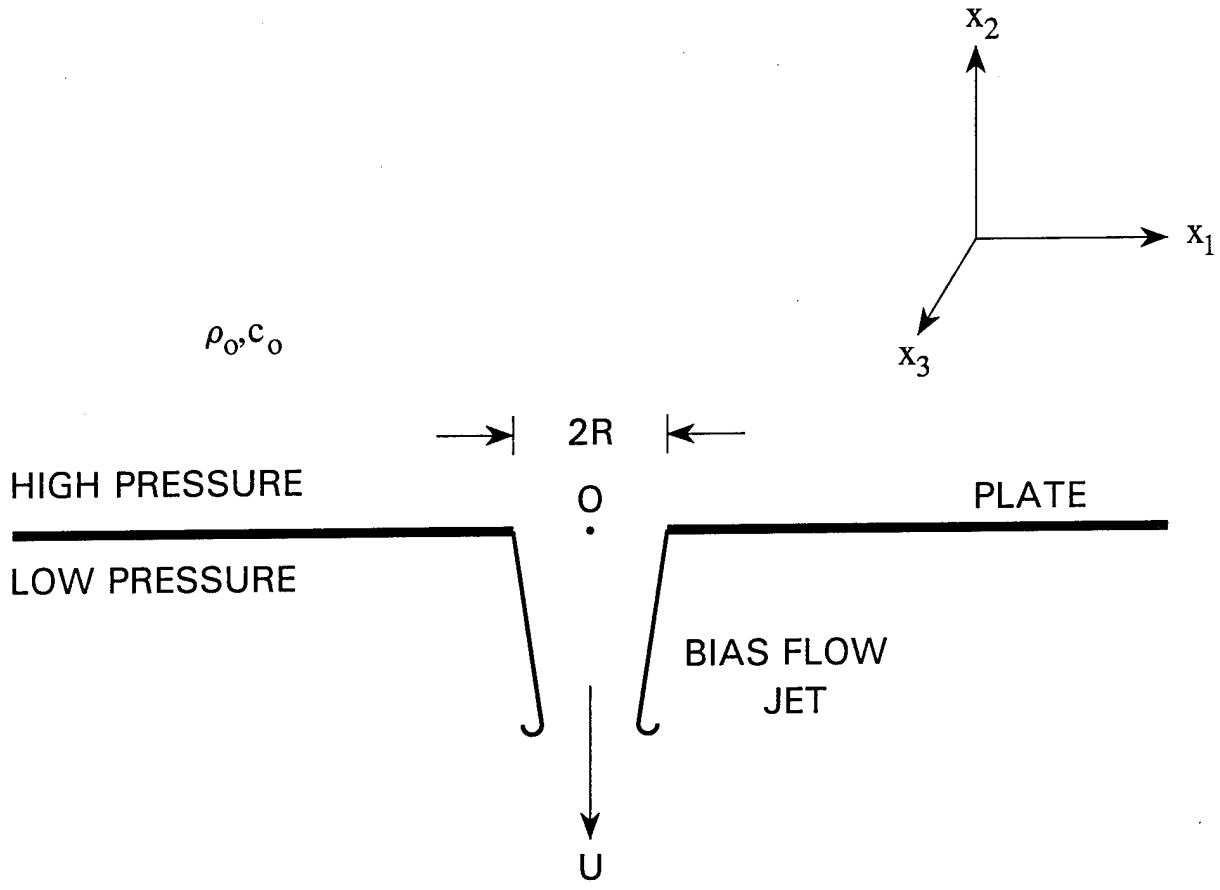

Figure 1. Configuration of the plate, aperture and bias flow.

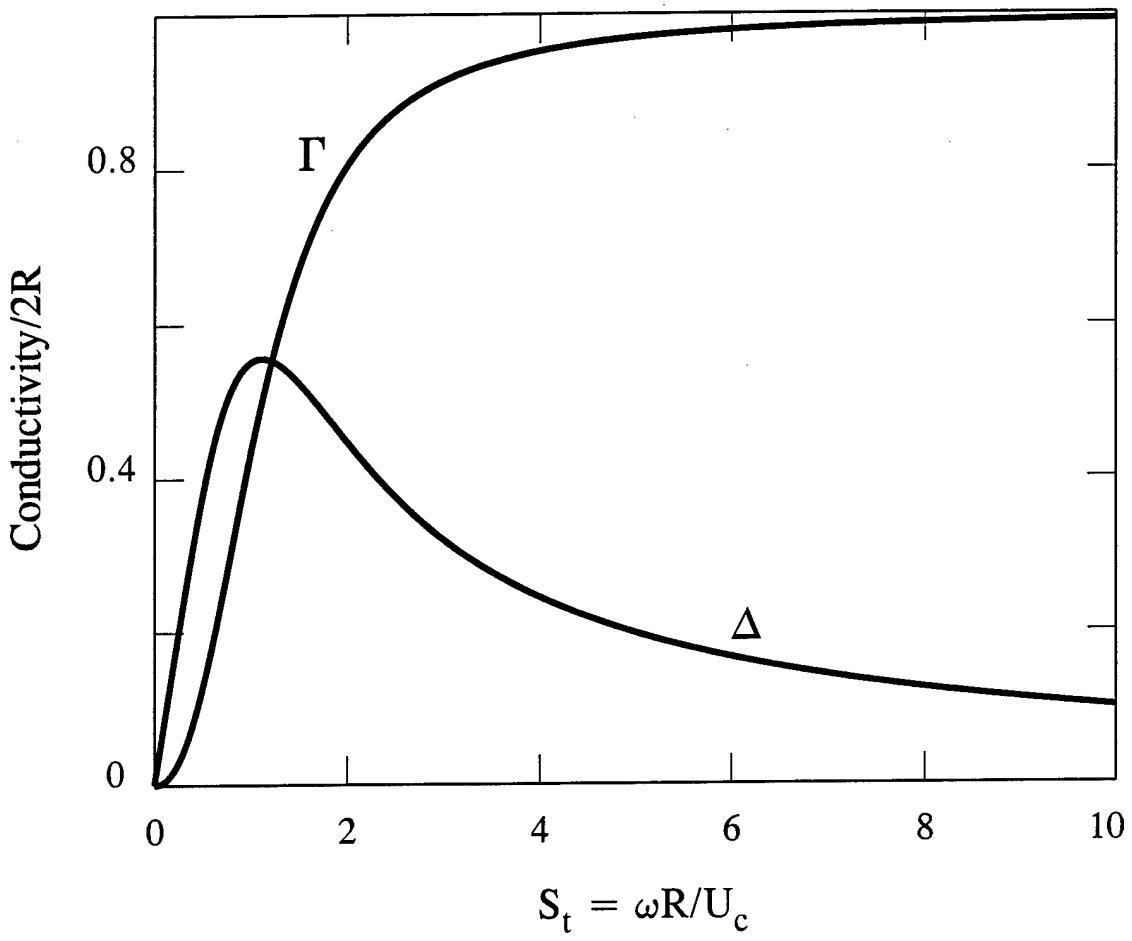

Figure 2. Dependence of the complex Rayleigh conductivity $K_R = 2R(\Gamma - i\Delta)$ on Strouhal number S_t.

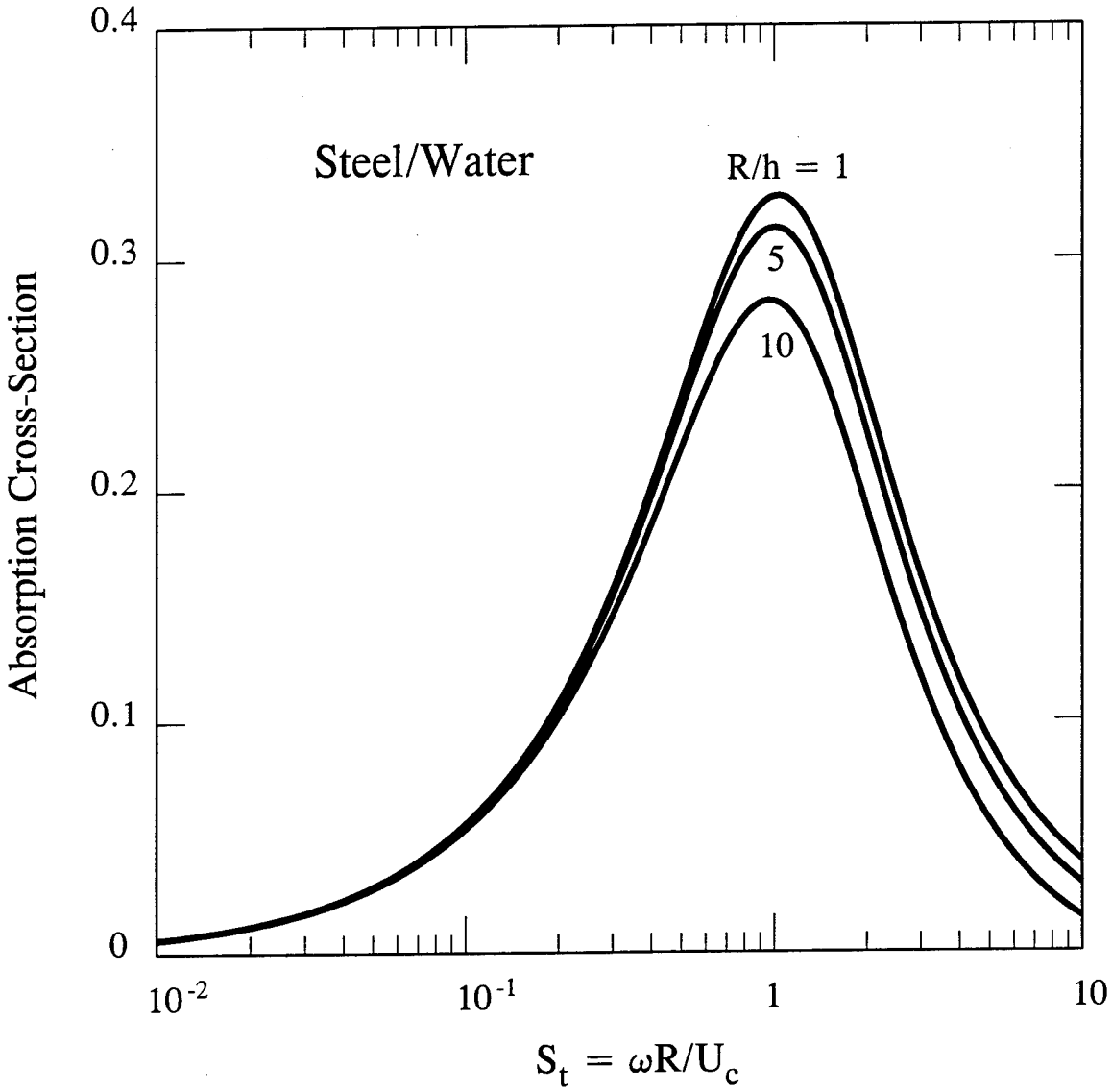

Figure 3. Bending wave absorption cross-section for a circular aperture in a steel plate in water when M = 0.003 ($U_c \approx 4.5$ m/s).

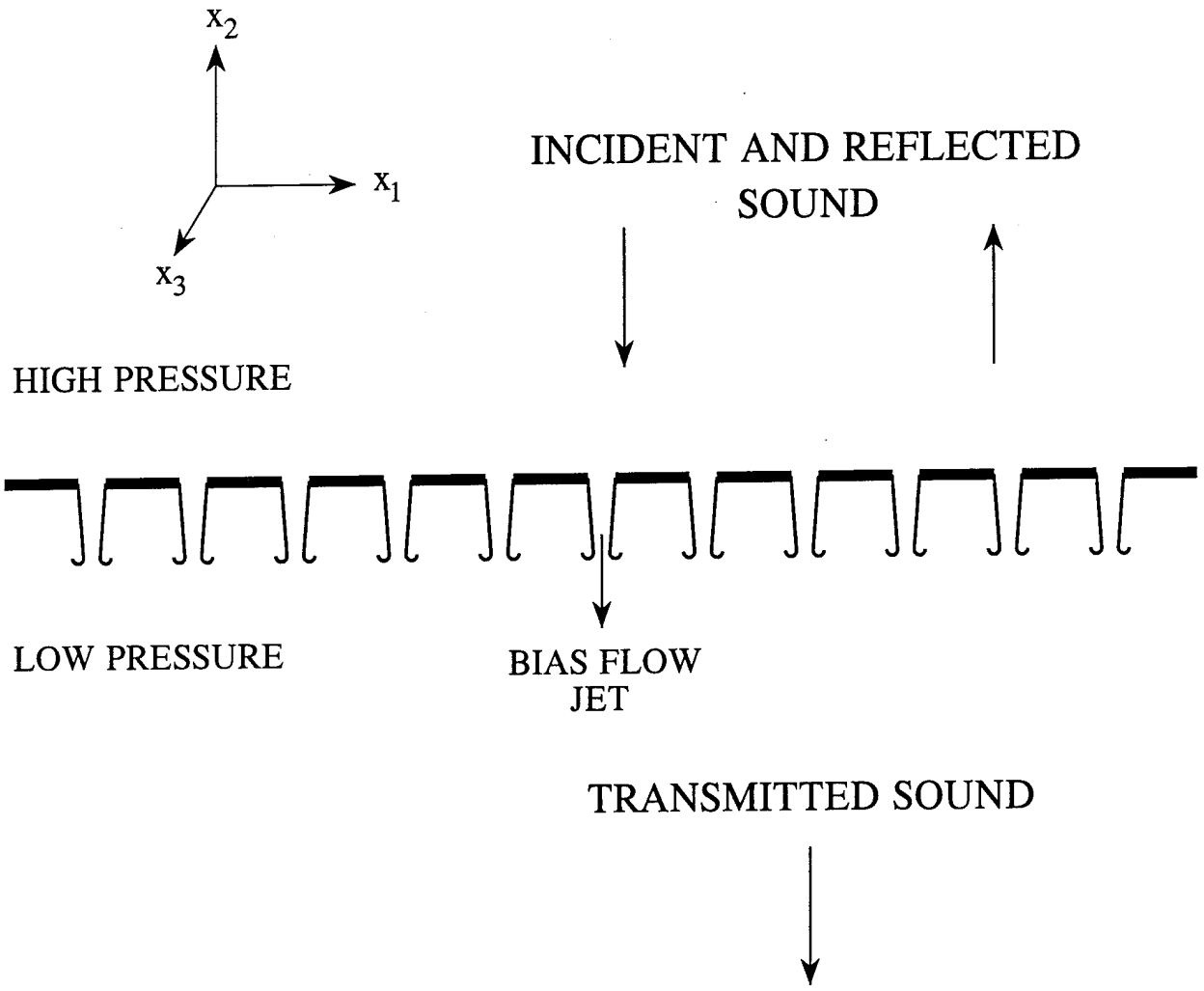

Figure 4. Reflection and transmission of sound by a bias-flow perforated plate.

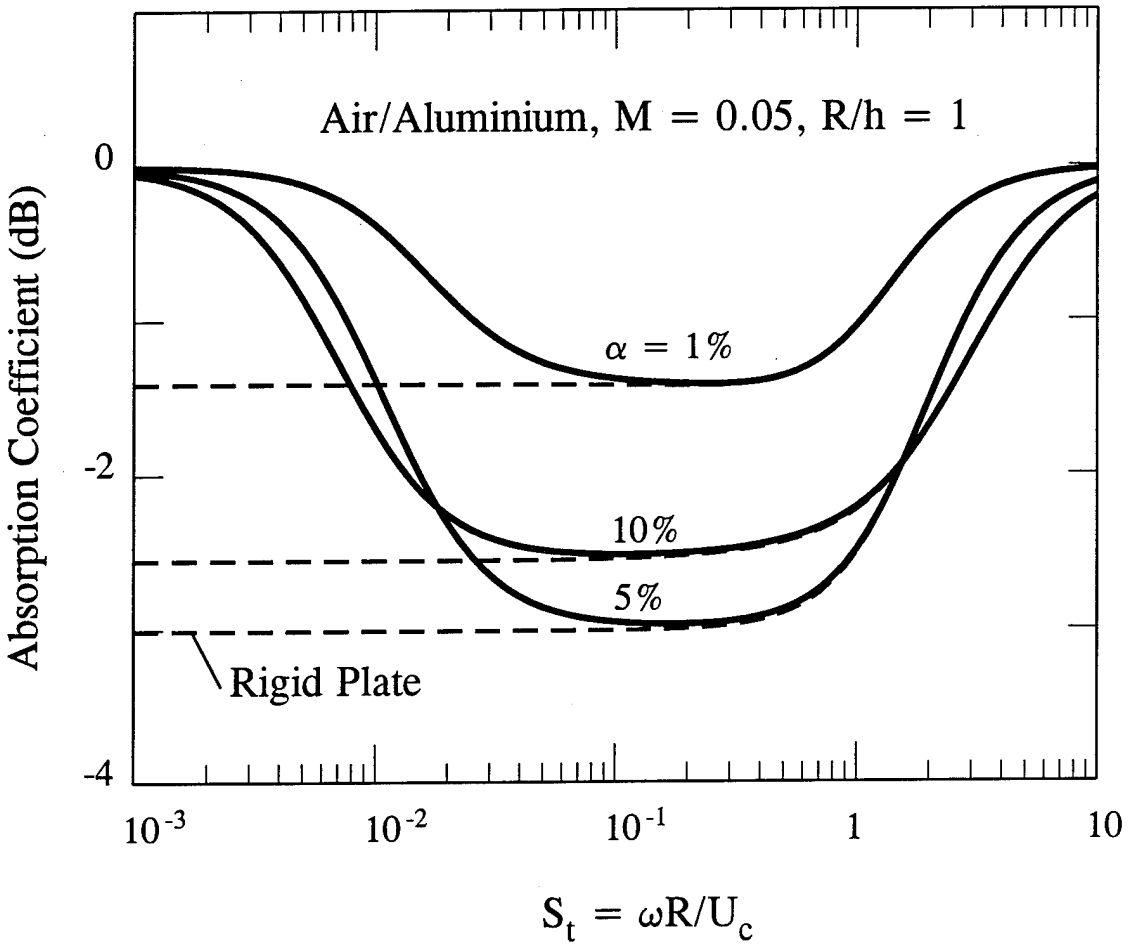

Figure 5. Absorption of normally incident sound by a bias flow perforated screen: ——, the absorption coefficient $10\times\log_{10}\{\delta\Pi_I/\Pi_I\}$ (equation (3.6)) for an aluminium screen in air at different open area ratios α; - - - - -, analogous predictions for a *rigid* screen in air.

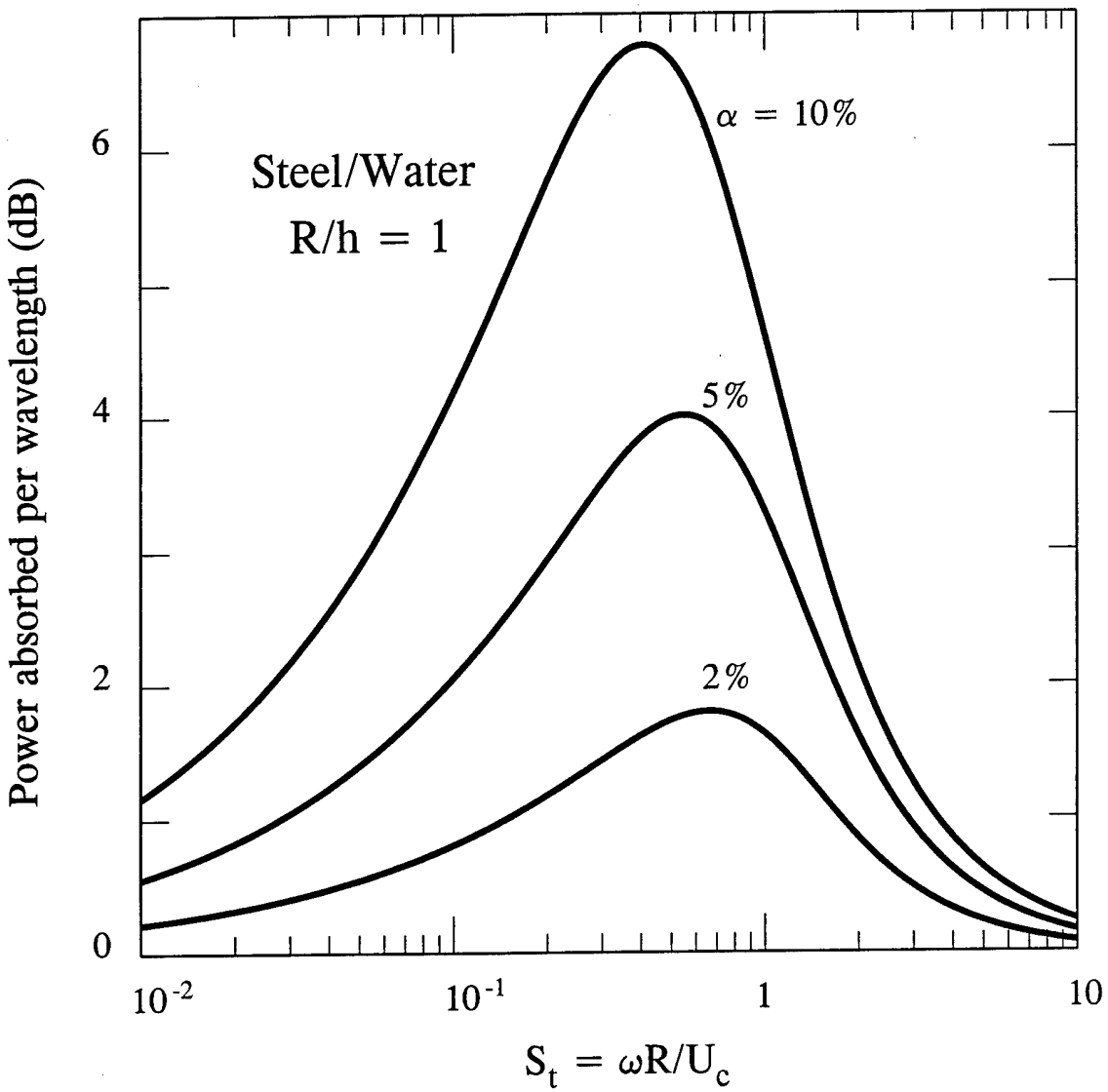

Figure 6. Attenuation of bending waves on a bias flow perforated steel screen in water; the vorticity convection Mach number M = 0.002 (U_c = 3 m/s).

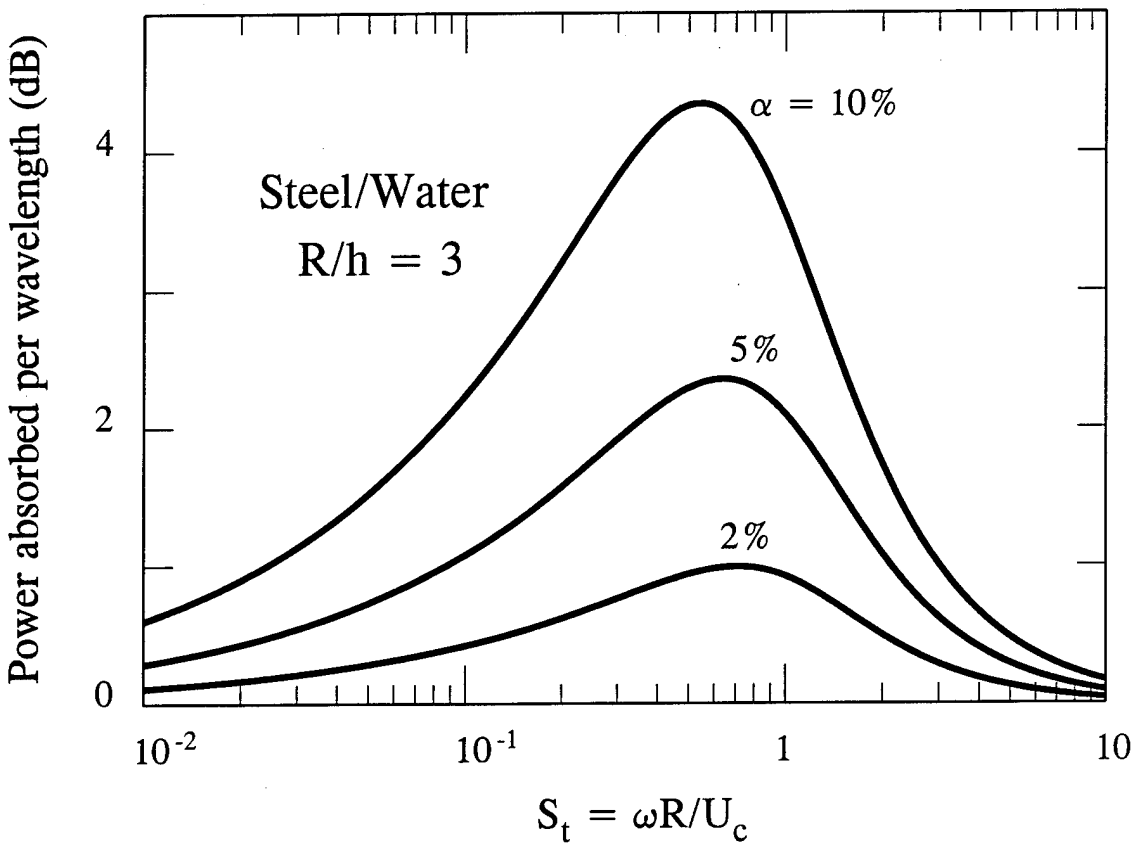

Figure 7. Attenuation of bending waves on a bias flow perforated steel screen in water; the vorticity convection Mach number M = 0.002 (U_c = 3 m/s).

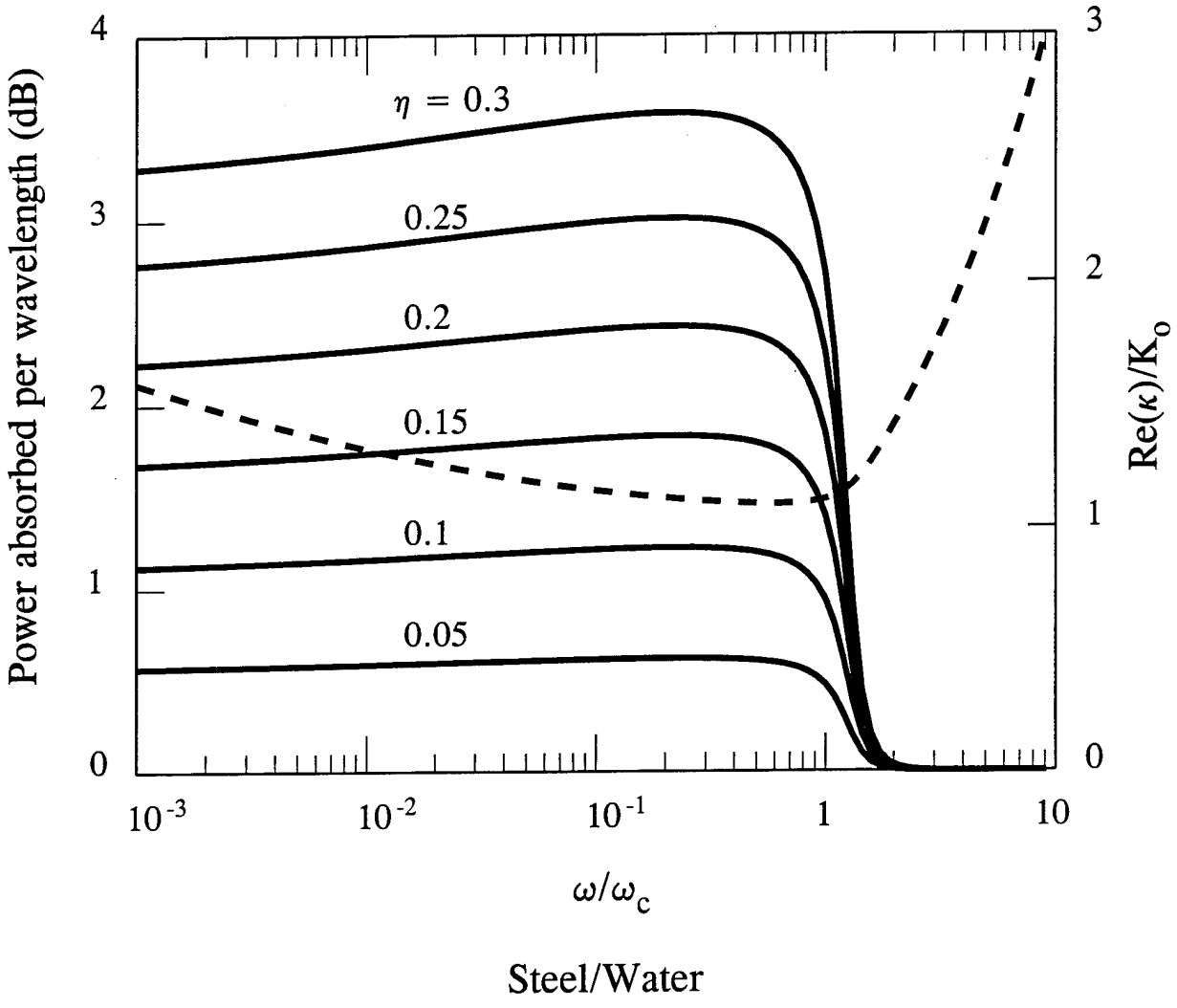

Figure 8. Bending waves on a coated steel plate in water: ——, attenuation for different values of the effective loss factor η; - - - -, $\mathrm{Re}(\kappa)/K_o$.

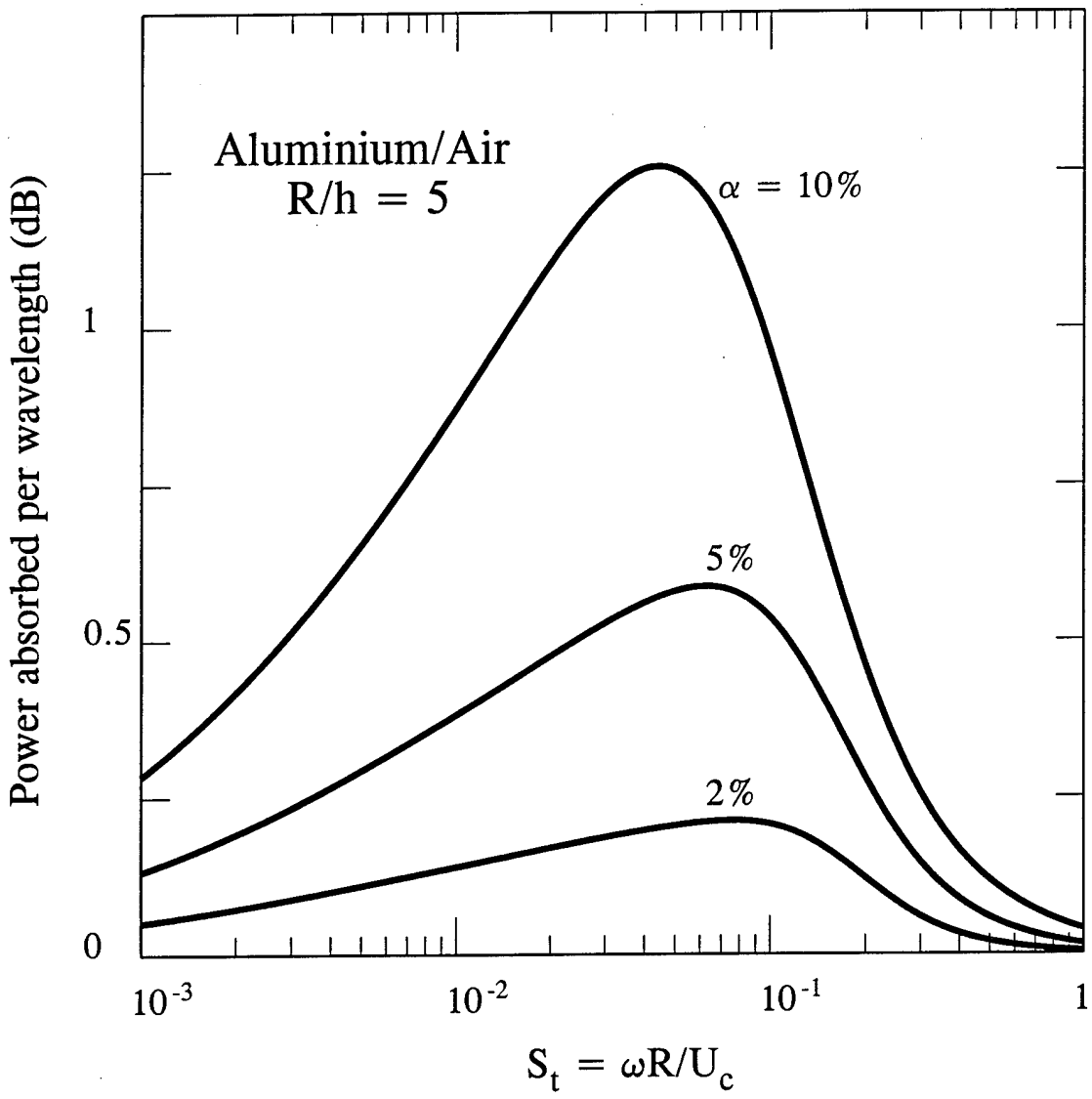

Figure 9. Attenuation of bending waves on a bias flow perforated aluminium screen in air with a bias flow jet velocity of 3.4 m/s.

CHAPTER 2

ENERGY CONSERVATION AND THE DAMPING OF FLEXURAL WAVES BY VORTICITY PRODUCTION

SUMMARY

An analysis is made of the transfer of energy between structural/acoustic vibrations and fluid kinetic energy in flows at very small Mach number. A general energy balance equation is discussed for a vibrating rigid body in either incompressible or low Mach number compressible mean flows. This equation can be used to calculate the growth or decay of structural or acoustic oscillations, and to locate regions of the flow where energy exchanges are significant. A similar general treatment for vibrating *elastic* bodies does not seem to be possible, except in simple cases involving thin elastic plates in parallel flow. Two such problems are discussed, involving the dissipation of structural vibrations by vorticity production (i) at the trailing edge of a large elastic plate, and (ii) in the circular apertures of a perforated elastic plate in a two-sided grazing mean flow. The interaction of boundary layer turbulence with the apertures of a perforated plate can be a particularly intense source of sound, but in applications where the characteristic frequencies are small, a grazing flow perforated screen has been shown to be an efficient sink of acoustic energy. In this paper predictions are given for the damping of bending waves by the same mechanism. When the fluid loading is large, such as for a steel plate in water, these predictions indicate that the damping of resonant bending waves can exceed that normally achieved by coating the plate with elastomeric damping materials, at least over a restricted range of frequencies.

1. INTRODUCTION

Vorticity is produced by fluid motion relative to a solid surface, the rate of production being greatest in regions where the pressure and velocity in the primary flow change rapidly, such as at corners and sharp edges. The kinetic energy of the motion induced by this vorticity is derived from the primary flow, and vorticity generation accordingly transfers energy from that flow to generally smaller scale vortex motions. When the primary motion is produced by a sound wave incident on, say, a sharp edge, vorticity diffuses from the edge by viscous action, causing the sound to be damped (e.g., see [1 - 3]). When the fluid is in a mean state of rest the dissipation is caused by the nonlinear convection of vorticity from the edge and subsequent viscous damping, both of which are weak because the growth of substantial levels of vorticity is inhibited by the periodic nature of the acoustic field, which leads to the generation of vorticity of fluctuating sign. The damping is significantly increased, however, in the presence of a high Reynolds number flow [4 - 16]. Viscous effects are now important only in the immediate vicinity of the edge, where vorticity is released into the flow; the shed vorticity is swept away from the edge by the flow, and its kinetic energy is permanently lost to the incident acoustic wave.

Practical devices for exploiting this mechanism of sound control usually involve bias or grazing flow perforated screens. In the bias flow case a mean pressure difference is maintained across the screen producing a steady flow through the apertures. Damping is caused by the modulation of vorticity production at the aperture edges by the impinging sound [6, 7, 12, 14 - 16]. A grazing flow screen works in a similar way: unsteady motion produced by the sound in the apertures generates vorticity which is swept away by the tangential flow past the screen. In practice high acoustic intensities are usually accompanied by significant structural vibrations. Since the near field (non-acoustic) pressure fluctuations produced by a vibrating body can modulate vorticity production at an edge, it seems likely that a neighboring perforated structure might also be used to suppress structural vibrations. This possibility has been examined theoretically by the author, who considered the damping of bending waves (i) incident on the trailing edge of a large plate in a mean flow [17], and (ii) propagating on a bias-flow perforated

elastic screen [18]. For a bias flow screen subject heavy fluid loading (a steel plate in water, say), it was predicted that damping is significant over a range of frequencies centered on a Strouhal number $\omega R/U \sim O(1)$, where ω denotes radian frequency, R the aperture radius, and U the mean flow velocity through an aperture. These frequencies are typically less than about $0.1\omega_c$, where ω_c is the coincidence frequency of the plate [19, 20]. The predicted damping can be comparable with that normally achieved by heavily coating the vibrating plate with a conventional elastomeric material, whose use frequently entails substantial and undesirable increases in the structural mass, especially at low frequencies.

In this paper equations are derived in §2 which describe the transfer of energy from acoustic and/or structural vibrations to the kinetic energy of the fluid in low Mach number flows, first for vibrations of arbitrary amplitude of rigid and elastic bodies, and second for small amplitude motions of elastic plates in parallel mean flow. These equations generalize results given previously in [12]. Illustrative applications of the theory are made in §3, and in §4 the analysis of [18] for a bias flow perforated plate is extended to investigate the damping of bending waves on a grazing flow perforated screen.

2. THE ENERGY EQUATION IN FLOW AT INFINITESIMAL MACH NUMBER

2.1 Rigid body vibrating in incompressible flow

Equations describing the damping of structural vibrations by vorticity production are easily established in the simplest possible case of a *rigid* body in an incompressible fluid. Consider a rigid body with surface S immersed in incompressible fluid of infinite extent and uniform mean density ρ_o and shear viscosity η. Let the body execute *translational* oscillations at velocity $\mathbf{u}^o$ (whose mean value is assumed to vanish) with respect to a fixed coordinate system (x_1, x_2, x_3), and let V denote the fluid region bounded internally by S and externally by a large control surface Σ (Figure 1). The fluid at large distances from the body is in steady motion at uniform velocity U^o. The velocity $\mathbf{v}$ at any point in the fluid can then be cast in the form

$$\mathbf{v} = \mathbf{U} + \mathbf{u} + \mathbf{v}_\omega \tag{1}$$

where $\mathbf{U}$ and $\mathbf{u}$ are the *irrotational* velocities due to the steady mean flow and the translational oscillations of the body that would exist if the fluid were ideal, and $\mathbf{v}_\omega$ is the additional velocity required to satisfy the no-slip condition on S and to account for the velocity induced by vorticity in the flow. This vorticity includes "gusts" convected in the incident stream, and that produced by vortex shedding from the body. The velocities can be defined more precisely as follows. Let ϕ_i^* denote the velocity potential of the flow that would be produced in an ideal fluid by translational motion of the body at unit speed in the i-direction. Then

$$\left.\begin{aligned} \mathbf{U} &= U_j^o \nabla X_j, \quad \mathbf{u} = u_j^o \nabla \phi_j^*, \\ X_j &= x_j - \phi_j^*, \end{aligned}\right\} \tag{2}$$

where $\mathbf{U}\cdot\mathbf{n} = 0$, $\mathbf{u}\cdot\mathbf{n} = \mathbf{u}^o\cdot\mathbf{n}$ on S, and $\mathbf{n}$ is the unit normal on S directed into the fluid (see Figure 1). The remaining velocity $\mathbf{v}_\omega$ is determined in terms of the vorticity ω by

$$\left.\begin{aligned} \mathbf{U} + \mathbf{u} + \mathbf{v}_\omega &= \mathbf{u}^o, \quad \mathbf{v}_\omega\cdot\mathbf{n} = 0 \text{ on S}, \\ \operatorname{curl}\mathbf{v}_\omega &= \omega \text{ in V}. \end{aligned}\right\} \tag{3}$$

At large distances from S, $|\mathbf{v}_\omega| \sim O(1/|\mathbf{x}|^3)$, and this and conditions (3) are sufficient to determine $\mathbf{v}_\omega$ [21].

The kinetic energy of the fluid $\int_V \frac{1}{2}\rho_o(\mathbf{U}+\mathbf{u}+\mathbf{v}_\omega)^2 d^3\mathbf{x}$ can be partitioned (with the assistance of the divergence theorem) in the form

$$\int_V \tfrac{1}{2}\rho_o(\mathbf{U}+\mathbf{v}_\omega)^2 d^3\mathbf{x} - \int_{S+\Sigma} \rho_o u_j^o \phi_j^* (\mathbf{U}+\mathbf{v}_\omega)\cdot d\mathbf{S} + \int_V \tfrac{1}{2}\rho_o \mathbf{u}^2 d^3\mathbf{x}.$$

The surface integral may be discarded. The integration over S vanishes identically because $(\mathbf{U}+\mathbf{v}_\omega)\cdot\mathbf{n} = 0$ on S. On Σ, $\rho_o u_j^o \phi_j^* (\mathbf{U}+\mathbf{v}_\omega) \approx -\rho_o (x_j P_j/|\mathbf{x}|^3)\mathbf{U}^o$, where $P_j = \oint_S X_j \mathbf{u}^o \cdot d\mathbf{S}$ is the *impulse* of the oscillatory motion [21]. The integration over Σ accordingly vanishes when Σ is large and geometrically symmetric; more generally its average value is null, since $\mathbf{u}^o$ has zero mean. The final volume integral is the ("reversible") kinetic energy of the local irrotational motion associated with the added mass of the body; it is equal to $\frac{1}{2}A_{ij} u_i^o u_j^o$, where A_{ij} is the added mass tensor for translational motion [21].

The transfer of energy from the body to the fluid is balanced by an increase in the kinetic energy of the fluid and the dissipation by viscosity, and can be evaluated from the rate of working of the net surface force F. Let $\mathbf{v}_{rel}$ denote fluid velocity relative to the body, i.e.,

$$\mathbf{v}_{rel} = \mathbf{v} - \mathbf{u}^o \equiv \mathbf{U} - u_j^o \nabla X_j + \mathbf{v}_\omega . \tag{4}$$

The net force F exerted on the fluid can be written [22, 23]

$$F_i = A_{ij}\frac{\partial u_j^o}{\partial t} - \rho_o \int_V \omega \wedge \mathbf{v}_{rel} \cdot \nabla X_i \, d^3\mathbf{x} + \eta \int_S \omega \wedge \nabla X_i \cdot d\mathbf{S}, \tag{5}$$

where the volume integral in (5) corresponds to the component of force produced by the normal (pressure) stresses on S, and the surface integral is the net contribution from the skin friction. The rate at which energy is supplied to the fluid is equal to $F_i u_i^o$.

If

$$Q = \tfrac{1}{2}\eta \int_V \left(\frac{\partial v_i}{\partial x_j} + \frac{\partial v_j}{\partial x_i}\right)^2 d^3\mathbf{x} \tag{6}$$

denotes the viscous energy dissipation rate, Q plus the rate of change of the fluid kinetic energy can be equated to $F_i u_i^o$ to yield the energy equation

$$\frac{\partial E}{\partial t} + Q = -\rho_o u_j^o \int_V \omega \wedge \mathbf{v}_{rel} \cdot \nabla X_j \, d^3\mathbf{x} + \eta u_j^o \int_S \omega \wedge \nabla X_j \cdot d\mathbf{S}, \tag{7}$$

where $E = \int_V \frac{1}{2}\rho_o (\mathbf{U}+\mathbf{v}_\omega)^2 d^3\mathbf{x}$ is the kinetic energy of the mean flow and the vortex field. The contributions from the added mass have canceled from both sides of this equation, which therefore expresses the rate of dissipation and production of non-reversible kinetic energy to the rate of working of the surface stresses on S. For a stationary body ($\mathbf{u}^o = \mathbf{0}$) the kinetic energy is absorbed entirely by viscous action in the body of the fluid. There are frequently circumstances, however, in which vortex shedding from a vibrating body becomes highly organized and correlated over large distances on S. Kinetic energy of the flow can then be extracted to drive unstable oscillations of the body [24, 25].

Let us repeat the above analysis in a reference frame in which the fluid is at rest at infinity. The kinetic energy is now

$$\int_V \tfrac{1}{2}\rho_o \mathbf{v}_\omega^2 d^3\mathbf{x} + \int_V \tfrac{1}{2}\rho_o (\mathbf{u}-U_j^o \nabla\phi_j^*)^2 d^3\mathbf{x}.$$

The second integral is the reversible, added mass component of the energy, which is equal to $\frac{1}{2}A_{ij}(u_i^o-U_i^o)(u_j^o-U_j^o)$. The force between the fluid and body is still given by equation (5), but the velocity of translation of the body is equal to $-\mathbf{U}^o+\mathbf{u}^o$, so that the rate of working of the surface force is $F_j(u_j^o-U_j^o)$. Evaluation of this using (5), leads to the following alternative energy equation

$$\frac{\partial E_W}{\partial t} + Q = -\rho_o u_j^o \int_V \omega \wedge \mathbf{v}_{rel} \cdot \nabla X_j \, d^3\mathbf{x} + \eta u_j^o \int_S \omega \wedge \nabla X_j \cdot d\mathbf{S}$$

$$+ \rho_o \int_V \omega \wedge \mathbf{v}_{rel} \cdot \mathbf{U} d^3\mathbf{x} - \eta U_j^o \int_S \omega \wedge \nabla X_j \cdot d\mathbf{S}, \tag{8}$$

where $E_W = \int_V \frac{1}{2}\rho_o \mathbf{v}_\omega^2 d^3\mathbf{x}$ is the kinetic energy of the vortex field alone (hereafter referred to as the "vortex kinetic energy"). Equations (7) and (8) correspond to alternative views of the motion. If the body does not vibrate ($\mathbf{u}^o = \mathbf{0}$), $E + \int^t Q dt$ is constant, and mean flow kinetic energy is transformed into vortex energy and thence dissipated by viscosity.

By subtracting equations (7) and (8), the variable mean "flow energy" $E_S = E - E_W$ is found to satisfy

$$\frac{\partial E_S}{\partial t} = -\rho_o \int_V \omega \wedge \mathbf{v}_{rel} \bullet \mathbf{U} d^3\mathbf{x} + \eta U_j^o \int_S \omega \wedge \nabla X_j \bullet d\mathbf{S}, \tag{9a}$$

$$\equiv F_i U_i^o . \tag{9b}$$

Since the component of -F in the direction of the uniform mean flow U^o is the *drag* experienced by the body, equation (9) equates the rate of change of the mean flow kinetic energy to minus the rate of working of the drag force. For a body at rest in a uniform stream, the kinetic energy lost by the mean flow in this way is transformed into vortical energy and dissipated by viscosity. For a vibrating body the drag force can be *negative*; the body experiences a force opposite to the mean flow direction and proceeds to "swim" against the stream. The energy transferred to the fluid goes into the wake and into accelerating the mean flow [26].

2.2 An arbitrary elastic body in low Mach number compressible flow

In a compressible fluid there can be a transfer of energy from structural motions into both *sound* and the kinetic energy of the flow. This can be important if sound waves are incident on the body, or when it is necessary to consider the production of aerodynamic sound by surface motions and vorticity. We shall consider low Mach number motions and write the velocity in the form

$$\mathbf{v} = \mathbf{U} + \mathbf{u} + \mathbf{v}_\omega + \nabla\varphi, \text{ where } \mathbf{n}\bullet\mathbf{u} = \mathbf{n}\bullet\mathbf{u}^o, \ \mathbf{n}\bullet\nabla\varphi = 0 \text{ on } S. \tag{10}$$

$\mathbf{U}$, $\mathbf{u}$ and $\mathbf{v}_\omega$ are defined as before, on the assumption that the motion is *incompressible*, and the velocity potential φ is taken to account for the whole effect of compressibility. For an elastic body the surface velocity $\mathbf{u}^o$ will generally vary with position on S. In a nonuniform mean flow, the velocity field $\mathbf{U}$ can be assumed to be incompressible when $M^2 \ll 1$, where $M = U^o/c_o$ is the free stream Mach number, c_o being the speed of sound (which can also be regarded as uniform throughout the fluid when $M^2 \ll 1$).

An equation describing the production of the kinetic energy $E = \int_V \frac{1}{2}\rho_o (\mathbf{U}+\mathbf{v}_\omega)^2 d^3\mathbf{x}$ of the mean flow and vorticity can be derived from the momentum equation taken in the form

$$\frac{\partial}{\partial t}\rho_o (\mathbf{U}+\mathbf{v}_\omega) + \nabla\left[p + \tfrac{1}{2}\rho_o v^2 + \rho_o \frac{\partial \psi}{\partial t} + \rho_o \frac{\partial \varphi}{\partial t}\right] = -\rho_o \boldsymbol{\omega}\wedge\mathbf{v} - \eta \mathrm{curl}\boldsymbol{\omega}\ , \qquad (11)$$

where (for $M^2 \ll 1$) the mean density ρ_o is constant, and ψ denotes the velocity potential of incompressible flow produced by oscillatory motion of the body in an ideal fluid (so that $\mathbf{u} = \nabla\psi$). Dissipation terms proportional to ηdivv and those associated with the bulk viscosity of the fluid have been neglected.

The scalar product of equation (11) with $\mathbf{U}+\mathbf{v}_\omega$ can be written

$$\frac{\partial}{\partial t}\left[\tfrac{1}{2}\rho_o (\mathbf{U}+\mathbf{v}_\omega)^2\right] + \mathrm{div}\left[(\mathbf{U}+\mathbf{v}_\omega)\left[p + \tfrac{1}{2}\rho_o v^2 + \rho_o \frac{\partial \psi}{\partial t} + \rho_o \frac{\partial \varphi}{\partial t}\right]\right] = \rho_o \boldsymbol{\omega}\wedge\mathbf{v}\bullet(\nabla\psi+\nabla\varphi)$$

$$- \eta(\mathbf{U}+\mathbf{v}_\omega)\bullet\mathrm{curl}\boldsymbol{\omega}. \qquad (12)$$

The argument of the divergence on the left hand side may be interpreted as the flux of the kinetic energy of the mean flow and vorticity when convection by sound and unsteady surface motions is neglected. In irrotational regions it reduces exactly to the energy flux vector $-\rho_o(\mathbf{U}+\mathbf{v}_\omega)\partial\Phi/\partial t$, where Φ is the velocity potential with contributions from unsteady surface motion and sound excluded [27].

The rate of production of mean flow and vortex kinetic energy is obtained by integrating equation (12) over the volume V. The motion of the surface S of the body is accounted for by recalling that

$$\int_V \frac{\partial}{\partial t}\left[\tfrac{1}{2}\rho_o (\mathbf{U}+\mathbf{v}_\omega)^2\right] d^3\mathbf{x} = \frac{\partial}{\partial t}\int_V \tfrac{1}{2}\rho_o (\mathbf{U}+\mathbf{v}_\omega)^2 d^3\mathbf{x} + \int_S \tfrac{1}{2}\rho_o (\mathbf{U}+\mathbf{v}_\omega)^2 \mathbf{u}^o \bullet d\mathbf{S}$$

If Q is the viscous dissipation calculated as for an incompressible fluid (as in (6) but with v defined by (10)), equation (12) then yields

$$\frac{\partial E}{\partial t} + Q = \rho_o \int_V \boldsymbol{\omega}\wedge(\mathbf{U}+\mathbf{v}_\omega)\bullet(\nabla\psi + \nabla\varphi) d^3\mathbf{x} - \tfrac{1}{2}\rho_o \int_S (\mathbf{U}+\mathbf{v}_\omega)^2 \mathbf{u}^o \bullet d\mathbf{S}$$

$$+ \eta\int_S \left[\boldsymbol{\omega}\wedge(\mathbf{U}+\mathbf{v}_\omega) - 2(\mathbf{u}^o\bullet\nabla)\mathbf{v}\right]\bullet d\mathbf{S}. \qquad (13)$$

When the viscous term on the right hand side of this formula is discarded, and the surface is at rest ($\mathbf{u}^o = 0$), this equation reduces to one given previously in [7, 12]. However, for a moving surface the second, surface integral on the right hand side of (13) was mistakenly omitted from the corresponding equation (2.5) of [12].

For a rigid body $\mathbf{u}^o$ is constant on S, $\psi = u_j^o \phi_j^*$, and the identity

$$\partial/\partial x_j (\tfrac{1}{2} v^2) = \partial/\partial x_i (v_i v_j) - (\omega \wedge v)_j, \quad v = U + v_\omega \quad (\text{div } v \equiv 0)$$

can be used to show that

$$\tfrac{1}{2}\rho_o \int_S (U+v_\omega)^2 u^o \cdot dS = \rho_o u_j^o \int_V \omega \wedge (U+v_\omega) \cdot \nabla x_j \, d^3x.$$

Thus, when small dissipative terms of order $\eta \text{div } \mathbf{v}$ are again discarded, so that $\oint_S (u^o \cdot \nabla) v \cdot dS \equiv 0$, (13) becomes

$$\frac{\partial E}{\partial t} + Q = -\rho_o u_j^o \int_V \omega \wedge v_{rel} \cdot \nabla X_j \, d^3x + \eta u_j^o \int_S \omega \wedge \nabla X_j \cdot dS$$

$$+ \rho_o \int_V \omega \wedge v_{rel} \cdot \nabla \varphi \, d^3x - \eta \int_S \omega \wedge \nabla \varphi \cdot dS, \tag{14}$$

where

$$v_{rel} = v - u^o \equiv U - u_j^o \nabla X_j + v_\omega + \nabla \varphi. \tag{15}$$

Equation (14) is the generalization to low Mach number compressible flow of equation (7).

The corresponding equations for the vortex kinetic energy E_W is obtained by taking the scalar product of (11) with v_ω. This gives

$$\frac{\partial E_W}{\partial t} + Q = \rho_o \int_V \omega \wedge v_\omega \cdot \{U + \nabla\psi + \nabla\varphi\} d^3x - \tfrac{1}{2}\rho_o \int_S v_\omega^2 u^o \cdot dS$$

$$+ \eta \int_S \left(\omega \wedge v_\omega - 2(u^o \cdot \nabla) v\right) \cdot dS. \tag{16}$$

For a rigid body this simplifies to

$$\frac{\partial E_W}{\partial t} + Q = -\rho_o u_j^o \int_V \omega\wedge\mathbf{v}_{rel}\bullet\nabla X_j\, d^3\mathbf{x} + \eta u_j^o \int_S \omega\wedge\nabla X_j \bullet d\mathbf{S}$$

$$+ \rho_o U_j^o \int_V \omega\wedge\mathbf{v}_{rel}\bullet\nabla X_j\, d^3\mathbf{x} - \eta U_j^o \int_S \omega\wedge\nabla X_j \bullet d\mathbf{S}$$

$$+ \rho_o \int_V \omega\wedge\mathbf{v}_{rel}\bullet\nabla\varphi d^3\mathbf{x} - \eta \int_S \omega\wedge\nabla\varphi\bullet d\mathbf{S}. \qquad (17)$$

When this is subtracted from (14), the rate of production of mean stream kinetic energy $E_S = E - E_W$ is found to be given by (9a), with $\mathbf{v}_{rel}$ defined as in (15).

A particular form of the rigid body formulae (14) and (17) arises when S is *acoustically compact*, i.e., when the characteristic wavelength λ of sound waves involved in the motion is much larger than the typical body dimension ℓ, say. The generation of sound by the unsteady flow near the body can then usually be neglected, and the principal contribution to the compressible velocity potential φ is from sound waves incident from remote sources. In a first approximation (correct to the neglect of terms $\sim O\{(\ell/\lambda)^2\}$) the behavior of φ near S is given by

$$\varphi(\mathbf{x},t) \approx \varphi(\mathbf{x}_o,t) + X_j\,\partial\varphi(\mathbf{x}_o,t)/\partial x_j,$$

where $\mathbf{x}_o$ may be taken as the center of volume of S. Equations (14), (15) and (17) then imply that the production of kinetic energy proceeds as in an incompressible fluid provided the vibrational velocity $\mathbf{u}^o$ of the body is increased by $-\partial\varphi(\mathbf{x}_o,t)/\partial x_j$, i.e., by an amount which is equal and opposite to the acoustic particle velocity of the sound incident on S.

2.3 Small amplitude vibrations of elastic plates in parallel mean flow

The surface velocity $\mathbf{u}^o$ cannot normally be assumed to be independent of position on S when the body is elastic, and it is not then possible to reduce the energy equation (13) to the simplified form (14). An important special case, however, occurs when all fluctuating quantities are small and the viscous term on the right of (13) may be discarded. The surface integral involving the shear viscosity η is negligible when the Reynolds number $U^o\ell\rho_o/\eta \gg 1$, where ℓ is the length scale of the unsteady motions near S. In making this approximation observe that, although viscosity is ultimately responsible for the diffusion of vorticity into flow, this fact has no bearing

on the relative magnitudes of the integrals in (13).

Consider interactions and vorticity production in the neighborhood of one or more thin elastic plates in high Reynolds number parallel mean flow at velocity $\mathbf{U}^\circ$. When all fluctuating quantities, including the vorticity $\boldsymbol{\omega}$, can be regarded as small perturbations, the leading order approximation to the terms on the right of (13) (omitting contributions of zero mean) is

$$\rho_o \int_V \boldsymbol{\omega} \wedge \mathbf{U}^\circ \bullet (\nabla\psi + \nabla\varphi) d^3\mathbf{x} - \rho_o \int_S (\mathbf{U}^\circ \bullet \mathbf{v}_\omega) \nabla\psi \bullet d\mathbf{S}.$$

These integrals can be combined by introducing the *bound* vorticity $\bar{\boldsymbol{\omega}}$, say, on the surfaces of the plates. This is done when there is only one plate as follows. Let the equation $\zeta(\mathbf{x},t) = 0$ define a surface in the fluid that just encloses the plate, where $\zeta > 0$ in the exterior fluid. Define the extended vorticity $\boldsymbol{\Omega}$ by

$$\begin{aligned} \boldsymbol{\Omega} \equiv \operatorname{curl}\{H(\zeta)\mathbf{v}_\omega\} &= H(\zeta)\boldsymbol{\omega} + \nabla H(\zeta) \wedge \mathbf{v}_\omega \\ &= H(\zeta)\boldsymbol{\omega} + \mathbf{n} \wedge \mathbf{v}_\omega \delta(x_n), \end{aligned} \tag{18}$$

where $H(x)$ is the Heaviside step function, and x_n is a local coordinate which vanishes on the plate and is orientated in the direction of the unit normal $\mathbf{n}$. The bound vorticity $\bar{\boldsymbol{\omega}} \equiv \mathbf{n} \wedge \mathbf{v}_\omega \delta(x_n)$. Recalling that $\mathbf{n} \bullet \nabla\varphi = 0$ on S, (13) is now reduced to

$$\frac{\partial E}{\partial t} + Q = \rho_o \int \boldsymbol{\Omega} \wedge \mathbf{U}^\circ \bullet (\nabla\psi + \nabla\varphi) d^3\mathbf{x}, \tag{19}$$

where the integration is taken over the whole of space. It is evident that this result is applicable to situations involving multiple parallel plates.

Similarly, since $\mathbf{U}^\circ$ is constant and $\mathbf{n} \bullet \mathbf{v}_\omega = 0$ on S, the vortex and mean stream energy equations become, in the same approximation,

$$\frac{\partial E_W}{\partial t} + Q = \rho_o \int_V \boldsymbol{\omega} \wedge \mathbf{v}_\omega \bullet \mathbf{U}^\circ d^3\mathbf{x} \equiv -\rho_o \int \boldsymbol{\Omega} \wedge \mathbf{U}^\circ \bullet \mathbf{v}_\omega d^3\mathbf{x}, \tag{20}$$

$$\frac{\partial E_S}{\partial t} = \rho_o \int \boldsymbol{\Omega} \wedge \mathbf{U}^\circ \bullet (\nabla\psi + \nabla\varphi + \mathbf{v}_\omega) d^3\mathbf{x}. \tag{21}$$

Equations (19) - (21) remain valid to second order for stationary surfaces. In that case, however, $\nabla\psi \equiv 0$, and the integrations need be taken only over the free field vorticity.

3. APPLICATIONS TO RIGID AND ELASTIC PLATES

3.1 The rigid airfoil

A rigid, two dimensional, flat airfoil of chord 2a is set at zero angle of attack to an incompressible, high Reynolds number mean flow of velocity U in the x_1-direction. In the undisturbed state the airfoil occupies the region $|x_1| < a$, $x_2 = 0$, of the rectangular coordinate system (x_1, x_2, x_3). The airfoil executes small amplitude time-harmonic, translational oscillations at velocity $\mathbf{u}^o = (0, u_2, 0)e^{-i\omega t}$ in the x_2-direction (where the real part is to be taken, and the harmonic time factor is henceforth suppressed), as indicated in Figure 2(a). Viscous forces are neglected except at the trailing edge, where vorticity is shed into a wake of infinitesimal thickness, in accordance with the Kutta condition of thin airfoil theory. Then $\boldsymbol{\omega} = (0, 0, \omega_3)$, where [28]

$$\omega_3 = \gamma_o H(x_1 - a)\delta(x_2)e^{i\kappa x_1}, \qquad \gamma_o = 4iu_2/\{H_0^{(1)}(\kappa a) + iH_1^{(1)}(\kappa a)\}, \tag{22}$$

$H_0^{(1)}$, $H_1^{(1)}$ are Hankel functions [29], and $\kappa = \omega/U$ is the wavenumber of the wake vorticity. In high Reynolds number flow the power $\Pi = \partial E/\partial t + Q$ fed into the mean flow and wake *per unit span* of the airfoil is given by the first integral in (7) with $j = 2$ and the integration over x_3 omitted. To evaluate the integral correct to second order in the amplitude u_2 of the oscillations, we can set $\mathbf{v}_{rel} = (U, 0, 0)$ and

$$X_2 = \mathrm{Re}\{-i\sqrt{z^2 - a^2}\}, \quad z = x_1 + ix_2 \tag{23}$$

[21]. After taking the real parts of all fluctuating quantities and averaging over the period $2\pi/\omega$ of the motion, we find

$$\Pi = \pi C_R \rho_o a U |u_2|^2, \tag{24}$$

where $C_R \equiv C_R(\kappa a)$ is the real part of the *Theodorsen* function

$$C(x) = iH_1^{(1)}(x)/\{H_0^{(1)}(x) + iH_1^{(1)}(x)\}. \tag{25}$$

C_R is positive for all real frequencies, so that the motion is always stable inasmuch as energy is always drawn from the oscillating body and ceded to the fluid [24].

A similar calculation shows that the power delivered to the wake per unit span is

$$\Pi_W = \frac{2\rho_o aU|u_2|^2}{(\kappa a)|H_0^{(1)}(\kappa a)+iH_1^{(1)}(\kappa a)|^2} \ . \tag{26}$$

The difference $\Pi_S = \Pi - \Pi_W$ represents the power absorbed directly by the mean stream. This is positive and arises from the working against the mean stream of the suction force at the leading edge (which is not balanced by an equal and opposite force at the trailing edge because of the application of the Kutta condition). The airfoil accordingly has a tendency to "swim" against the mean stream under the action of a propulsive force equal to Π_S/U (see [26] and the references cited therein for an extensive discussion of problems of this type relating to aquatic propulsion, etc).

When the characteristic wavelength of the vortex wake is much smaller than the airfoil chord, i.e., when the *reduced frequency* $\kappa a \to \infty$, it follows by use of the asymptotic formulae for the Hankel functions in (25) and (26) that,

$$\Pi_W = \Pi_S = \tfrac{1}{4}\pi\rho_o aU|u_2|^2 \ \text{ as } \kappa a \to \infty, \tag{27}$$

so that the power absorbed by the flow is ultimately shared equally by the mean flow and wake. At low frequencies, however, $\Pi_W \sim O(\kappa a)\Pi$, and the energy flows primarily into the mean stream.

A similar calculation can be performed for the case of a sound wave incident on the airfoil in mean flow of Mach number $M = U/c_o \ll 1$, when the chord is acoustically *compact* (wavelength of the sound $\gg$ airfoil chord). In these circumstances it is permissible to neglect the convection of sound by the flow, and we may consider an incident, time-harmonic plane acoustic wave whose pressure is given by

$$p = p_I e^{i\kappa_o(x_1\cos\theta + x_2\sin\theta)}, \tag{28}$$

where p_I is constant, $\kappa_o = \omega/c_o$ is the acoustic wavenumber and θ is the propagation direction measured from the positive x_1-axis (see Figure 2(b)).

Assume the airfoil to be fixed. For a compact airfoil $\kappa_o a$ is small, and the velocity potential of the acoustic field near the airfoil can be approximated by

$$\varphi = -\frac{ip_I}{\rho_o \omega}\left(1 + i\kappa_o x_1 \cos\theta + i\kappa_o X_2 \sin\theta\right), \tag{29}$$

where X_2 is given by (23). The wake vorticity is again given by equations (22) with u_2 replaced by $-p_I \sin\theta/\rho_o c_o$. Using these results in (14) and (17) (in which only the volume integrals involving φ are retained), we find, correct to second order,

$$\frac{\Pi}{\Pi_I} = \pi C_R(\kappa a) M \sin\theta \ , \qquad \frac{\Pi_W}{\Pi_I} = \frac{2M\sin\theta}{(\kappa a)\left|H_0^{(1)}(\kappa a) + iH_1^{(1)}(\kappa a)\right|^2} \ , \tag{30}$$

where $\Pi_I = |p_I|^2 a \sin\theta/\rho_o c_o$ is the acoustic power incident on unit span of the plate. At high reduced frequencies the absorbed sound power is shared equally between the wake and mean stream, but as $\kappa a \to 0$, the wake power becomes negligible relative to that ceded to the mean stream. As in the case of the vibrating plate, the sound induces a leading edge suction force and a tendency for the plate to be propelled against the stream.

The interaction of sound with the trailing edge of a stationary rigid airfoil whose chord is much larger than the acoustic wavelength ($\kappa_o a \gg 1$) can also be investigated in this way [12, 30]. When the airfoil is modeled by a semi-infinite rigid plate in flow of infinitesimal mean flow Mach number, and the incident wave is defined as in (28), the acoustic power dissipated per unit span of the trailing edge is [12]

$$\Pi = \frac{2|p_I|^2 M}{\rho_o \omega}\cos^2\left(\frac{\theta}{2}\right), \qquad M \ll 1. \tag{31}$$

In this limit it is again found that $\Pi_W = \Pi_S$, i.e., that the dissipated acoustic power is shared equally by the wake and mean flow, but this relation is not maintained at higher Mach numbers (see [12] for details).

3.2 Damping of bending waves on a large plate

Vortex shedding from the trailing edge of a thin elastic plate is probably the simplest model problem for studying the exchanges of energy which occur when a vibrating *elastic* structure interacts with mean flow. Small amplitude flexural motions of the plate are governed by the linearized bending wave equation [20], and the canonical structural vibration problem is that in which a bending wave impinges normally on the edge. Part of the incident wave energy is reflected, part is transformed into kinetic energy of the mean flow and wake and, for a compressible fluid, part is scattered into sound. A linearized analysis of these events is discussed in [17] for a plate that is immersed in a mean flow of infinitesimal Mach number flow.

Let a thin, semi-infinite elastic plate of bending stiffness B and mass m per unit area occupy the half-plane $x_1 < 0$, $x_2 = 0$, in fluid in uniform motion at speed U (where $M = U/c_o \ll 1$) in the positive x_1-direction (Figure 3). Time-harmonic flexural displacements $\zeta(x_1)e^{-i\omega t}$ $(\omega > 0)$ of the plate (measured in the x_2-direction) satisfy the bending wave equation [20],

$$\{B\partial^4/\partial x_1^4 - m\omega^2\}\zeta = p(x_1,-0) - p(x_1,+0), \quad x_1 < 0, \tag{32}$$

where $p(x_1,x_2)$ denotes pressure, and the terms on the right hand side give the net normal stress on the plate (here and henceforth the harmonic time factor $e^{-i\omega t}$ is suppressed). The displacement and the pressure are also related by the x_2-component of the fluid momentum equation $\rho_o\{\omega+iU\partial/\partial x_1\}^2\zeta = \partial p/\partial x_2$, $x_2 = \pm 0$.

A steady state bending wave $\zeta = \zeta_o e^{i\kappa_+ x_1}$ propagating towards the edge has subsonic phase velocity ω/κ_+ $(< c_o)$ and the structural motion is accompanied by a traveling pressure field that decays exponentially with distance from the plate

$$p = -\mathrm{sgn}(x_2)\rho_o\{(\omega-U\kappa_+)^2/\sqrt{\kappa_+^2-\kappa_o^2}\}\zeta_o e^{i\kappa_+ x_1 - \sqrt{\kappa_+^2-\kappa_o^2}|x_2|}. \tag{33}$$

provided the Mach number is sufficiently small that convection of sound by the flow can be neglected

It follows from (32) that κ_+ is the positive real root of the dispersion equation

$$D(k,\omega) \equiv Bk^4 - m\omega^2 - 2\rho_o(\omega - Uk)^2/\sqrt{k^2 - \kappa_o^2} = 0. \tag{34}$$

A reflected bending wave $\zeta = R\zeta_o e^{-i\kappa_- x_1}$ emerges from the localized, complex fluid-structure interaction at the edge and propagates without attenuation to $x_1 = -\infty$. The reflection coefficient R is a function of frequency, Mach number M, and the mechanical constraints imposed on the motion of the plate at the edge; κ_- is the positive root of (34) when the sign of U is reversed. In addition, sound is generated, and vorticity is shed into a wake extending downstream from the edge. The strength of the shed vorticity can be estimated by application of the unsteady Kutta condition. The analysis of this problem in [17] is based on linear perturbation theory, in which the wake is treated as a vortex sheet.

The flexural wave power Π_I, say, incident on unit length of the edge (including that conveyed in the evanescent fluid motions on both sides of the plate) can be calculated from the formula $\Pi_I = \frac{1}{4}\omega|\zeta_o|^2 \partial D/\partial k$, where the derivative is evaluated at $k = \kappa_+$ [31]. The total flexural wave power dissipated per unit length of edge consists of a portion Π_A scattered into sound and a component Π_K which increases the kinetic energy of the mean flow and wake. The total dissipated power is therefore given by

$$\Pi_A + \Pi_K = \tfrac{1}{4}\omega|\zeta_o|^2\left[\left(\frac{\partial D}{\partial k}(k,\omega)\right)_{k=\kappa_+} - |R|^2\left(\frac{\partial D}{\partial k}(k,\omega)\right)_{k=\kappa_-}\right]. \tag{35}$$

Using formulae given in [17], the fractional power dissipated at the edge, $\Delta = \{\Pi_A + \Pi_K\}/\Pi_I$, has been plotted in Figure 4(a) for a steel plate in water for several values of the Mach number when the edge of the plate is "free" ($\partial^2\zeta/\partial x_1^2 = \partial^3\zeta/\partial x_1^3 = 0$ at $x_1 = -0$ [20]). In this figure the frequency is normalized by the *coincidence frequency* $\omega_c = c_o^2(m/B)^{1/2}$, above which the *in vacuo* bending wave phase speed exceeds c_o.

For M = 0 all of the dissipation of bending wave power can be attributed to sound radiated from the edge. When $M \neq 0$ there is a significant increase in the bending wave power loss at low frequencies caused by the transfer of energy to the mean flow and wake, with negligible changes in the radiated sound power (at least for $M \ll 1$). This is clear from Figure 4(b), which

compares the total power loss Δ for a steel plate in water (solid curve) with the acoustic power (dashed curve) when M = 0.01. Inspection of Figures 4(a) and (b) confirms that the sound power is hardly influenced by the flow. However, at high frequencies dissipation is caused entirely by the radiation of sound; this is because, as $\omega \to \omega_c$, bending wave energy is contained principally in the evanescent motions on either side of the plate, and propagates with negligible plate motion at a velocity which is only slightly less than the speed of sound.

The dotted curve in Figure 4(b) shows the fraction of the dissipated energy which appears as vortex kinetic energy. This indicates that, over the range of frequencies within which acoustic dissipation is negligible, the dissipated energy is shared equally between the mean flow (E_S) and the vortex motions (E_W); this is not generally the case, but depends on the nature of mechanical constraints at the edge. The momentum of the mean flow increases at a rate equal to Π_S/U, so that the plate experiences an equal and opposite thrust and a tendency to swim against the mean stream.

4. DAMPING OF FLEXURAL WAVES ON A GRAZING FLOW PERFORATED SCREEN

Perforated screens have been used to attenuate sound in low Mach number flows. The flow is usually turbulent, and typically the sound is generated by the interaction of the mean flow and turbulence with solid bodies, such as the cross-tubes in a flow-through heat exchanger. Vér [10, 13] has described the use of grazing flow perforated plates in the tube bank cavity of a nuclear reactor heat exchanger that successfully eliminated acoustic resonances which had not responded to more conventional means of attenuation. Acoustic attenuation by this means is useful only when the dominant frequencies are small. At higher frequencies boundary layer turbulence (which is enhanced by flow over the perforations) can interact strongly with the apertures to produce intense sound (and vibration) [32]. Analytical studies [33 - 35] suggest that boundary layer generated noise is increased by several orders of magnitude by the presence of the apertures.

4.1 Modified bending wave equation

The attenuation of low frequency sound and structural vibrations by a grazing flow perforated plate can be estimated by a simple extension of the method developed in [18] for a *bias flow* screen. A generalized form of the bending wave equation (32) was derived in [18] for a plate with circular apertures when the length scale of the sound and plate motion is large compared to both the aperture radius R and the distance between neighboring apertures. For an infinite, thin elastic plate, with N apertures per unit area, and occupying the plane $x_2 = 0$ in the undisturbed state, long wavelength, small amplitude motions (proportional to $e^{-i\omega t}$) are governed by the equation

$$\left(\left[1 - \frac{2\alpha\sigma}{(1-\sigma)}\right]B\nabla_2^4 - m\omega^2\right)\zeta + \left(1 + 2NRK_R\left[1 - \frac{1}{2R\rho_o\omega^2}\left(\left[1 - \frac{2\alpha\sigma}{(1-\sigma)}\right]B\nabla_2^4 - m\omega^2\right)\right]\right)[p] = 0. \tag{36}$$

where $\alpha = N\pi R^2$ is the fractional open area, σ is Poisson's ratio for the plate, $\nabla_2^4 \equiv (\partial^2/\partial x_1^2 + \partial^2/\partial x_3^2)^2$, and K_R is the *Rayleigh conductivity*.

The conductivity determines the volume flux Q, say, through an aperture caused by a long wavelength perturbation $[p] = p(x_1,+0,x_3) - p(x_1,-0,x_3)$ in the pressure difference across the plate according to the relation

$$Q = K_R[p]/i\rho_o\omega. \tag{37}$$

This definition is a generalization of that originally proposed by Rayleigh [36, 37] in terms of the electrical analogue $Q = K_R[\Phi]$, where Φ is the perturbation *velocity potential*, and the motion is imagined to be driven by the potential difference $[\Phi]$ across the aperture. In more general situations, however, where the flow in an aperture can contain vorticity, local variations in the velocity potential need not be continuous through the aperture and Rayleigh's definition must be expressed in terms of the pressure (which *is* continuous).

It was argued in [18] that K_R is well approximated by its value for a *rigid* plate provided the length scale of the plate motion is much larger than the aperture radius R. K_R has the dimensions of length and is equal to 2R in a stationary ideal fluid, but becomes complex valued and frequency dependent in the presence of flow, because of the unsteady shedding of vorticity from the aperture edges.

We consider the application of equation (36) to the case in which the low Mach number mean flow is tangential to the plate at uniform speed U in the x_1-direction on both sides (Figure 5), and where the Reynolds number based on aperture radius is large. In the linearized approximation the pressure p and velocity potential Φ are then related by $p = \rho_o(i\omega - U\partial/\partial x_1)\Phi$. The conductivity is a function of the Strouhal number $S \equiv \omega R/U$, and can be set in the form

$$K_R = 2R\{\Gamma(S) - i\Delta(S)\}. \tag{38}$$

The real and imaginary parts Γ and Δ are not known in analytic form, but have been computed by Scott [38] for high Reynolds number flow. Scott applied linear perturbation theory and the unsteady Kutta condition to determine the strength of vorticity shed from the upstream semi-circular arc of the aperture as a result of the unsteady aperture flow; the vorticity was assumed to occupy a vortex sheet in the plane of the aperture and to convect downstream at the

mean velocity U.

The calculated dependencies of Γ and Δ on Strouhal number are depicted in Figure 6. Γ and Δ are approximately periodic (with period $\approx \pi$) when $\omega R/U$ exceeds about 3. The imaginary component Δ governs the damping of aperture motions by vorticity production and acoustic radiation losses. The latter can be neglected when $\kappa_o R$ is small, so that the value of Δ then determines the exchange of perturbation energy with the mean flow; aperture motions are *damped* by vorticity production provided $\Delta > 0$; when $\Delta < 0$, the unsteady motion in the aperture is enhanced at the expense of mean stream kinetic energy. This extraction of energy from the flow is caused by the interaction of shed vorticity with the semi-circular "leading edge" on which it impinges after convecting across the aperture. The aperture motion should *not* be regarded as unstable, however, since the transfer of energy from the mean flow occurs only when an incident disturbance contains a component with frequency within an interval where $\Delta_R < 0$. This means that, in the absence of an incident pressure differential [p] (and on the basis linear theory), large amplitude, unsteady motions within the aperture cannot arise spontaneously as a result of a random fluctuation in the mean flow; mathematically this conclusion follows from the fact that the Rayleigh conductivity $K_R(\omega)$ for this problem can be shown to be a *regular* function of ω in the upper half of the complex frequency plane.

4.2 Attenuation of resonant bending waves

To examine the damping of bending waves consider a time harmonic displacement $\zeta = \zeta_o e^{i(\kappa x_1 - \omega t)}$ $(\omega > 0)$; from (33) we have

$$[p] = -2\rho_o \{(\omega - U\kappa)^2/\sqrt{\kappa^2 - \kappa_o^2}\}\zeta_o e^{i\kappa x_1}.$$

The flexural wave dispersion equation is obtained by substituting these expressions for ζ and [p] into equation (36), which supplies

$$\bar{D}(\kappa,\omega) \equiv \left[1 - \frac{2\alpha\sigma}{(1-\sigma)}\right]B\kappa^4 - m\omega^2$$

$$- \frac{2\rho_o(\omega - U\kappa)^2}{\sqrt{\kappa^2 - \kappa_o^2}}\left(1 + 2NRK_R\left[1 - \frac{1}{2R\rho_o\omega^2}\left(\left[1 - \frac{2\alpha\sigma}{(1-\sigma)}\right]B\kappa^4 - m\omega^2\right)\right]\right) = 0. \qquad (39)$$

When there is no mean flow $K_R \to 2R$, and $\bar{D}(\kappa,\omega)$ has two real zeros of

opposite sign that correspond to undamped flexural waves propagating in the positive and negative x_1-directions. They satisfy $|\kappa| > \kappa_o$, so that $\sqrt{\kappa^2-\kappa_o^2}$ is real and positive. In the presence of flow the bending wavenumber acquires a small imaginary component that accounts for the exchange of wave energy with the flow via vorticity production. The wave power dissipated in propagating a distance δs is equal to $20|\mathrm{Im}\{\kappa\}|\delta s \log_{10}(e)$ dB, and the power absorbed per wavelength of propagation is therefore $40\pi \log_{10}(e)\mathrm{Im}\{\kappa\}/\mathrm{Re}\{\kappa\} \approx 54.6\mathrm{Im}\{\kappa\}/\mathrm{Re}\{\kappa\}$ dB. Figures 7 - 9 illustrate typical predictions of the absorption for a perforated steel plate in water at different fractional open areas α and aperture radii (for R/h = 3 and 6, where h is the thickness of the plate) and mean flow velocities. The solid and dashed curves are respectively for waves propagating in the $\pm x_1$-direction, i.e., with and against the mean stream. The case of a lightly fluid loaded plate is illustrated in Figure 10 (aluminium in air: R/h = 10, U = 10 m/s). The ability of the bending wave motions to force fluid through the apertures is now much reduced, and the maximum losses are correspondingly very much smaller than for a plate in water. Waves propagating against the mean flow are more strongly damped than those propagating in the mean flow direction. Increases in flow velocity or aperture radius reduce the maximum possible attenuation. In all case, waves can experience small *negative* damping when $\omega R/U > 3$.

To assess the significance of these predictions, it should be noted that the largest attenuations usually achieved by conventional means, i.e., by coating a nominally homogeneous plate with one or more layers of an absorptive material, are of the order of 4 dB per wavelength of propagation [19]. The present results are accordingly comparable with the best obtainable by coating, at least for Strouhal numbers in the interval 0.7 - 2. However, conventional coating materials tend to be effective over a much broader range of frequencies.

5. CONCLUSION

Energy is transferred between structural and acoustic vibrations and the kinetic energy of essentially incompressible fluid motions by vorticity production at the surface of a solid. In many instances this can lead to unstable and catastrophic structural motions and the generation of intense acoustic noise, but there exist regimes in which vibrational and/or acoustic modes may be dissipated through the generation of vorticity. This energy transfer mechanism has been discussed for elementary rigid body vibrations of a solid in low Mach number flow, and the effects of structural and acoustic damping have been illustrated by reference to the classical problem of the vibrating airfoil. At low Mach numbers the dissipated energy appears first as an increase in the kinetic energy of the mean flow and wake before being ultimately dissipated by viscosity. Modified versions of these formulae are applicable also to vibration problems involving parallel flat plates in a mean flow, but such problems are usually so complicated that it is generally easier to make direct predictions of the energy distribution from the analytical solution. The simplest problem of this kind involves the generation of vorticity at the trailing edge of a large, vibrating elastic plate in a nominally uniform mean flow. At low Mach numbers energy is dissipated both by the generation of sound and by the conversion of plate energy into kinetic energy of the flow. At low frequencies (well below the coincidence frequency) most of the dissipated energy is ceded to the flow, but as the frequency increases towards coincidence the damping is progressively dominated by acoustic radiation.

The exploitation of vorticity production in the apertures of a perforated elastic plate for vibration damping has been examined for low Mach number, two-sided grazing mean flow. As in the case of the "bias flow" screen discussed in [18], the efficiency with which bending waves are damped increases with the fluid loading. The attenuation experienced by waves on a perforated steel plate in water is significant for aperture Strouhal numbers $S = \omega R/U$ in the range 0.7 - 2, and can exceed that usually obtained when an unperforated plate is heavily coated with damping material.

REFERENCES

1. B. T. Zinn 1970 *Journal of Sound and Vibration* **13**, 347 - 356. A theoretical study of nonlinear damping by Helmholtz resonators.
2. T. H. Melling 1973 *Journal of Sound and Vibration* **29**, 1 - 65. The acoustic impedance of perforates at medium and high sound pressure levels.
3. A. Cummings 1983 *American Institute of Aeronautics and Astronautics Paper 83-0739*. Acoustic nonlinearities and power losses at orifices.
4. P. D. Dean & B. J. Tester 1975 *National Aeronautics and Space Administration Contractor Report CR-134998*. Duct wall impedance control as an advanced concept for acoustic suppression.
5. D. Bechert, U. Michel & E. Pfizenmaier 1977 *American Institute of Aeronautics and Astronautics Paper 77-1278*. Experiments on the transmission of sound through jets.
6. D. W. Bechert 1979 *American Institute of Aeronautics and Astronautics Paper* 79-0575. Sound absorption caused by vorticity shedding, demonstrated with a jet flow.
7. M. S. Howe 1980 *Journal of Sound and Vibration.* **70**, 407 - 411. The dissipation of sound at an edge.
8. M. S. Howe 1979 *Proceedings of the Royal Society of London* **A366**, 205 - 233. On the theory of unsteady high Reynolds number flow through a circular aperture.
9. M. S. Howe 1980 *Proceedings of the Royal Society of London* **A370**, 523 - 544. On the diffraction of sound by a screen with circular apertures in the presence of a low Mach number grazing flow.
10. I. L. Vér 1982 *Perforated baffles prevent flow-induced acoustic resonances in heat exchangers*. Paper presented at 1982 meeting of the Federation of the Acoustical Societies of Europe; Göttingen, September 1982.
11. A. M. Cargill 1982 *Journal of Fluid Mechanics* **121**, 59 - 105. Low frequency sound radiation and generation due to the interaction of unsteady flow with a jet pipe.

12. M. S. Howe 1984 *Institute of Mathematics and its Applications, Journal of Applied Mathematics* **32**, 187 - 209. On the absorption of sound by turbulence and other hydrodynamic flows.

13. I. L. Vér 1990 *Noise Control Engineering Journal* **35** (Nov/Dec issue) pp. 115 - 125. Practical examples of noise and vibration control: case history of consulting projects.

14. I. J. Hughes & A. P. Dowling 1990 *Journal of Fluid Mechanics*. **218**, 299 - 336. The absorption of sound by perforated linings.

15. Y. Fukumoto & M. Takayama 1991 *Physics of Fluids* **A3**, 3080 - 3082. Vorticity production at the edge of a slit by sound waves in the presence of a low Mach number bias flow.

16. A. P. Dowling & I. J. Hughes 1992 *Journal of Sound and Vibration* **156**, 387 - 405. Sound absorption by a screen with a regular array of slits.

17. M. S. Howe 1992 *Journal d'Acoustique* 5, 603 - 620. On the damping of structural vibrations by vortex shedding.

18. M. S. Howe 1994 *European Journal of Applied Mathematics*. (in press). The damping of flexural and acoustic waves by a bias-flow perforated elastic plate.

19. L. L. Beranek & I. L. Vér 1992 *Noise and Vibration Control Engineering* New York: John Wiley.

20. L. Cremer, M. Heckl & E. E. Ungar 1988 *Structure-borne sound* (2nd ed). New York: Springer-Verlag.

21. Batchelor, G. K. 1967 *An introduction to fluid dynamics*. Cambridge University Press.

22. M. S. Howe 1989 *Journal of Fluid Mechanics* **206**, 131 - 153. On unsteady surface forces, and sound produced by the normal chopping of a rectilinear vortex.

23. M. S. Howe 1994 *Quarterly Journal of Mechanics and Applied Mathematics* (in press). On the force and moment exerted on a body in an incompressible fluid, with application to rigid bodies and bubbles at high and low Reynolds numbers.

24. T. Theodorsen 1935 *National Advisory Committee for Aeronautics Report 496*. General theory of aerodynamic instability and the mechanism of flutter.

25. R. D. Blevins 1977 *Flow induced vibration*. New York: Van Nostrand Reinhold.

26. Sir James Lighthill 1975 *Mathematical Biofluiddynamics*. Philadelphia: Society of Industrial and Applied Mathematics.

27. L. D. Landau and E. M. Lifshitz 1987 *Fluid Mechanics* (Second edition). Oxford: Pergamon.

28. Y. C. Fung 1993 *An Introduction to the Theory of Aeroelasticity*. New York: Dover Publications Inc.

29. M. Abramowitz & I. A. Stegun (editors) 1970 *Handbook of Mathematical Functions* (Ninth corrected printing), US Dept. of Commerce, Nat. Bur. Stands. Appl. Math. Ser. No.55.

30. S. W. Rienstra 1981 *Journal of Fluid Mechanics* **108**, 443 - 460. Sound diffraction at a trailing edge.

31. M. S. Howe 1992 *Proceedings of the Royal Society of London* **A436**, 351 - 372. Sound produced by an aerodynamic source adjacent to a partly coated, finite elastic plate.

32. P. A. Nelson 1982 *Journal of Sound and Vibration* **83**, 11 - 26. Noise generated by flow over perforated surfaces.

33. M. S. Howe 1990 *Journal of Sound and Vibration* **139**, 227 - 240. Sound produced by turbulent flow over a perforated inlet.

34. K. L. Chandiramani 1993 *Flow induced vibration and noise of a perforated panel*. Paper presented at American Society of Mechanical Engineers, Winter Annual Meeting, Nov. 28 - Dec. 3, New Orleans.

35. M. S. Howe 1994 *Journal of the Acoustical Society of America* (in press). Influence of mean shear on sound produced by turbulent flow over surface slots.

36. Lord Rayleigh 1870 *Philosophical Transactions of the Royal Society of London* **161**, 77 - 118. On the theory of resonance.

37. Lord Rayleigh 1945 *Theory of Sound*, Vol 2. New York: Dover.

38. M. I. Scott 1994 *The Rayleigh conductivity of a circular aperture in the presence of grazing flow*. M.Sc. thesis, Boston University.

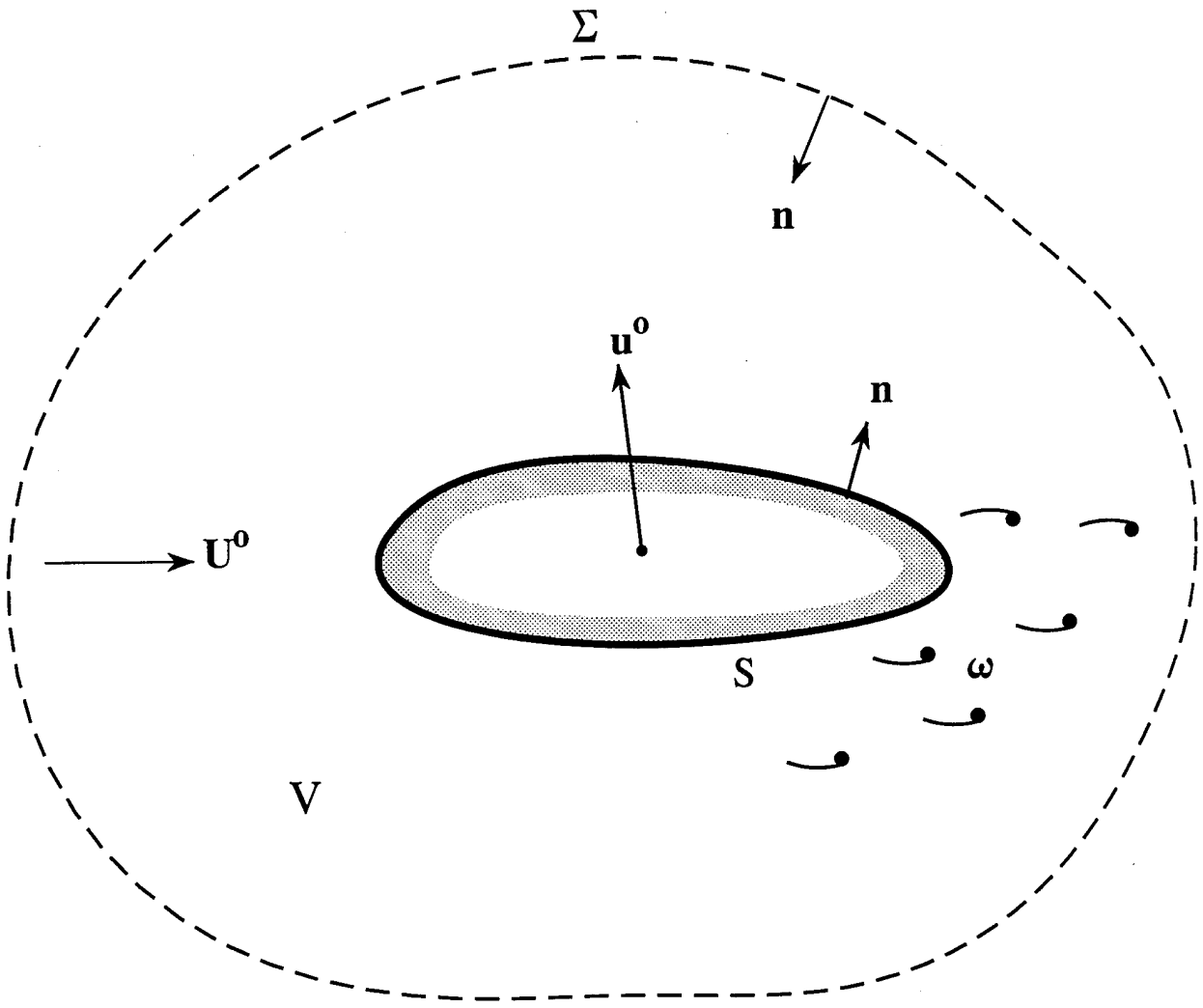

Figure 1. A rigid body in oscillatory motion in an incompressible fluid in uniform mean flow at velocity U^o.

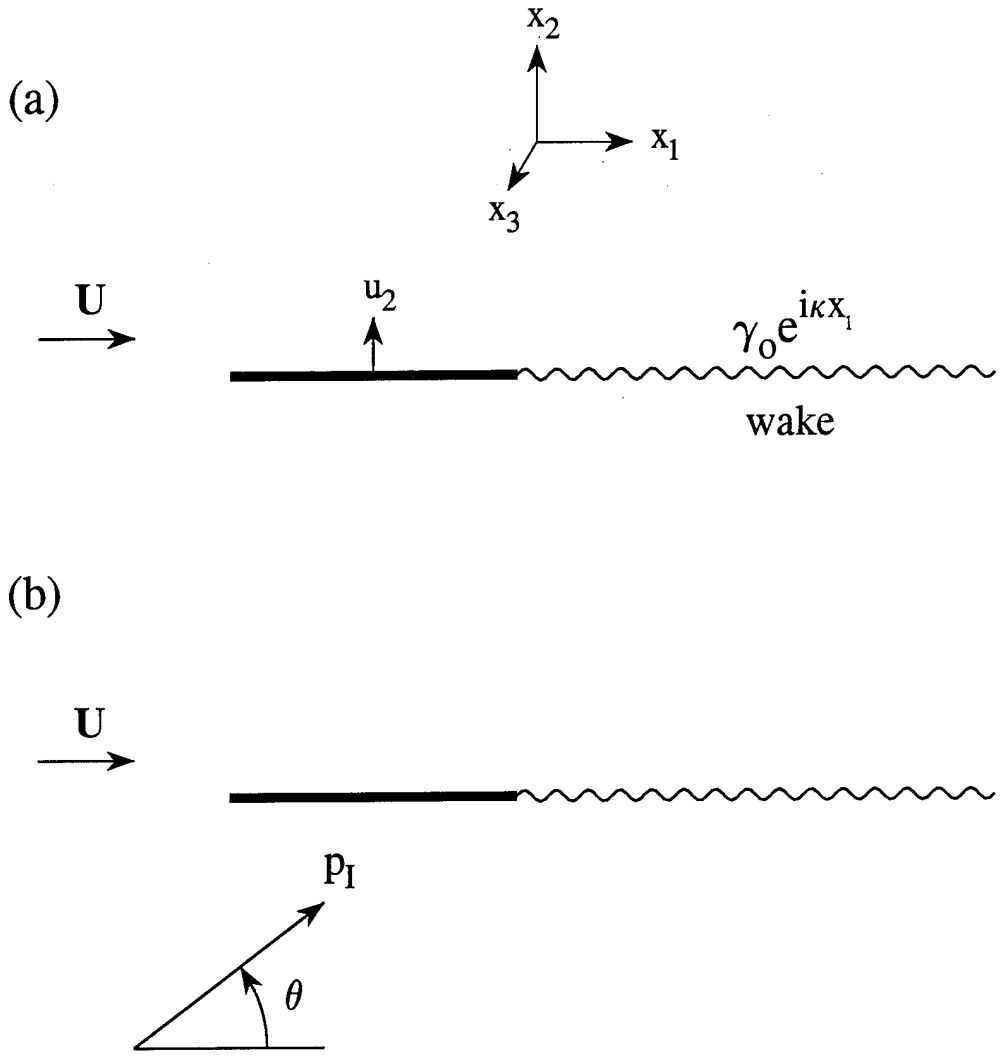

Figure 2. (a) Rigid airfoil vibrating in a mean stream.
(b) Sound incident on a stationary airfoil in a mean stream.

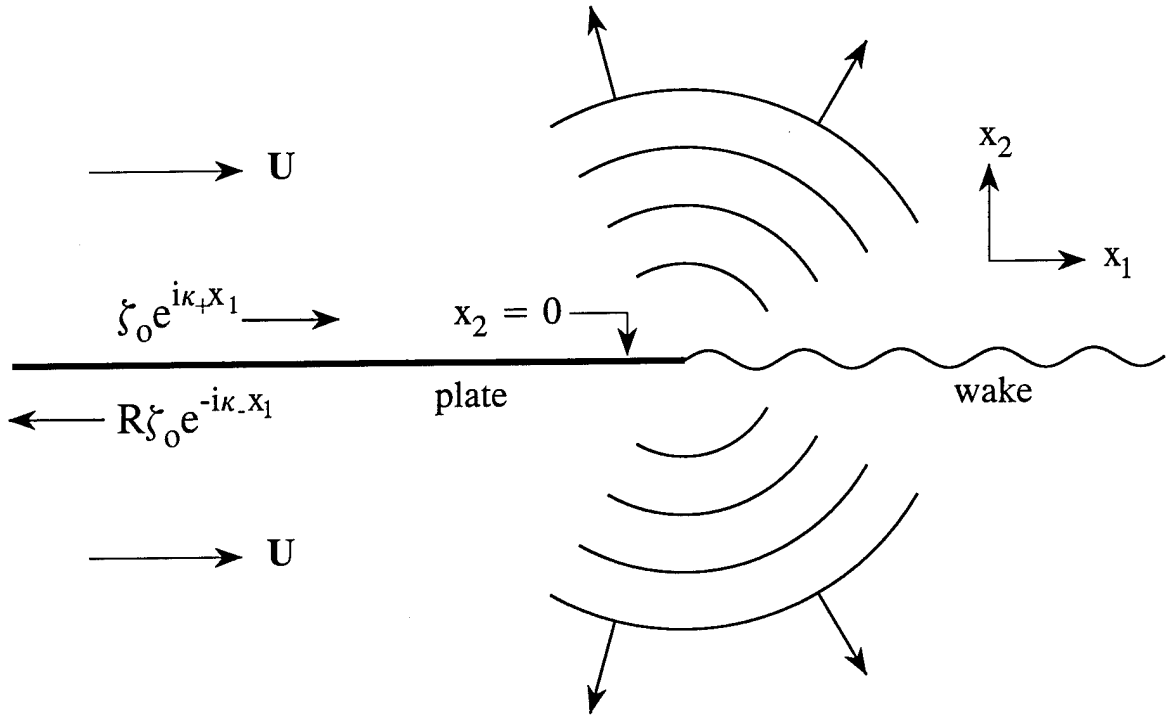

Figure 3. Flexural vibrations near the trailing edge of a large plate in uniform mean flow.

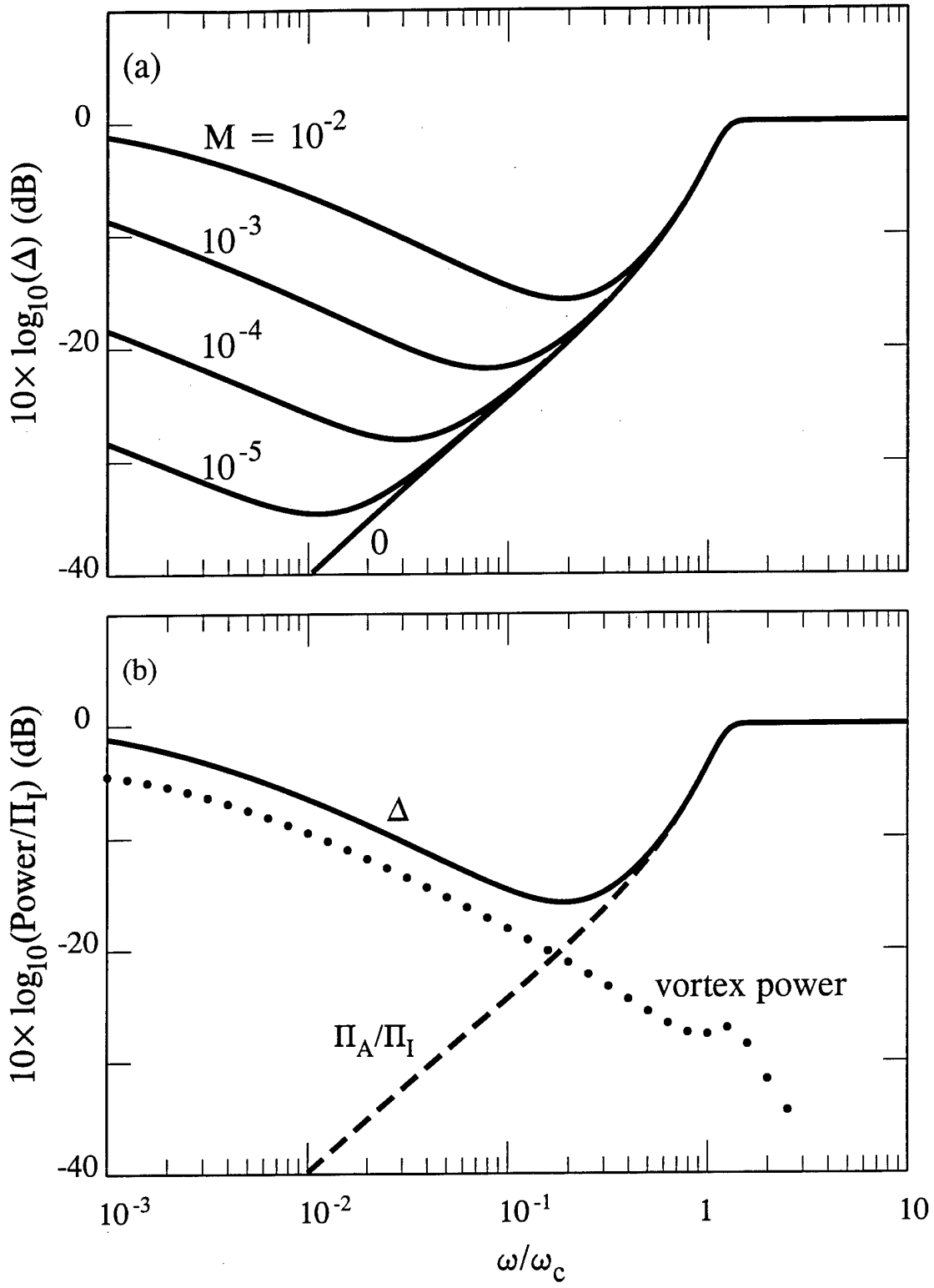

Figure 4. (a) Fractional power Δ dissipated when a bending wave is reflected at the freely vibrating trailing edge of a steel plate in water at various mean flow Mach numbers.
(b) Comparison of Δ (———) and Π_A/Π_I (– – – –) when M = 0.01. The dotted curve is the fractional vortex power Π_W/Π_I.

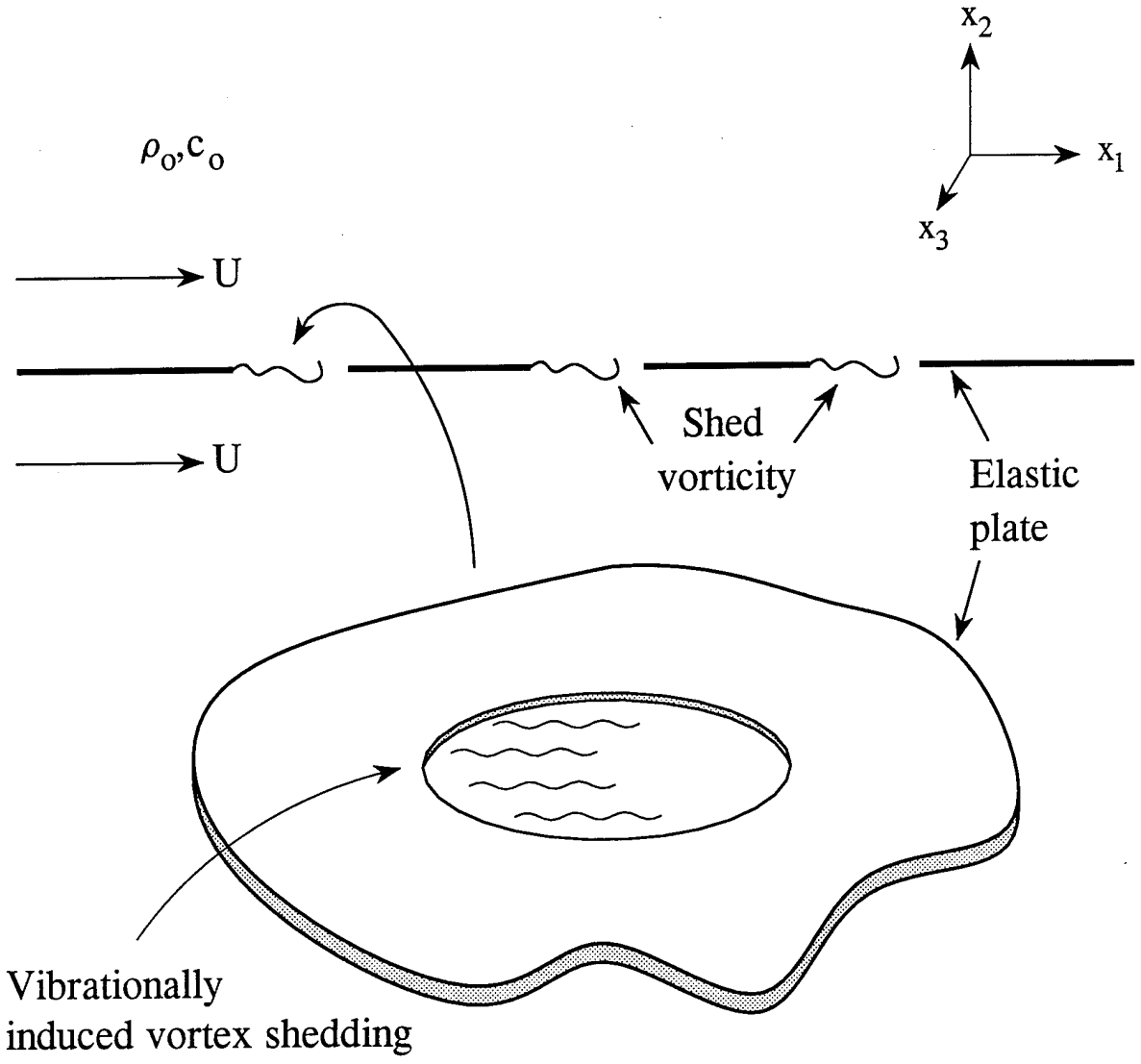

Figure 5. Schematic grazing flow perforated elastic plate.

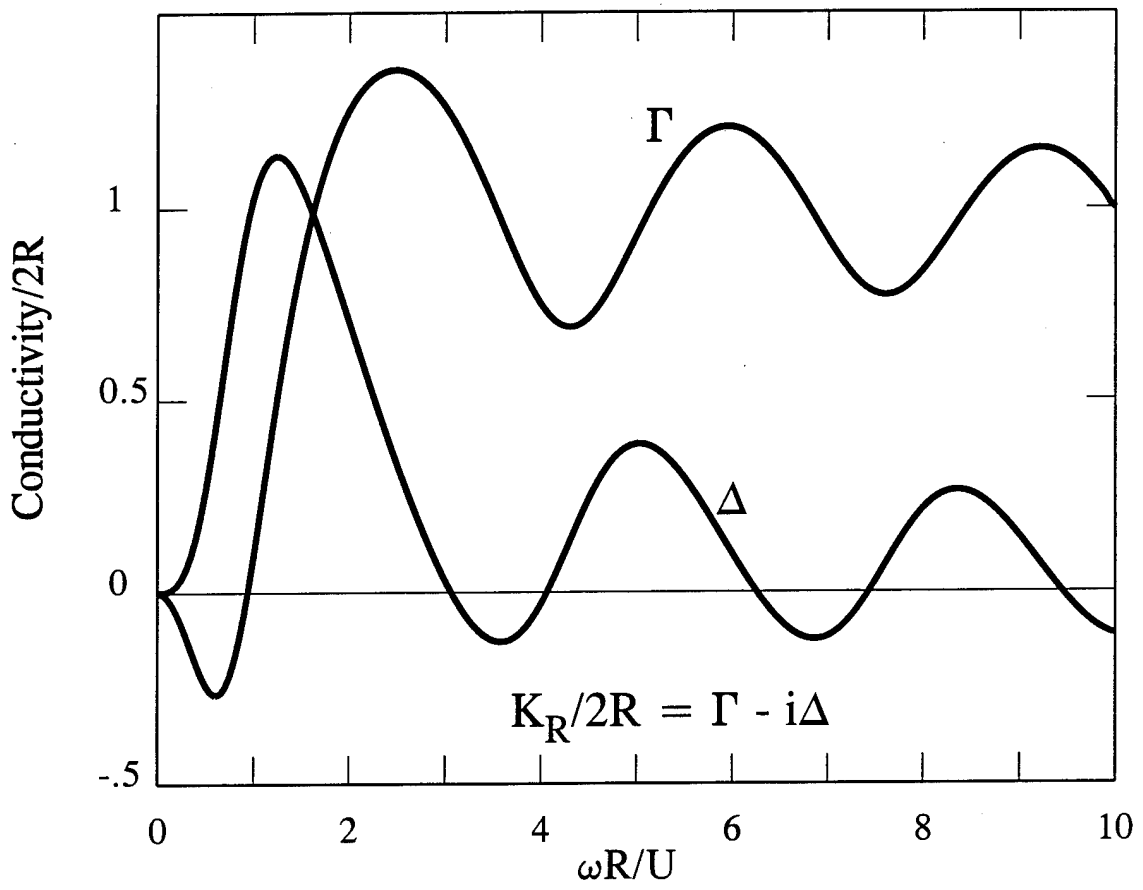

Figure 6. The Rayleigh conductivity of a circular aperture in uniform, two-sided grazing mean flow.

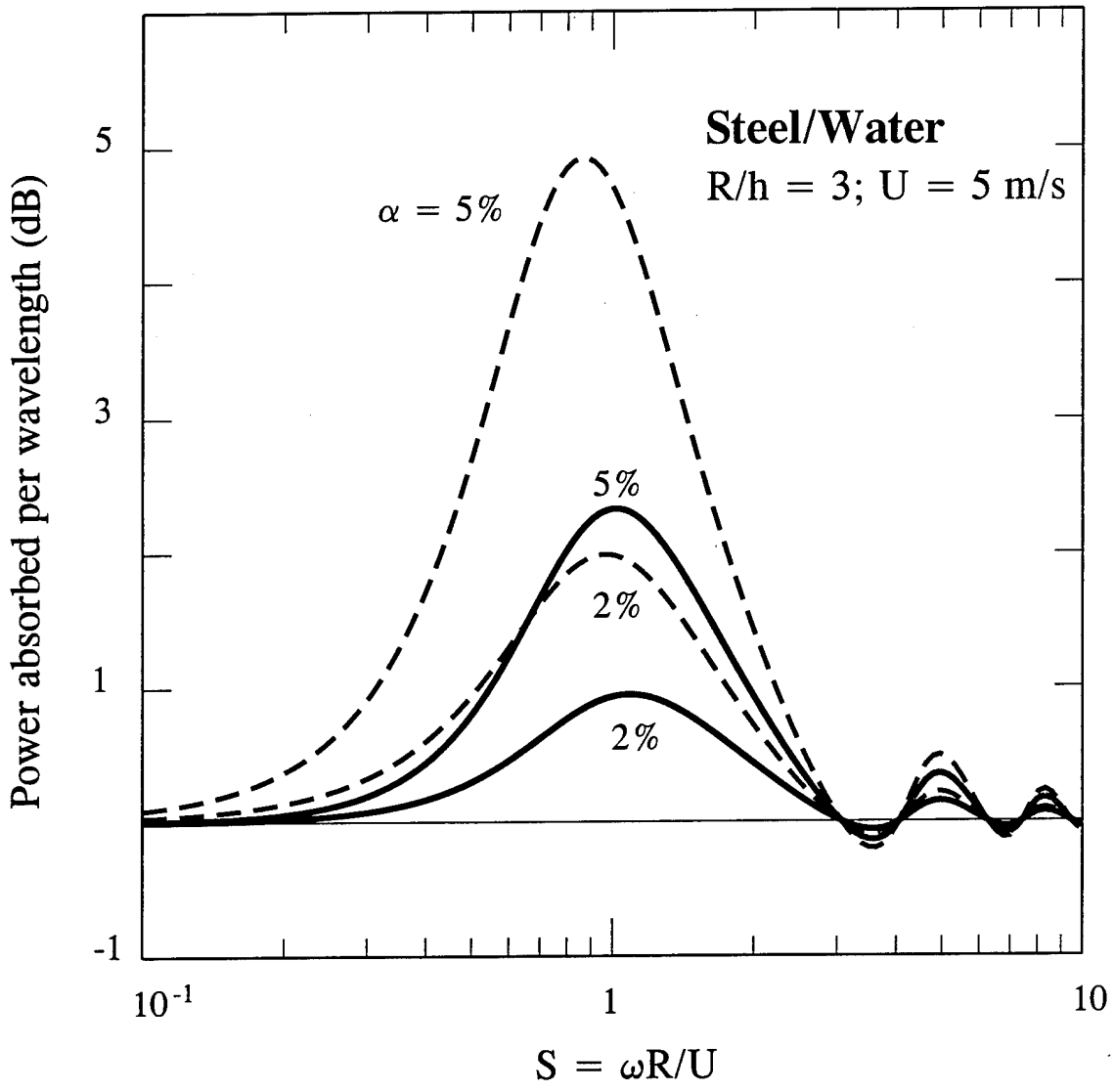

Figure 7. Flexural wave power dissipated per wavelength of propagation on a perforated steel plate in water for different values of the fractional open area α, and for R/h ≡ aperture radius/plate thickness = 3, U = 5 m/s: ———, wave propagating in the mean stream direction; – – – –, wave propagating against the mean stream.

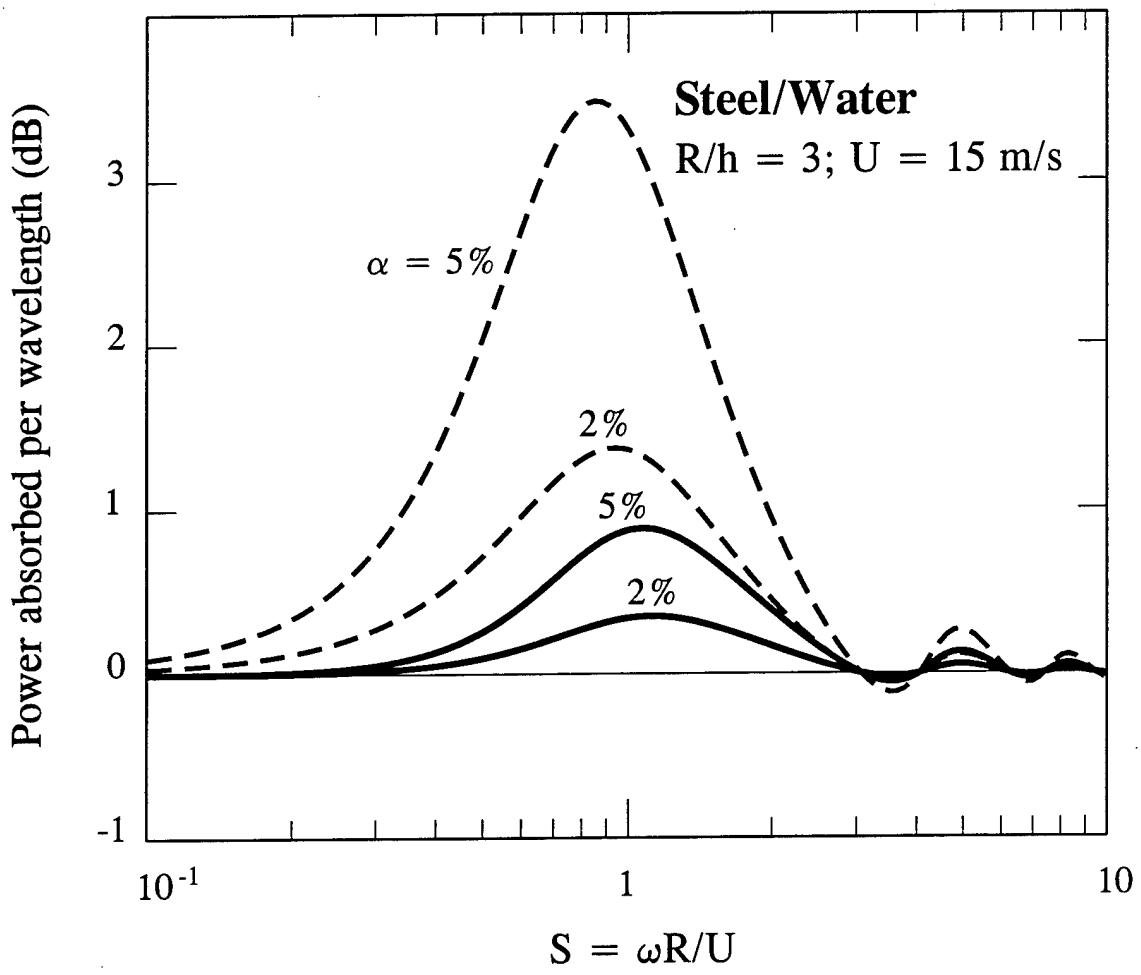

Figure 8. As for Figure 7 with U = 15 m/s.

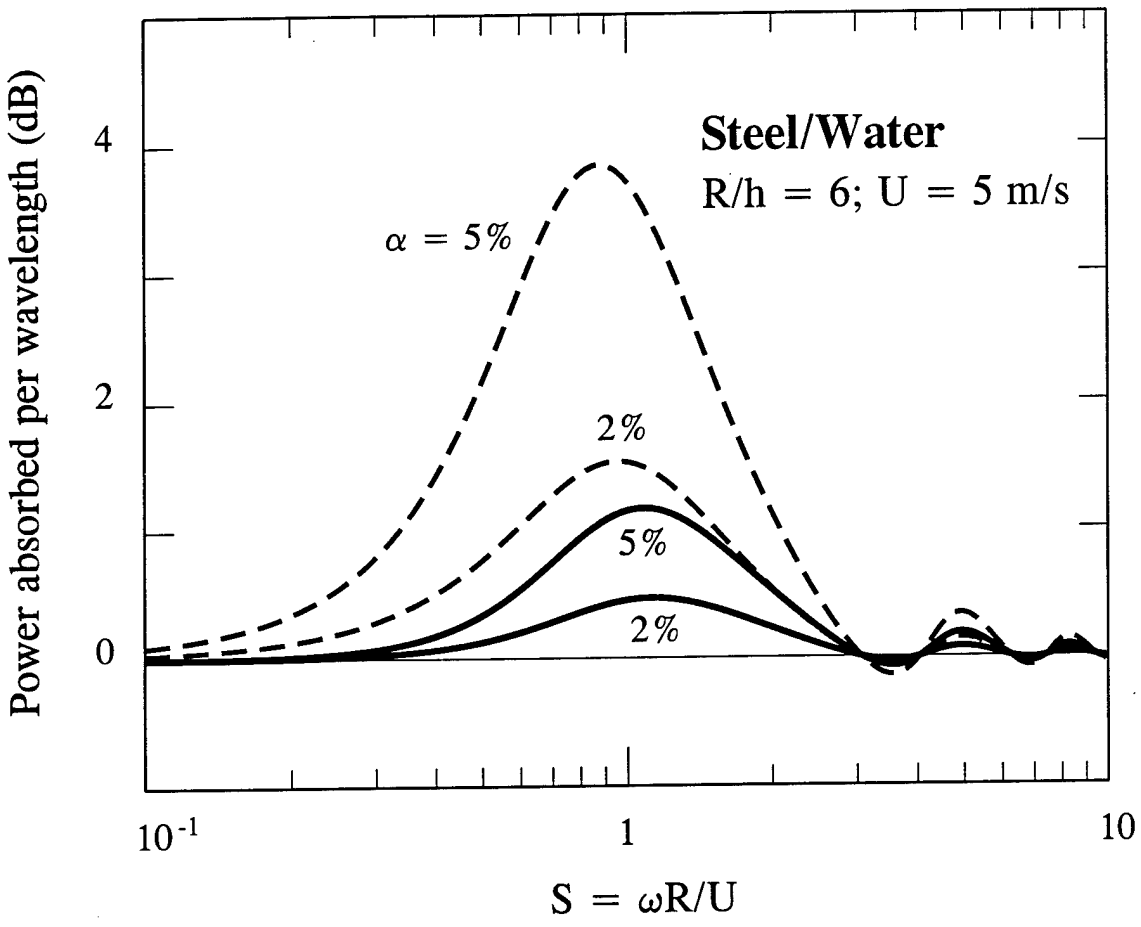

Figure 9. As for Figure 7 with R/h = 6, U = 5 m/s.

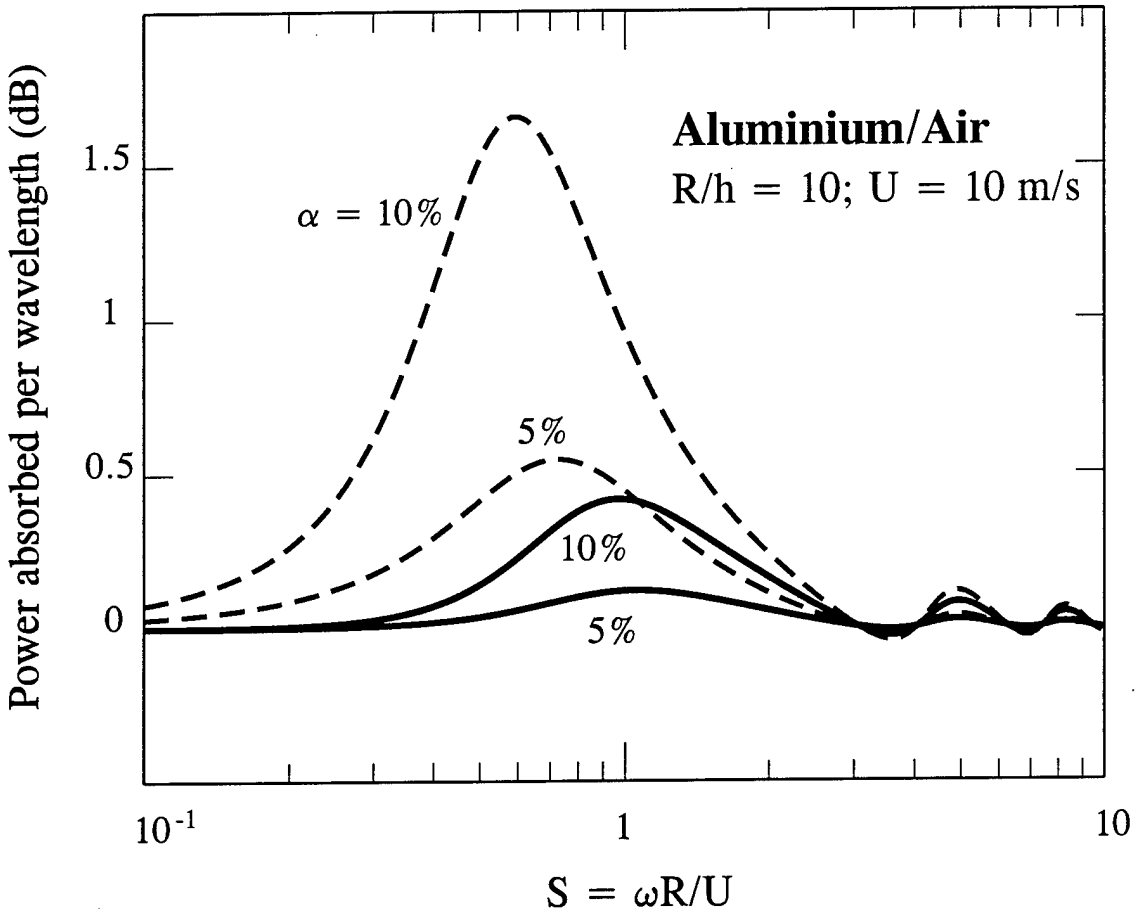

Figure 10. Flexural wave power dissipated per wavelength of propagation on a perforated aluminium plate in air for different values of the fractional open area α, and for R/h = 10, U = 10 m/s: ———, wave propagating in the mean stream direction; – – – –, wave propagating against the mean stream.

CHAPTER 3

THE INFLUENCE OF TANGENTIAL MEAN FLOW ON THE RAYLEIGH CONDUCTIVITY OF AN APERTURE

SUMMARY

An investigation is made of the influence of grazing mean flow on the Rayleigh conductivity of an aperture in a thin rigid plane. The fluid is assumed to be incompressible and inviscid, but the Kutta condition is applied to permit the generation of vorticity at the edge of the aperture by an applied time-varying pressure field. Numerical results are given for a circular aperture in the two cases of (i) one-sided mean flow, when the aperture is spanned by a plane vortex sheet in the undisturbed state, and (ii) two-sided mean flow, when the mean velocity is the same on both sides of the plane, so that the undisturbed motion is irrotational. In both cases there exist frequency ranges within which perturbation energy is either absorbed or generated by the mean flow. The numerical results are supplemented by an approximate analytical treatment of the same problem for a rectangular aperture of large aspect ratio (with its long edge transverse to the mean flow direction). The aperture flux for one-sided flow is shown to be absolutely unstable, and may in principle be triggered by an arbitrary, small disturbance in the mean stream. For two-sided flow the motion is conditionally unstable, in the sense that perturbations are amplified by the extraction of energy from the mean flow only when the frequency of the applied pressure lies in certain discrete bands.

1. INTRODUCTION

Consider the unsteady flow of fluid through an aperture of area A in a rigid plane of negligible thickness produced by a uniform, time-harmonic pressure load $[p] = (p_+ - p_-)e^{-i\omega t}$ ($\omega > 0$) applied across the plane. The "upper" and "lower" faces of the plane are taken to coincide respectively with surfaces $z = \pm 0$ of the coordinate plane $z = 0$ of the rectangular system (x,y,z), and p_+, p_- are the respective amplitudes of the applied pressures above and below the plane. The induced motion through the aperture is assumed to be *incompressible* and to be governed by the linearized equations of motion. Let Q denote volume flux through the plane (in the positive z-direction), where here and henceforth the exponential time factor $e^{-i\omega t}$ is suppressed. Then the *Rayleigh conductivity* K_R of the aperture is defined by (Rayleigh 1870, 1945)

$$K_R = i\omega\rho_0 Q/(p_+ - p_-), \tag{1.1}$$

where ρ_0 denotes the density of the fluid.

The pressure varies continuously through the aperture, and $p_\pm$ are its limiting values at large distances ($\gg \sqrt{A}$) on either side. When there is no *mean* flow, and the motion at large distances can be regarded as irrotational, the definition (1.1) is equivalent to

$$K_R = Q/(\varphi_+ - \varphi_-), \tag{1.2}$$

where $\varphi_\pm$ are the *uniform* velocity potentials above and below the plane, determined by $p_\pm = -\rho_0 \partial\varphi_\pm/\partial t$. This form of the definition is analogous to *Ohm's law* in electricity. Conductivity has the dimensions of length; for example, it is equal to 2R for a circular aperture of radius R in an ideal, stationary fluid.

For an ideal, inviscid fluid, K_R is real and the motion through the aperture is entirely irrotational and conservative. In practice, however, viscous action causes dissipation, and the dissipated power Π, say, is given in terms of $[p]$ and the normal component v_n of fluid velocity at $z = 0$ by

$$\Pi = -\int_{-\infty}^{\infty} \langle [p] v_n \rangle dxdy,$$

where the angle brackets denote a time average, and the real parts of $[p]$, v_n are to be taken after restoration of the time factor $e^{-i\omega t}$. It follows that

$$\Pi = -\tfrac{1}{2}\mathrm{Im}\{K_R\}|[p]|^2/\rho_0\omega, \tag{1.3}$$

and therefore that energy is dissipated provided the imaginary part of K_R is negative.

The dissipation is frequently enhanced for certain frequencies by the presence of a high Reynolds number mean tangential flow over the aperture or a "bias" flow through the plane (Bechert 1979; Crighton 1981), and perforated screens have been deployed in mean flow environments to eliminate harmful acoustic resonances (for example, in heat exchanger cavities (Vér 1990)). For a bias flow screen with circular apertures, the dissipation can be estimated from (1.3) by use of an approximate formula for K_R given by Howe (1979), which has been validated experimentally by Hughes & Dowling (1990). The mean flow is maintained by a steady pressure differential across the screen. If U is the average velocity within an aperture, and $U\sqrt{A}/\nu \gg 1$, the motion will be uninfluenced by viscosity except in the immediate vicinity of the aperture edge, where the flow separates to form a jet. The undisturbed motion is no longer irrotational, and a superimposed, fluctuating pressure $[p]$ causes additional vorticity to be generated, which is then swept away in the jet. The energy required to produce this vorticity is supplied by the applied pressure $[p]$, and dissipation occurs by its transfer to the kinetic energy of the jet.

In this paper we consider the determination of K_R for an aperture in the presence of a tangential mean flow. When the mean velocities are at speeds U_+, U_- above and below the plane (see Figure 1) and the Reynolds number is large, the undisturbed mean shear layer in the aperture can be approximated by a vortex sheet. The sheet is deformed by a small amplitude applied pressure $[p]$, and additional vorticity is shed from the upstream edge of the aperture. However, because the vortex sheet is unstable (Lamb 1932), perturbation energy may be expected to be either created or absorbed by the interaction, depending on the frequency ω of the applied pressure. This problem was examined by Howe (1980), who obtained high and low frequency approximations for K_R for a circular aperture when $U_+ = U_-$, so that the undisturbed motion may be regarded

as irrotational. The applied pressure was assumed to induce separation from the upstream semi-circular edge of the aperture in the form of a thin vortex sheet, the strength of which was set by the *Kutta* condition (Crighton 1985), and it was concluded that $\mathrm{Im}\{K_R\} < 0$ for all ω. We shall argue below (§2) that Howe's (1980) solution is erroneous, because proper account was not taken of conditions at the downstream edge of the aperture.

The tangential flow problem is formulated in §2, and solved numerically for a circular aperture for the two cases of (i) one-sided mean flow, when the fluid is at rest on one side of the plane in the undisturbed state, and (ii) two-sided flow at the same velocity on both sides. The problem is amenable to approximate analytical treatment for a *rectangular* aperture of large aspect ratio, orientated with its long edges perpendicular to the mean flow direction. This is discussed in §3, and comparison made with the numerical results. In all cases there exist frequency ranges where $\mathrm{Im}\{K_R\} > 0$, within which perturbation energy is extracted from the mean flow. For both the circular and rectangular apertures we show in case (ii), for which the undisturbed motion is irrotational, that the motion is *conditionally* unstable (§4), i.e., that energy is extracted from the mean flow only when $[p] \neq 0$; in case (i), on the other hand, the motion is *absolutely* unstable, and an arbitrarily small disturbance can trigger the release of mean flow kinetic energy.

A brief discussion is given in the Appendix of the *generalized* Rayleigh conductivity $K_R(\mathbf{k},\omega)$, which is defined as in (1.1), but for an applied pressure $[p] = p_o e^{i(\mathbf{k}\bullet\mathbf{x}-\omega t)}$, where p_o is constant and $\mathbf{k}$ is an arbitrary "trace-wavenumber" parallel to plane. Rayleigh's (1870) definition corresponds to $K_R(\mathbf{0},\omega)$. The reverse flow reciprocal theorem (Howe 1975; Möhring 1979), extended to problems involving vortex sheets, can be invoked to express $K_R(\mathbf{k},\omega)$ in terms of the vortex sheet displacement in the reverse flow problem for $\mathbf{k} = \mathbf{0}$.

2. CIRCULAR APERTURE WITH A GRAZING MEAN FLOW

2.1 The vortex sheet model

Consider incompressible, uniform mean flows over the upper and lower surfaces of the rigid plane $z = 0$ which is pierced by a circular aperture of radius R whose center is at the coordinate origin. Let the mean velocities be at speeds $U_\pm$ in the x-direction respectively in $z \gtrless 0$, as in Figure 1. The Reynolds number is assumed to be sufficiently large that viscosity can be neglected except for its role in generating vorticity at sharp edges. In the steady state, when $U_+ \neq U_-$, the aperture is spanned by a vortex sheet.

When the plane is subject to a small amplitude, time harmonic pressure load $[p] = p_+ - p_-$, the velocity potentials $\varphi_\pm(\mathbf{x})$ of the unsteady motion above and below the plane may be expressed in the form (Lamb 1932)

$$\varphi_\pm(\mathbf{x}) = \frac{\mp 1}{2\pi} \int_{-\infty}^{\infty} \frac{v_\pm(x',y')}{|\mathbf{x}-\mathbf{x}'|}\, dx'dy', \quad \mathbf{x}' = (x',y',0), \tag{2.1}$$

where $v_\pm$ is the z-component of velocity as $z \to \pm 0$, which vanishes on the plane except at the aperture. In the linearized approximation, the z-component of displacement $\zeta(x,y)$ of fluid particles initially lying just above or below the plane ($z = \pm 0$) vanishes outside the aperture, and equals the displacement of the vortex sheet within the aperture. Thus

$$v_\pm(x,y) = (\partial/\partial t + U_\pm \partial/\partial x)\zeta \equiv -i(\omega + iU_\pm \partial/\partial x)\zeta, \tag{2.2}$$

and integration by parts permits (2.1) to be cast in the form

$$\varphi_\pm(\mathbf{x}) = \frac{\pm i}{2\pi}\left(\omega + iU_\pm \frac{\partial}{\partial x}\right)\int_S \frac{\zeta(x',y')}{|\mathbf{x}-\mathbf{x}'|}\, dx'dy' \ , \tag{2.3}$$

where the final integration may be restricted to the area S occupied by aperture provided $\zeta \sim O(1/|X|^\alpha)$, $\alpha < 1$, near the aperture edge, where X denotes distance from the edge.

The volume flux Q through the aperture is needed to calculate the conductivity K_R from the definition (1.1). This is given by

$$Q = \int_{-\infty}^{\infty} -i(\omega + iU_{\pm}\partial/\partial x)\zeta \, dxdy \equiv -i\omega\int_S \zeta(x,y)dxdy. \qquad (2.4)$$

The equation determining $\zeta(x,y)$ in terms of [p] is obtained from the condition that the pressures just above and below the vortex sheet must be equal. The linearized Bernoulli equation supplies the perturbation pressure in the form

$$p_{\pm} + i\rho_0(\omega+iU_{\pm}\partial/\partial x)\varphi_{\pm}, \quad (z \gtrless 0).$$

Continuity of pressure across the vortex sheet therefore requires that

$$\left[\left(\omega+iU_+\frac{\partial}{\partial x}\right)^2 + \left(\omega+iU_-\frac{\partial}{\partial x}\right)^2\right]\int_S \frac{\zeta(x',y')}{2\pi|x-x'|}\,dx'dy' = (p_+-p_-)/\rho_0,$$

$$\text{for } z = 0, \ (x^2+y^2)^{1/2} < R, \qquad (2.5)$$

Integrating with respect to the second order differential operator on the left hand side, we find (for constant $(p_+-p_-)/\rho_0$)

$$\int_S \frac{Z(\xi',\eta')d\xi'd\eta'}{\sqrt{\{(\xi-\xi')^2+(\eta-\eta')^2\}}} = 1 + \alpha_1(\eta)e^{i\sigma_1\xi} + \alpha_2(\eta)e^{i\sigma_2\xi}, \ (\xi^2+\eta^2)^{1/2} < 1, \qquad (2.6)$$

where $Z = \{\rho_0\omega^2R/\pi(p_+-p_-)\}\zeta$ is the displacement in dimensionless form, $\xi = x/R$, $\eta = y/R$, etc (so that the integration is over the unit disk $(\xi'^2+\eta'^2)^{1/2} < 1$), and σ_1 and σ_2 are the dimensionless *Kelvin-Helmholtz* wavenumbers of instability waves on the vortex sheet (Lamb 1932)

$$\sigma_1 = \frac{\omega R(1+i)}{U_+ + iU_-}, \quad \sigma_2 = \frac{\omega R(1-i)}{U_+ - iU_-}. \qquad (2.7)$$

The amplitudes $\alpha_1(\eta)$, $\alpha_2(\eta)$ of these waves are constant along any line drawn on the sheet in the streamwise direction, but vary with transverse location η. They must be chosen (in accordance with the Kutta condition) to ensure that the vortex sheet leaves the upstream semi-circular arc of the aperture edge tangentially, i.e., such that $Z(\xi,\eta) = \partial Z(\xi,\eta)/\partial\xi = 0$ for $(\xi^2+\eta^2)^{1/2} = 1$, $\xi < 0$. Evidently, $\alpha_1(\eta)$, $\alpha_2(\eta)$ are even functions of η. Potential theory (Kellogg 1954; Sneddon 1966) implies that ζ will generally exhibit a mild singularity of order $1/\sqrt{R-r}$ at the downstream edge $r \equiv (x^2+y^2)^{1/2} = R$, $x > 0$, of the aperture. The singularity is integrable, however

(yielding a finite value for the volume flux Q (2.4)), and is a physically acceptable, linear theory representation of the large amplitude and violent motions produced by vortex impingement on an edge (Rockwell 1983). A correction that incorporates the influence of displacement thickness waves on the downstream surfaces of the plane (modeling vorticity convected in the boundary layers after ejection from the aperture) can be introduced to eliminate the singularity, but this cannot be done in a unique manner and is not expected to modify significantly the conclusions of the present simpler approach (Howe 1981b).

The solution of the integral equation (2.6) determines the volume flux Q via (2.4). The definition (1.1) then yields

$$K_R = \pi R \int_S Z(\xi,\eta)\,d\xi\,d\eta. \tag{2.8}$$

In the absence of flow the conductivity is real and equal to 2R. In the more general case it is convenient to set

$$K_R = 2R(\Gamma_R - i\Delta_R), \tag{2.9}$$

where Γ_R and Δ_R are real valued and depend on the frequency ω.

2.2 Numerical results

Numerical solutions of equation (2.6) have been obtained by discretizing the integral. The aperture was overlaid by a mesh of square integration elements within each of which Z, α_1 and α_2 were assumed to be constant, and the Kutta condition imposed by requiring Z to vanish in those elements overlapping the upstream edge (where the flow separates) *and* in each of the contiguous elements just downstream. The application of (2.6) in each element of the mesh supplies a sufficient number of equations to determine the discretized values of Z, α_1 and α_2. Further details of the procedure are given by Scott (1995). In the degenerate case in which the mean velocities on each side of the plane are the same and equal to U (so that $\sigma_1 = \sigma_2 = \omega R/U$), the right hand side of equation (2.6) was taken in the modified form

$$1 + \left(\alpha_1(\eta) + \alpha_2(\eta)\xi\right)e^{i\sigma\xi}, \text{ where } \sigma = \omega R/U.$$

The real and imaginary parts of the conductivity (2.9) are functions of

the Strouhal number $\omega R/U_+$ and the velocity ratio U_-/U_+. Their calculated values are given in Tables 1 and 2 for the two cases of (i) one-sided flow: $U_+ = U$, $U_- \equiv 0$, and (ii) two-sided flow: $U_+ = U_- = U$. In applications these tabulated results can be approximated by cubic splines, and this has been done in plotting Γ_R and Δ_R for these two cases in Figure 2.

For one-sided flow (Case (i)) $\Gamma_R \approx 4$ when $\omega R/U$ becomes large and the imaginary part $\Delta_R \to 0$. Δ_R is negative for $1.9 < \omega R/U < 3.9$. According to equation (1.4), a negative amount of work is then done by the applied pressure $[p] = p_+ - p_-$, i.e., energy is extracted from the mean flow. In Case (ii) ($U_+ = U_-$) the motion is irrotational when $[p] = 0$. However, there still exist periodically spaced frequency bands (of period π when $\omega R/U > 3$) within which $\Delta_R < 0$, and where perturbations grow at the expense of the mean flow. This extraction of mean flow energy is not associated with vortex sheet instability, but should in this case be regarded as a consequence of the interaction of the vorticity with the semi-circular "leading edge" on which it impinges after convecting across the aperture. We shall show in §4 that cases (i) and (ii) are fundamentally different, inasmuch as the aperture motions are respectively absolutely and conditionally unstable.

Conductivity of a circular aperture for one-sided grazing flow

$U_+ = U$, $U_- = 0$

$\omega R/U$	Γ_R	Δ_R	$\omega R/U$	Γ_R	Δ_R
0.00	0.000	0.000	1.50	1.949	0.623
0.10	-0.030	0.005	1.75	2.097	0.244
0.20	-0.119	0.041	2.00	2.233	-0.131
0.30	-0.253	0.145	2.25	2.409	-0.540
0.40	-0.395	0.360	2.50	2.708	-1.006
0.50	-0.464	0.710	2.75	3.277	-1.459
0.60	-0.350	1.140	3.00	4.184	-1.555
0.70	-0.016	1.503	3.25	4.887	-0.969
0.80	0.439	1.673	3.50	4.897	-0.300
0.90	0.872	1.652	3.75	4.628	-0.000
1.00	1.216	1.515	4.00	4.398	0.059
1.10	1.466	1.333	4.25	4.258	0.033
1.20	1.644	1.142	4.50	4.189	0.003
1.30	1.774	0.959	4.75	4.175	0.011
1.40	1.872	0.786	5.00	4.182	0.115

Table 1

Conductivity of a circular aperture for two-sided grazing flow

$U_+ = U_- = U$

$\omega R/U$	Γ_R	Δ_R	$\omega R/U$	Γ_R	Δ_R
0.00	0.000	0.000	4.00	0.749	-0.031
0.10	-0.015	0.002	4.25	0.691	0.102
0.20	-0.057	0.019	4.50	0.714	0.242
0.30	-0.119	0.063	4.75	0.805	0.345
0.40	-0.187	0.143	5.00	0.928	0.385
0.50	-0.243	0.264	5.25	1.048	0.363
0.60	-0.268	0.420	5.50	1.141	0.297
0.70	-0.247	0.594	5.75	1.195	0.203
0.80	-0.174	0.767	6.00	1.208	0.099
0.90	-0.055	0.916	6.25	1.180	0.002
1.00	0.096	1.030	6.50	1.115	-0.076
1.10	0.263	1.101	6.75	1.023	-0.120
1.20	0.431	1.133	7.00	0.920	-0.117
1.30	0.590	1.131	7.25	0.830	-0.065
1.40	0.734	1.103	7.50	0.778	0.026
1.50	0.860	1.057	7.75	0.781	0.130
1.75	1.102	0.894	8.00	0.836	0.215
2.00	1.252	0.705	8.25	0.922	0.259
2.25	1.331	0.514	8.50	1.014	0.256
2.50	1.354	0.333	8.75	1.091	0.213
2.75	1.329	0.169	9.00	1.139	0.143
3.00	1.260	0.029	9.25	1.152	0.062
3.25	1.152	-0.074	9.50	1.130	-0.017
3.50	1.015	-0.127	9.75	1.075	-0.079
3.75	0.870	-0.114	10.00	0.998	-0.112

Table 2

2.3 Comparison with previous work

The two-sided flow problem where $U_+ = U_- = U$ has been investigated by Howe (1980), who derived the following integral equation for the dimensionless normal velocity $v' = -i(\sigma + i\partial/\partial\xi)Z$ of the vortex sheet

$$\int_S \frac{v'(\xi',\eta')d\xi'd\eta'}{\sqrt{\{(\xi-\xi')^2+(\eta-\eta')^2\}}} = C + \alpha(\eta)e^{i\sigma\xi}, \quad (\xi^2+\eta^2)^{1/2} < 1, \tag{2.10}$$

where C is a known constant. The Kutta condition was imposed by choosing $\alpha(\eta)$ to ensure that v' is finite over the upstream edge $(\xi^2+\eta^2)^{1/2} = 1$, $\xi < 0$ of the aperture. Consequently, $v \sim O(1/\sqrt{R-r})$ at the downstream edge, on which the shed vorticity impinges after convecting across the aperture. In fact, equation (2.10) is invalid because the range of integration in (2.10) cannot be restricted to the region S of the aperture unless account is taken of a *singular* contribution to v' from the downstream edge. When $v \sim O(1/\sqrt{R-r})$ at this edge, the displacement ζ will have a simple discontinuity there, with limiting value ζ_D, say, as $r \to R-0$ $(x > 0)$, and the singular velocity at the edge would equal $-U\zeta_D\delta(r-R)$. This should appear as a separate contribution in (2.10) and must be included in the evaluation of the volume flux Q. A finite limiting behavior of ζ at the downstream edge is possible only when $U_+ = U_-$, since in general the edge singularity is much stronger than a simple discontinuity, being proportional to $1/\sqrt{R-r}$, although the aperture flux remains finite.

3. THE RECTANGULAR APERTURE

It is of interest to compare the numerical predictions for a circular aperture with corresponding results that can be derived in analytical form for a rectangular aperture of large aspect ratio.

Take the mean flow in the x-direction with velocities $U_\pm$ above and below the plate, as before, and let the rectangular aperture occupy the region $|x| < s$, $|y| < \frac{1}{2}b$, where the *aspect ratio* $b/2s \gg 1$ (Figure 3). In the notation of §2, the vortex sheet displacement ζ satisfies the integro-differential equation (2.5), in which S now denotes the rectangular area. An approximate solution of this equation can be obtained when b/2s is large by assuming the motion of the vortex sheet to be two-dimensional, i.e., by neglecting the dependence of $\zeta(x',y')$ on the spanwise coordinate y'. The integration with respect to y' over $(-\frac{1}{2}b,\frac{1}{2}b)$ in (2.5) may then be performed explicitly. If we also integrate over $-\frac{1}{2}b < y < \frac{1}{2}b$, the resulting equation may be regarded as satisfying the condition of pressure continuity across the vortex sheet in a spanwise averaged sense.

To do this observe that, when x and x' both lie within the aperture, so that $|x-x'| < 2s$,

$$\iint_{-b/2}^{b/2} \frac{dy'\,dy}{\sqrt{(x-x')^2+(y-y')^2}} = 2b\,\sinh^{-1}(b/|x-x'|) - 2\{\sqrt{b^2+(x-x')^2} - |x-x'|\}.$$

$$= 2b\left(\ln\{2b/e|x-x'|\} + \frac{|x-x'|}{b} - \frac{|x-x'|^2}{4b^2} + \ldots\right), \quad (3.1)$$

where e is the exponential constant. When $b/2s \gg 1$ only the first term in the brace brackets of this expansion need be retained. Making this approximation in (2.5), and integrating with respect to the differential operator, we obtain

$$\int_{-1}^{1} Z(\xi')\ln\left(\frac{2b}{es|\xi-\xi'|}\right)d\xi' = 1 + \alpha_1 e^{i\sigma_1\xi} + \alpha_2 e^{i\sigma_2\xi}, \quad |\xi| < 1, \quad (3.2)$$

where

$$Z = \{2\rho_0\omega^2 s/\pi(p_+ - p_-)\}\zeta, \quad \xi = x/s, \quad \xi' = x'/s$$

and σ_1 and σ_2 are nondimensional Kelvin-Helmholtz wavenumbers defined as in (2.7) with R replaced by s. The coefficients α_1 and α_2 are *constants* whose values are fixed by the Kutta condition $Z = \partial Z/\partial\xi = 0$ at $\xi = -1$.

The solution of (3.2) satisfying these conditions has been given by Howe (1981b). Z varies like $(\xi+1)^{3/2}$ near the upstream edge $\xi = -1+0$ of the aperture, and is singular like $1/(1-\xi)^{1/2}$ at the downstream edge ($\xi \to 1-0$) where the vortex sheet impinges on the solid surface. The volume flux

$$Q = \{\pi b(p_+ - p_-)/2i\rho_0\omega\}\int_{-1}^{1} Z(\xi)d\xi,$$

and the Rayleigh conductivity is therefore equal to $\frac{\pi}{2}b\int_{-1}^{1} Z(\xi)d\xi$. Using the solution given by Howe (1981b) we find

$$K_R = \frac{\pi b}{2\{F(\sigma_1,\sigma_2) + \Psi\}}, \tag{3.3}$$

where

$$F = \frac{-\sigma_1 J_0(\sigma_2)[J_0(\sigma_1)-2W(\sigma_1)] + \sigma_2 J_0(\sigma_1)[J_0(\sigma_2)-2W(\sigma_2)]}{\sigma_1 W(\sigma_2)[J_0(\sigma_1)-2W(\sigma_1)] - \sigma_2 W(\sigma_1)[J_0(\sigma_2)-2W(\sigma_2)]}, \quad \Psi = \ln(4b/es), \tag{3.4}$$

$W(x) = ix[J_0(x) - iJ_1(x)]$, and J_0 and J_1 are Bessel functions.

The conductivity in the absence of flow is also given by (3.3) by formally setting F = 0. For that case we can write

$$K_R/2R_e = (\pi^3 b/32s)^{1/2}/\ln\{4b/se\}, \tag{3.5}$$

where $R_e = (2sb/\pi)^{1/2}$ is the radius of the circle of area 2sb (that of the rectangle). According to Rayleigh (1945) the circular aperture has the minimum conductivity of all apertures of the same area, and indeed the right hand side of (3.5) has a minimum value of about 1.1, and does not exceed 1.2 when $2.5 < b/s < 12.8$.

Figure 4(i) illustrates the dependence of the real and imaginary parts of $K_R(\omega)/2R_e = \Gamma_R - i\Delta_R$ on $\sigma = \omega s/U$ for one sided flow, $U_+ = U$, $U_- = 0$ when the aspect ratio b/2s = 10. These curves are qualitatively the same as the corresponding plots in Figure 2(i) for the circular aperture. It follows from equations (3.3), (3.4) for the rectangular aperture that

$$\left.\begin{aligned} \Gamma_R &\approx \frac{(\pi^3 b/32s)^{1/2}}{\ln(4b/se^3)}, \qquad \Delta_R \approx 0, \ \sigma \to \infty, \\ \Gamma_R &\approx -3\sigma^2(\pi^3 b/32s)^{1/2}, \ \Delta_R \approx 8\sigma^3(\pi^3 b/32s)^{1/2}, \ \sigma \to 0. \end{aligned}\right\} \tag{3.6}$$

Thus, at high frequencies the conductivity is real and exceeds that in the absence of the vortex sheet (provided $4b/se^3 > 1$).

For two-sided flow with $U_+ = U_- = U$, there is no vortex sheet in the steady state and $\sigma_1 \to \sigma_2 \to \sigma = \omega s/U$. The corresponding limiting form of function F of (3.4) is

$$F(\sigma,\sigma) = \frac{i\sigma J_0(J_0 - iJ_1) - [J_0 - 2i\sigma(J_0 - iJ_1)][J_0 - i\sigma(J_0 + iJ_1)]}{\sigma[J_0 J_1 + \sigma\{J_1^2 + (J_0 - 2iJ_1)^2\}]}, \tag{3.7}$$

where the Bessel functions are evaluated at $\sigma = \omega s/U$. The variations of Γ_R and Δ_R with σ are shown in Figure 4(ii) for $b/2s = 5$. Once again, the results are qualitatively similar to those in Figure 2(ii) for the circular aperture. However, whereas Figure 2(ii) indicates that the oscillatory behavior of K_R ultimately dies out, and that $\Gamma_R \to 1$, $\Delta_R \to 0$ as $\sigma \to \infty$, the limiting behaviors for the rectangular aperture remain oscillatory, with period π, since $F \approx 4/\{5\sin(2\sigma) + 4i\cos(2\sigma) - 3\}$ when $\sigma > 2$. As $\sigma \to 0$ we find

$$\Gamma_R \approx -\tfrac{3}{2}\sigma^2(\pi^3 b/32s)^{1/2}, \ \Delta_R \approx 6\sigma^3(\pi^3 b/32s)^{1/2}. \tag{3.8}$$

4. ABSOLUTE AND CONDITIONAL INSTABILITY

The volume flux Q is determined by the applied pressure $[p] \equiv p_+ - p_-$ and the conductivity K_R. All of these quantities are generally functions of the frequency ω, and the real form of (1.1) is

$$\rho_o \partial Q(t)/\partial t = -\int_{-\infty}^{\infty} K_R(\omega)[p(\omega)]e^{-i\omega t}\, d\omega. \qquad (4.1)$$

The integration is nominally taken over all real values of ω. However, if the integrand has singularities in the upper half of the complex ω-plane, the integration contour must pass above them to ensure that causality is satisfied. Since [p(t)] is arbitrary, and may be assumed to vanish prior to some initial instant, any singularities in $\mathrm{Im}(\omega) > 0$ must be associated with $K_R(\omega)$. When they are present the system is unstable, and an unsteady flux through the aperture can develop spontaneously. Also, because Q(t) and [p(t)] are real valued quantities, it follows that $K_R(-\omega^*) = K_R^*(\omega)$, where the asterisk denotes complex conjugate.

Consider the stable case in which $K_R(\omega) \equiv 2R\{\Gamma_R(\omega) - i\Delta_R(\omega)\}$ is regular in $\mathrm{Im}\{\omega\} > 0$. For *real* ω we have

$$\Gamma_R(-\omega) = \Gamma_R(\omega), \quad \Delta_R(-\omega) = -\Delta_R(\omega). \qquad (4.2)$$

In general $\Gamma_R(\omega) \to \Gamma_\infty$ = constant as $|\omega| \to \infty$ and $\Delta_R(\omega) \to 0$. The function $f(\omega) = \Gamma_R(\omega) - \Gamma_\infty - i\Delta_R(\omega)$ is regular in $\mathrm{Im}(\omega) > 0$ and vanishes as $|\omega| \to \infty$. Cauchy's theorem (Carrier, *et al* 1966) applied in the usual way to a closed contour consisting of the real axis and a semi-circle in the upper half-plane whose radius grows without limit, then implies that

$$f(\omega) = (1/2\pi i)\int_{-\infty}^{\infty} f(\xi)\,d\xi/(\xi-\omega) \text{ for } \mathrm{Im}(\omega) > 0,$$

where the integration is along the real axis. The real and imaginary parts of this expression as $\mathrm{Im}(\omega) \to +0$ yield the *Kramers-Kronig* formulae

$$\Gamma_R(\omega) - \Gamma_\infty = -\frac{2}{\pi}\int_0^{\infty} \frac{\lambda\Delta_R(\lambda)\,d\lambda}{\lambda^2-\omega^2}, \quad \Delta_R(\omega) = \frac{2\omega}{\pi}\int_0^{\infty} \frac{[\Gamma_R(\lambda)-\Gamma_\infty]\,d\lambda}{\lambda^2-\omega^2}, \quad (\omega \text{ real}) \qquad (4.3)$$

where the integrals are principal values.

When the motion is stable these equations can be used to determine Γ_R, say, when $\Delta_R(\omega)$ is known. If $K_R(\omega)$ vanishes at zero frequency (as it would when vortex shedding completely blocks the aperture flux), the constant Γ_∞ is found by setting $\omega = 0$ in the first of (4.3).

Alternatively, when $\Gamma_R(\omega)$ and $\Delta_R(\omega)$ are known for real ω, equations (4.3) can be used to investigate the stability of the flow. If the equations are *not* satisfied $K_R(\omega)$ must be singular in $\mathrm{Im}(\omega) > 0$, and the motion is *absolutely unstable*. This is the case for one-sided grazing flow over the circular and rectangular apertures of §§3, 4, and is presumably a consequence of vortex sheet instability. According to Figures 2(ii) and 4(ii), $\Delta_R < 0$ for discrete ranges of real frequencies for two-sided flow when $U_+ = U_- = U$. Equation (1.4) indicates that energy is extracted from the mean flow at these frequencies. However, the Kramers-Kronig formulae *are* satisfied by the numerical data for two-sided flow in Figures 2(ii) and 4(ii). The dots in these figures represent values of Γ_R computed from the first of the Kramers-Kronig equations (4.3) using the respective values of Δ_R shown in the figures (taking $\Delta_R(\lambda) = 0$ for $\lambda > 20$). The motion is therefore *conditionally unstable*: energy is extracted from the mean flow only when the applied pressure [p] contains a component with frequency within an interval where $\Delta_R < 0$.

When the aperture is backed by a cavity (in which $U_- \equiv 0$) whose dimensions are large compared to the aperture diameter, the instability of the shear layer can excite and sustain cavity acoustic resonances. This can occur only when the frequency lies within the range where $\Delta_R(\omega) < 0$. For the circular aperture it is usual to express the frequency at which a resonance is excited in terms of the Strouhal number fD/U, where $f = \omega/2\pi$ and D is the diameter. According to Figure 2(i) flow excited cavity resonances must occur for $0.6 < fD/U < 1.15$. This range is consistent with experimentally observed Strouhal numbers for laminar, high Reynolds number flow over cavity openings in cases where the shear layer is well approximated by a vortex sheet, i.e., when the shear layer thickness is very much smaller than D (see, e.g., DeMetz and Farabee 1977).

5. CONCLUSION

The Rayleigh conductivity K_R of an aperture in a thin plane determines the volume flux through the aperture generated by a small amplitude, time harmonic pressure load. When the motion is incompressible and irrotational K_R is real and constant, and depends only on the shape of the aperture. The conductivity is complex for a real fluid. If there is a tangential flow over the plane, and the Reynolds number based on aperture diameter is large, the pressure load can be assumed to generate vorticity at the aperture edge, which causes perturbation energy to be absorbed or generated by the mean flow, according as $\mathrm{Im}\{K_R\} \lessgtr 0$.

In this paper K_R has been calculated numerically for tangential flow over a circular aperture of radius R by modeling the shear layer as a vortex sheet. For one-sided flow at speed U, energy is extracted from the mean flow when the Strouhal number $\omega R/U$ is between about 1.9 and 3.9. The aperture motion is absolutely unstable, in the sense that a small perturbation in the mean stream can trigger motion of the vortex sheet that becomes unbounded on the basis of linear theory. When the mean velocity is the same on both sides of the plane the flow is irrotational in the steady state. Vorticity is generated by an applied pressure (in accordance with the Kutta condition) and there are discrete, quasi-periodic frequency intervals within which perturbation energy is alternately absorbed and generated by the mean flow. However, this motion is conditionally unstable, in that perturbation energy grows at the expense of the mean flow only when the applied pressure is non-zero and of the appropriate frequency.

The numerical results for a circular aperture are in qualitative agreement with analytical predictions for a rectangular aperture of large aspect ratio, whose long edge is transverse to the mean flow direction.

REFERENCES

Bechert, D. W. 1979 *AIAA Paper* 79-0575. Sound absorption caused by vorticity shedding, demonstrated with a jet flow.

Carrier, G. F., Krook, M. & Pearson, C. E. 1966 *Functions of a complex variable*. New York: McGraw-Hill.

Crighton, D. G. 1981 *J. Fluid Mech.* **106**, 261 - 298. Acoustics as a branch of fluid mechanics.

Crighton, D. G. 1985 *Ann. Rev. Fluid Mech.* **17**, 411 - 445. The Kutta condition in unsteady flow.

DeMetz, F. C. & Farabee, T. M. 1977 *AIAA Paper 77-1293*. laminar and turbulent shear flow induced cavity resonances.

Howe, M. S. 1975 *J. Fluid Mech.* **67**, 579 - 610. The generation of sound by aerodynamic sources in an inhomogeneous steady flow.

Howe, M. S. 1979 *Proc. Roy. Soc. Lond.* **A366**, 205 - 233. On the theory of unsteady high Reynolds number flow through a circular aperture.

Howe, M. S. 1980 *Proc. Roy. Soc. Lond.* **A370**, 523 - 544. On the diffraction of sound by a screen with circular apertures in the presence of a low Mach number grazing flow.

Howe, M. S. 1981a *Phil. Trans. Roy. Soc. Lond.* **A303**, 151 - 180. On the theory of unsteady shearing flow over a slot.

Howe, M. S. 1981b *J. Fluid Mech.* **109**, 125 - 146. The influence of mean shear on unsteady aperture flow, with application to acoustical diffraction and self-sustained cavity oscillations.

Howe, M. S. 1995 *J. Acoust. Soc. Am.* **97**, 1522 - 1533. Influence of mean shear on sound produced by turbulent flow over surface slots.

Hughes, I. J. & Dowling, A. P. 1990 *J. Fluid Mech.* **218**, 299 - 336. The absorption of sound by perforated linings.

Kellogg, O. D. 1954 *Foundations of Potential Theory*. Dover: New York.

Lamb, H. 1932 *Hydrodynamics* (6th. edition; Reprinted 1993). Cambridge University Press.

Möhring, W. 1979 *Modelling low Mach number noise*, pp 85 - 96, *Proc. Symp. Mechanics of Sound Generation in Flows*, Göttingen, August 28 - 31 (editor E.-A. Müller: Springer, Berlin, 1979).

Rayleigh, Lord. 1870 *Phil. Trans. Roy. Soc. Lond.* **161**, 77 - 118. On the theory of resonance.

Rayleigh, Lord 1945 *Theory of Sound, Vol 2*. New York: Dover.

Rockwell, D. 1983 *AIAA J.* **21**, 645 - 664. Oscillations of impinging shear layers.

Scott, M. I. 1995 MS thesis, Boston University, College of Engineering. *The Rayleigh conductivity of a circular aperture in the presence of a grazing flow.*

Sneddon, I. N. 1966 *Mixed boundary value problems in potential theory.* Amsterdam: North Holland.

Vér, I. L. 1990 *Noise Control Eng. J.* **35** (Nov/Dec issue) pp. 115 - 125. Practical examples of noise and vibration control: case history of consulting projects.

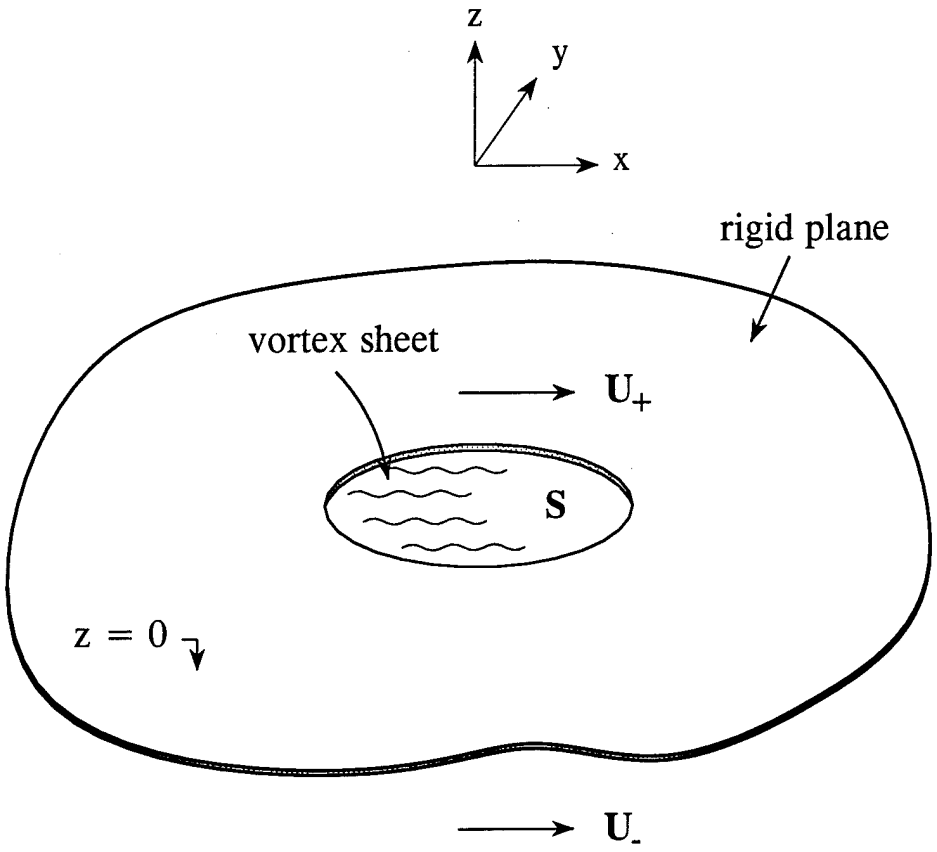

Figure 1. Tangential flow over the upper and lower surfaces of a thin, rigid plane with a circular aperture.

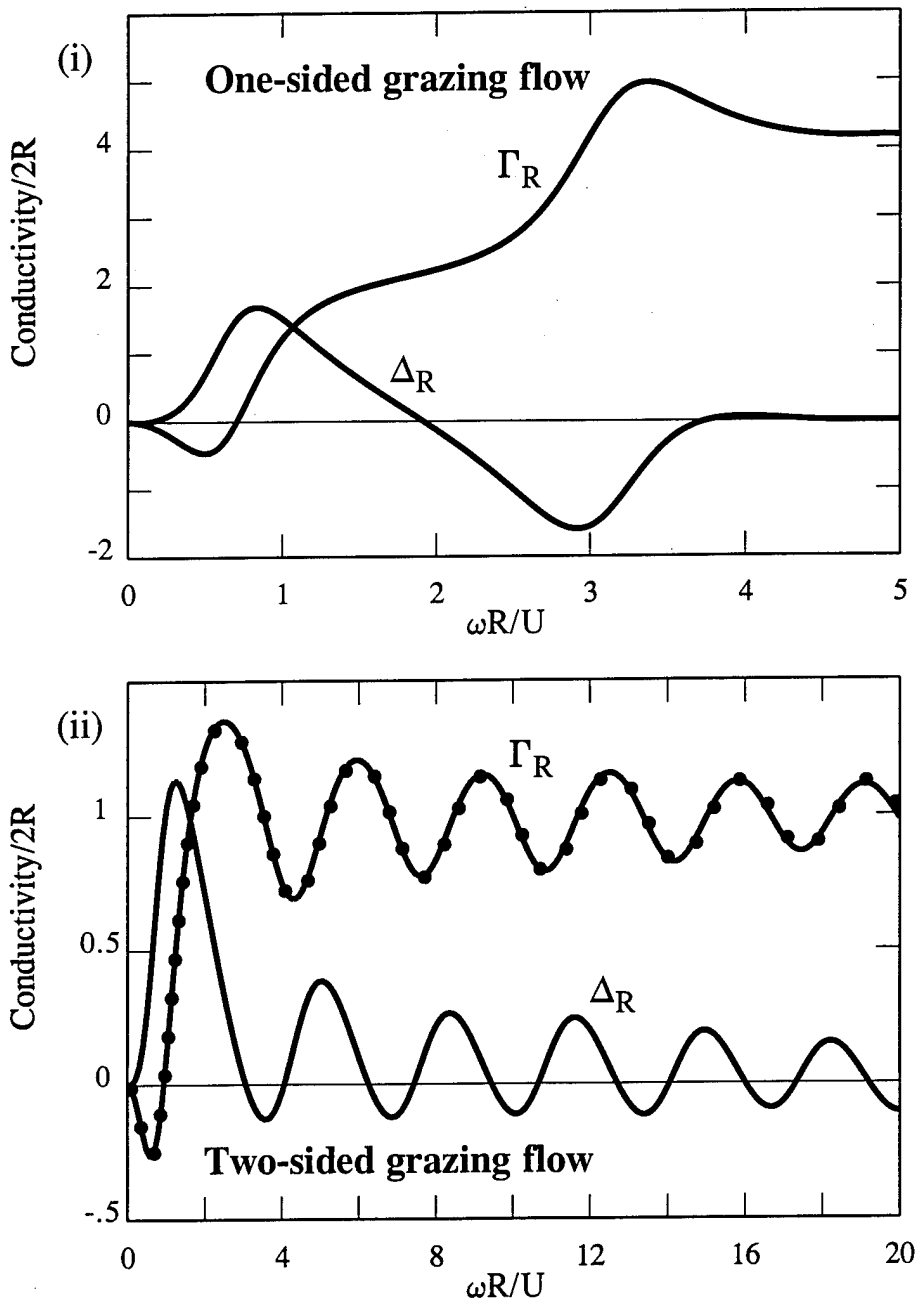

Figure 2. Conductivity of a circular aperture in grazing flow (i) $U_+ = U$, $U_- = 0$; (ii) $U_+ = U_- = U$. The dotted curve in Case (ii) is discussed in §4.

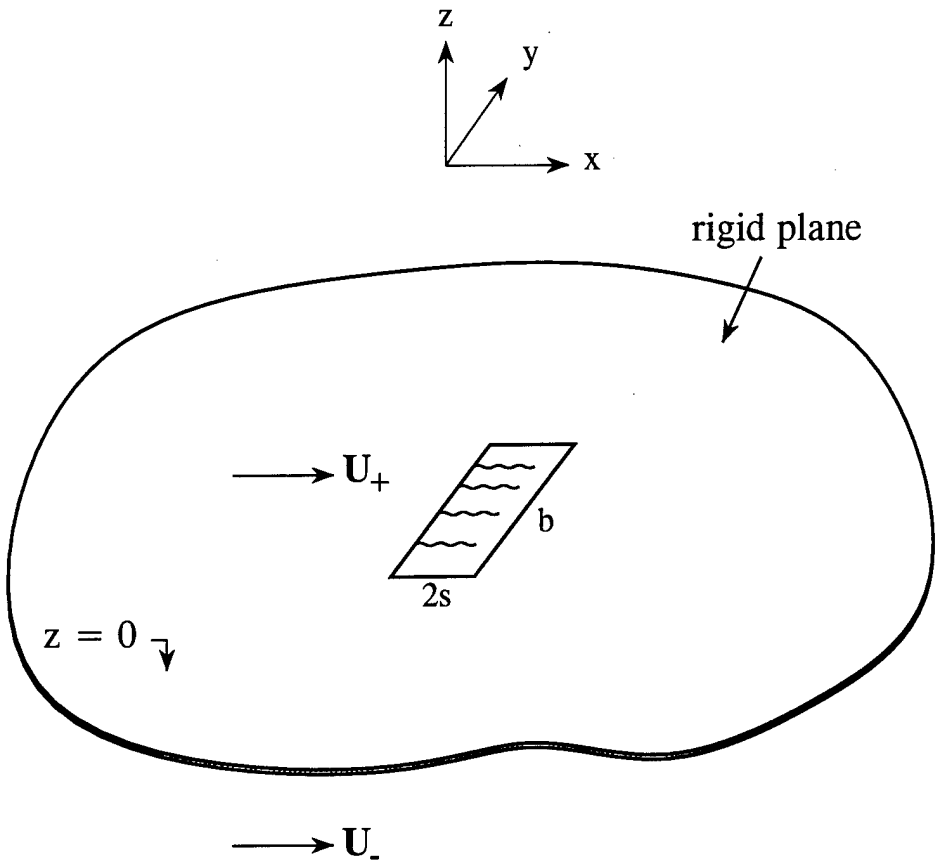

Figure 3. Rectangular aperture of large aspect ratio. The long edges of the aperture are transverse to the mean flow direction.

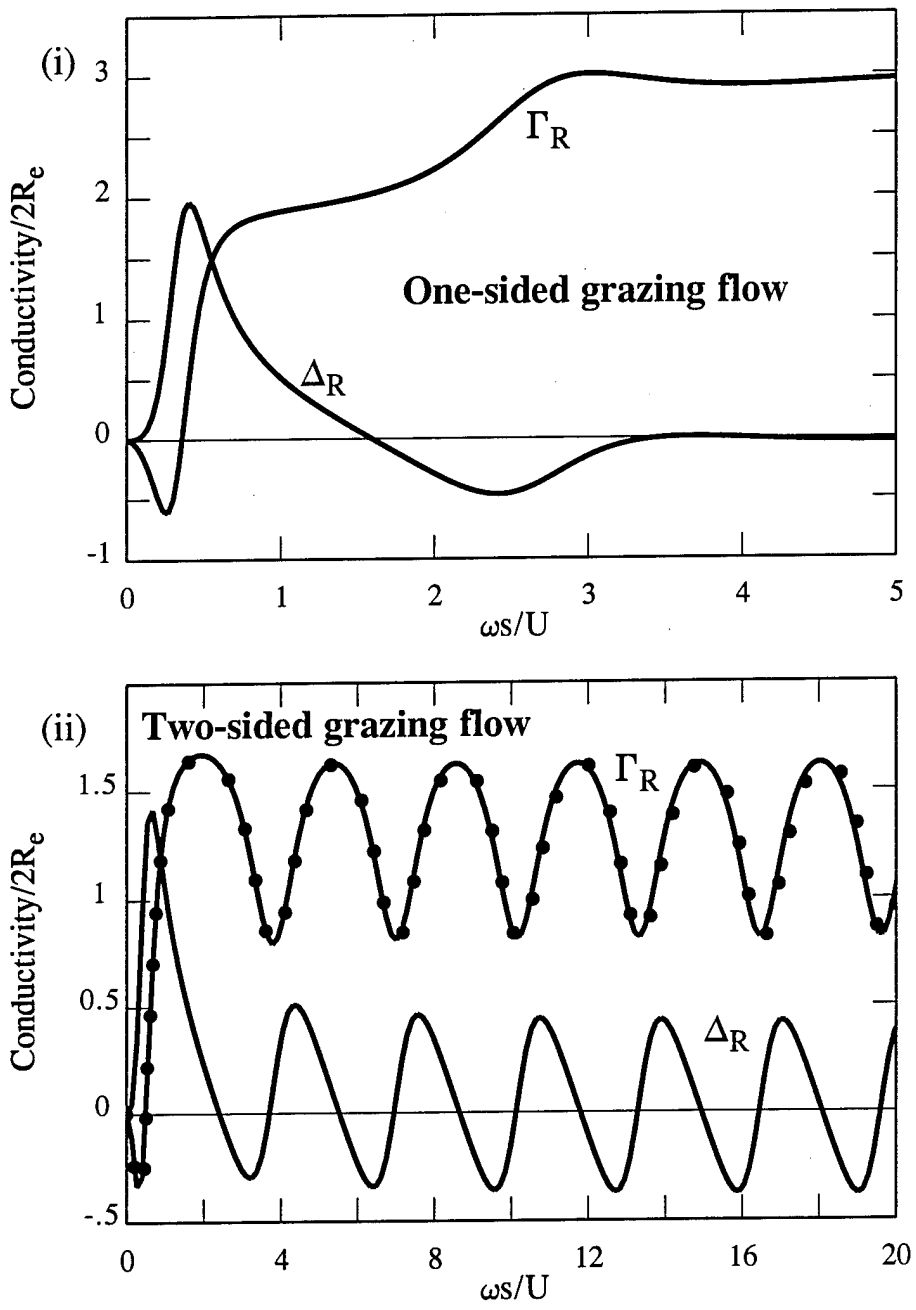

Figure 4. Conductivity $K_R(\omega)/2R_e = \Gamma_R - i\Delta_R$ of a rectangular aperture of aspect ratio b/2s = 10 in grazing flow (i) $U_+ = U$, $U_- = 0$; (ii) $U_+ = U_- = U$. The dotted curve in Case (ii) is discussed in §4.

CHAPTER 4

DAMPING OF SOUND AND VIBRATION BY FLOW NONLINEARITY IN THE APERTURES OF A PERFORATED ELASTIC SCREEN

SUMMARY

An analysis is made of the influence of flow nonlinearity in the apertures of a perforated elastic plate on the damping of sound and flexural vibrations. Fluid is forced through the perforations by the pressure differential established across the plate by the incident disturbance. The Reynolds number is assumed to be sufficiently large that separation occurs, and the reciprocating aperture flows form "jets" on alternate sides of the plate. The growth of these jets is modeled by means of a nonlinear equation proposed by Cummings (1986). This equation is solved simultaneously with a generalized bending wave equation derived by the author (Howe 1995a) which governs motions of a perforated elastic plate whose lengths scales are large compared to the aperture spacing. It is shown that significant attenuations of large amplitude acoustic waves can occur except when the frequency is so small that the plate is acoustically transparent. Bending waves are also damped provided the amplitude of the plate surface velocity is not too large and the frequency is small enough to ensure the formation of substantial jets in the apertures. Numerical results are given for large amplitude sound waves incident on a perforated screen in air, and for bending waves propagating over aluminium and steel screens immersed in either air or water.

1. INTRODUCTION

When a sound wave impinges on a solid surface in the absence of mean flow dissipation usually occurs through the direct action of viscous and molecular thermal diffusion. At very high acoustic amplitudes, however, free vorticity is formed at sharp edges, and dissipation takes place by the transfer of energy to the kinetic energy of the vorticity, which is convected away from the interaction region by *self-induction*. This nonlinear mechanism can be particularly important when sound generates motions in small perforates or apertures; when the acoustic Reynolds number $\omega R^2/\nu$ is large (ω being the acoustic frequency, R the aperture radius, and ν the kinematic viscosity) it is independent of the viscosity, except insofar as viscosity must be called into play to permit vorticity to be released into the fluid (Sivian 1935; Thurston, Hargrove & Cook 1957; Ingard & Ising 1967; Zinn 1970; Melling 1973; Cummings 1984, 1986; Salikuddin 1990; Salikuddin & Brown 1990). In addition, aperture nonlinearity typically causes sinusoidally varying incident sound to produce periodic reflected and transmitted waves containing multiple harmonics of the incident wave frequency.

This mechanism of attenuation by kinetic energy production has long been exploited to increase the damping of *moderate amplitude* sound by the simple expedient of introducing a high Reynolds number mean flow (Barthel 1958; Bechert, Michel & Pfizenmaier 1977; Bechert 1979; Howe 1979, 1980a, b; Rienstra 1981; Cargill 1982; Hughes & Dowling 1990; Guo 1991). For example, the absorption of acoustic energy by a perforated screen is enhanced when a "bias flow" is maintained through the apertures. Viscous effects are important only in the immediate vicinity of the surface, where vorticity is produced by the acoustic oscillations; the vorticity is subsequently swept away by the mean flow and its kinetic energy is permanently lost to the incident sound. When the *fluid loading* is small, such as for a steel plate in air, it is usually permissible to estimate the damping by assuming the screen to be rigid, but for plates immersed in liquids the loading is often large enough that high acoustic intensities are accompanied by significant structural vibrations. Vorticity production is then modulated both by the sound *and* the surface motions. Thus, a bias flow may be expected to cause

enhanced absorption of *structural vibrations* as well as sound.

An experimental investigation is currently in progress at Boston University to quantify the influence of grazing and bias flows on the absorption of structural vibrations by a perforated plate. In this paper the importance of nonlinear aperture motions on damping is examined in the *absence* of mean flow. An objective is to assess the likely contribution of aperture nonlinearity to the observed attenuations. A generalized bending wave equation governing the propagation of small amplitude flexural motions of a thin, fluid loaded, perforated elastic plate has previously been applied (Howe 1995a, b) to determine the influence of mean flow (either a bias flow, or a tangential mean flow) on damping. This equation is also applicable in the absence of mean flow and for nonlinear aperture motions, provided the plate motion is linear. Cummings (1986) has proposed a simple and convenient system of nonlinear equations for fluctuating forced motions in small circular apertures in the absence of mean flow, predictions of which have been validated by comparison with experiment. These equations are here adapted and used in conjunction with the generalized bending wave equation to investigate the interaction of long wavelength sound and flexural vibrations with apertures in a thin elastic plate. In particular, we consider the problems of the transmission of sound through a perforated plate, and the damping of bending waves.

The governing equations are reviewed in §2. The sound transmission problem is discussed in §3, where a comparison is made with corresponding predictions for a rigid screen. In §4 we investigate the interaction of a bending wave on a fluid loaded elastic plate with a single, isolated aperture, and make extension to bending waves propagating over a homogeneously perforated plate.

2. THE GOVERNING EQUATIONS

2.1 Nonlinear theory of unsteady high Reynolds number flow through a circular aperture

Consider a rigid wall of thickness h containing a circular cylindrical aperture of radius R. The wall is immersed in fluid of uniform mean density ρ_o and sound speed c_o, and a time-periodic pressure differential $[p] = p_2(t)-p_1(t)$ (of radian frequency $\omega > 0$) is applied across the wall as illustrated schematically in Figure 1. The mean value of [p] is assumed to vanish, so that there is no mean flow through the aperture; the aperture radius R and wall thickness h are assumed to be much smaller than the characteristic acoustic wavelength $2\pi/\kappa_o$, where $\kappa_o = \omega/c_o$ is the acoustic wavenumber. During the interval of time in which $p_1 > p_2$, fluid is forced through the aperture from left to right in the figure. The Reynolds number is assumed to be sufficiently large that the flow through the aperture separates and forms a jet.

To motivate the following discussion, the motion within the jet will first be assumed to be irrotational, and the pressure on the free surface of the jet is taken to be p_2. Let $V_A(t)$ denote the mean axial velocity of the jet where it enters the aperture (at O in the figure). Bernoulli's equation applied to the axial streamline within the jet between O and the point marked J just within the potential flow region at the head of the jet, where the velocity is V_J and the pressure p_2, implies that

$$\frac{\partial}{\partial t}\{\varphi_J-\varphi_A\} + \tfrac{1}{2}V_J^2 - \tfrac{1}{2}V_A^2 = \frac{p_A-p_2}{\rho_o} , \qquad (2.1)$$

where φ_A and φ_J are the values of the velocity potential at O and J. The flow into the aperture may be regarded as entirely irrotational, so that we also have

$$\frac{\partial}{\partial t}\{\varphi_A-\varphi_1\} + \tfrac{1}{2}V_A^2 = \frac{p_1-p_A}{\rho_o} , \qquad (2.2)$$

where the motion at large distances ($\gg$ R) from the aperture in the irrotational domain is assumed to be small enough to be governed by linearized equations, i.e., $p_1 \approx -\rho_o \partial\varphi_1/\partial t$.

Rayleigh's formula (Rayleigh 1945) can be used to write $\varphi_A - \varphi_1 = \lambda_1 V_A(t)$, where $\lambda_1 \approx 0.82R$ is the "end-correction" of the circular opening into the irrotational region. Also,

$$\partial\varphi_J/\partial t - \partial\varphi_A/\partial t = \int_0^{z_J} \partial v(\xi,t)/\partial t \, d\xi,$$

where $v(z,t)$ is the velocity on the axis of the jet at distance z from the inlet plane. The value of the integral in this formula is denoted by $\ell'(t)\partial V_A/\partial t$, where $\ell'(t)$ is a suitable, time dependent length.

Inserting these expressions into equations (2.1), (2.2) and adding, we find

$$\ell(t)\frac{\partial V_A}{\partial t} + \tfrac{1}{2}V_J^2 = \frac{-[p]}{\rho_o} , \tag{2.3}$$

where $\ell(t) = \lambda_1 + \ell'(t)$. Equation (2.3) describes the motion of a slug of fluid of variable effective length $\ell(t)$ and variable mass $\rho_o A_o \ell(t)$ (where $A_o \equiv \pi R^2$ is the area of the aperture) subject to a driving pressure $p_1 - p_2$ and a resistive force $-\frac{1}{2}\rho_o A_o V_J^2$. In the half-cycle during which the flow through the aperture is from right to left in Figure 1, equation (2.3) remains valid provided the sign of the nonlinear resistive term is reversed. The velocity V_J can be eliminated by writing $V_J = V_A(t)/\eta$, where η is a contraction coefficient. By this means we arrive at the following equation describing reciprocating, periodic flow through the aperture (Cummings & Eversman 1983; Cummings 1986)

$$\ell(t)\frac{\partial V_A}{\partial t} + \frac{V_A|V_A|}{2\eta^2} = \frac{-[p]}{\rho_o} . \tag{2.4}$$

If the flow were entirely irrotational (no jet formation) the length $\ell(t)$ would be constant and equal to $\lambda_1+\lambda_2$, where $\lambda_2 \approx \lambda_1+h \approx 0.82R + h$ (Rayleigh 1945). When separation occurs $\ell(t)$ can be expressed in terms of an effective length of the jet defined by

$$L(\tau) = \int_0^{\tau} |V_A(t)| dt , \tag{2.5}$$

where the time τ is measured from the beginning of the half cycle during which the sign of $V_A(t)$ is constant. From an analysis of data derived from aperture flow experiments performed by Ingard (1953), Thurston, Hargrove & Cook (1957) and Ingard & Ising (1967), in which the working fluid was either water or air,

Cummings (1986) deduced the following empirical relation between the lengths $\ell(t)$ and L,

$$\ell(t) = \lambda_1 + \frac{\lambda_2}{1+\beta(L/D)^{1.585}}, \quad \beta = \tfrac{1}{3}, \quad D = 2R. \tag{2.6}$$

There is no corresponding formula for the dependence of the contraction ratio η on τ. This would be expected to vary significantly only near the beginning of a half cycle when, however, the nonlinear resistance is small. Experiments for *steady flow* suggests that $\eta \approx 0.61$, but in a careful comparison of predictions of equations (2.4) - (2.6) with experiments involving high amplitude sound incident on small circular apertures, Cummings (1986) has concluded that η may be regarded as constant and equal to 0.75.

2.2 The generalized bending wave equation

Consider next a thin elastic plate of bending stiffness B, mass density $\rho_s = m/h$ (m being the mass of unit area of the plate) and Poisson's ratio σ, perforated with small circular apertures of equal radius R which are distributed uniformly with N per unit area. In the undisturbed state, let the median plane of the plate occupy the plane $z = 0$ of the rectangular coordinate system (x,y,z). The *fractional open area* $\alpha = N\pi R^2$ is assumed to be small, so that the average distance d ($\sim 1/\sqrt{N}$) between neighboring apertures is very much greater than R. When $\alpha \ll 1$ the average equation governing motion of the fluid-coupled plate whose length scale is large relative to d can be cast in the form (Howe 1995a)

$$(1-\alpha)\left(\left[1 - \frac{2\alpha\sigma}{(1-\sigma)}\right]B\nabla_2^4 + m\frac{\partial^2}{\partial t^2}\right)\zeta_P + [p] = 2\alpha R\rho_o\frac{\partial^2\zeta_A}{\partial t^2}, \tag{2.7}$$

where $\nabla_2^4 \equiv (\partial^2/\partial x^2+\partial^2/\partial y^2)^2$, ζ_P, ζ_A respectively denote the displacement of the plate and the mean fluid displacement in the apertures, both measured in the x_2-direction, $[p] = p(x,y,+0,t) - p(x,y,-0,t)$ is the pressure jump across the plate, and all quantities are averaged over a region of the plate containing many apertures. The flexural motions of the plate are small, and governed by linear theory, but the fluid motion in the apertures can be large, and satisfy in a first approximation (Howe 1995a) equations (2.4) - (2.6), wherein $V_A \equiv V_A(x,y,t) = \partial\zeta_A/\partial t$.

3. ABSORPTION OF SOUND AT A PERFORATED ELASTIC SCREEN

3.1 Equations of motion

The equations of §2 are first applied to estimate the influence of flexural motions on the transmission of sound through a perforated screen (the average aperture spacing d being small compared to the characteristic wavelength of the sound). Consider the simplest case, depicted in Figure 2, in which a plane, time-harmonic acoustic wave of pressure $p = p_I \cos\{\omega(t-z/c_o)\}$ (where p_I is constant and $\omega > 0$) is incident from $z < 0$ on a thin elastic screen of thickness h, whose median plane is $z = 0$. The transmitted and reflected acoustic pressures at distances $|z| > d$ from the screen must also be plane periodic waves, so that

$$\begin{aligned} p &= p_I \cos\{\omega(t-z/c_o)\} + p_R(t+z/c_o), \quad z < 0, \\ &= p_T(t-z/c_o), \quad z > 0, \end{aligned} \tag{3.1}$$

where, because of the nonlinear motions in the apertures, the transmitted and reflected waves $p_T(t+z/c_o)$ and $p_R(t+z/c_o)$ are generally not simple harmonic.

Equation (2.10) supplies the functional relations

$$p_T(t) = \rho_o c_o V(t), \quad p_R(t) = p_I \cos(\omega t) - \rho_o c_o V(t), \tag{3.2}$$

which determine the reflected and transmitted waves in terms of the aggregate normal velocity V of the perforated plate, and yield

$$[p] = 2p_I \cos(\omega t) - 2\rho_o c_o V(t).$$

Substituting this expression for [p] in equations (2.3), (2.7), and expressing ζ_A and ζ_P in terms of V and V_A, the equations governing the fluid-structure interaction reduce to

$$\left.\begin{aligned} \ell(t)\frac{\partial V_A}{\partial t} + \frac{V_A|V_A|}{2\eta^2} + 2c_o V(t) &= \frac{2p_I}{\rho_o}\cos(\omega t), \\ m\frac{\partial V}{\partial t} + 2\rho_o c_o V - \alpha(m + 2R\rho_o)\frac{\partial V_A}{\partial t} &= 2p_I \cos(\omega t), \end{aligned}\right\} \tag{3.3}$$

where $\ell(t)$ is determined by equation (2.6), in which L is the discontinuous

function defined by the differential form of (2.5):

$$\frac{\partial L}{\partial t} = |V_A|, \quad L = 0 \text{ when } V_A = 0. \tag{3.4}$$

The periodic solution of these equations must be determined numerically for prescribed values of the incident pressure amplitude p_I and frequency ω. This is done by assuming that p_I vanishes for $t < 0$, that $V = V_A = 0$ at $t = 0$, and integrating for $t > 0$ until the solution becomes stably periodic, usually after three or four cycles.

The acoustic power incident on unit area of the screen is

$$\Pi_I = p_I^2/2\rho_o c_o$$

when averaged over one cycle $2\pi/\omega$. Similarly, the mean reflected and transmitted sound powers per unit area are given respectively by

$$\Pi_R = \frac{\omega}{2\pi\rho_o c_o}\int \left(p_I\cos(\omega t) - \rho_o c_o V(t)\right)^2 dt, \quad \Pi_T = \frac{\omega\rho_o c_o}{2\pi}\int V^2(t)\, dt, \tag{3.5}$$

where the integrations are over one acoustic cycle.

An absorption coefficient may also be defined by

$$\Delta = 1 - \frac{\Pi_R + \Pi_T}{\Pi_I} = \frac{2\rho_o c_o \omega}{\pi p_I^2}\int V(t)[p_I\cos(\omega t) - \rho_o c_o V(t)]\, dt, \tag{3.6}$$

which is the fractional acoustic power absorbed by vorticity production at the screen.

3.2 Numerical results

It is convenient to introduce dimensionless velocities and time as follows:

$$\bar{V} = V/(\omega R), \quad \bar{V}_A = V_A/(\omega R); \quad T = \omega t/2\pi. \tag{3.7}$$

Let the fluid be an ideal gas of mean pressure $p_o = \rho_o c_o^2/\gamma$, where γ is the ratio of specific heats. The incident wave amplitude p_I may then be normalized with respect to p_o, and equations (3.3) - (3.6) become

$$\left.\begin{aligned} \frac{M}{R}\frac{\partial \bar{V}_A}{\partial T} + \frac{\pi}{\eta^2}\bar{V}_A|\bar{V}_A| + \frac{4\pi\bar{V}}{(\kappa_o R)} &= \frac{4\pi(p_I/p_o)}{\gamma(\kappa_o R)^2}\cos(2\pi T) \\ \frac{\partial \bar{V}}{\partial T} + \frac{4\pi\bar{V}}{(\kappa_o R)}\left(\frac{R\rho_o}{m}\right) - \alpha\left(1 + \frac{2R\rho_o}{m}\right)\frac{\partial \bar{V}_A}{\partial T} &= \frac{4\pi(p_I/p_o)}{\gamma(\kappa_o R)^2}\left(\frac{R\rho_o}{m}\right)\cos(2\pi T) \\ \frac{\partial}{\partial T}\left(\frac{L}{D}\right) &= \pi|\bar{V}_A|, \quad D = 2R, \end{aligned}\right\} \quad (3.8a, b, c)$$

$$\Delta = \frac{4(\gamma\kappa_o R)^2}{(p_I/p_o)^2}\int_0^1 \bar{V}(T)\left(\frac{(p_I/p_o)}{\gamma\kappa_o R}\cos(2\pi T) - \bar{V}(T)\right) dT, \quad (3.9)$$

where $\kappa_o = \omega/c_o$ is the acoustic wavenumber of the fundamental mode, and ℓ/R is defined by (2.6) with $\lambda_1 = 0.82R$, $\lambda_2 = 0.82R + h$. In this form the equations clearly exhibit the dependence of the fluid-structure interaction on the dimensionless quantities

$$p_I/p_o,\ \rho_o/\rho_s,\ R/h,\ \kappa_o R \text{ and } \alpha.$$

Figures 3 - 5 depict typical numerical predictions for an aluminium plate in air with fractional open area $\alpha = 0.03$ and $R = 10h$. The thick and thin curves in Figure 3 represent the respective contributions of the components αV_A and $(1-\alpha)V_P$ of the normal velocity V (i.e., the respective contributions from the aperture fluxes and the plate motion) for $\kappa_o R = 0.1$ and different incident wave amplitudes. Each pair of curves is plotted to the same scale for a given value of p_I/p_o, but the scales for different values of p_I/p_o are not the same. At low acoustic amplitudes the motion is dominated by the aperture flows, which are essentially simple harmonic; the very much smaller amplitude plate motions are seen to be in phase with the aperture velocity. As the acoustic amplitude increases, higher harmonic components of the fundamental frequency make progressively larger contributions to the aperture flux, and the plate motion becomes larger, but still simple harmonic. However, the phases of the plate and aperture motions diverge as p_I/p_o increases, the difference being close to 90° when $p_I/p_o = 0.1$.

The dependence of the absorption coefficient Δ on the acoustic amplitude is plotted in Figure 4 for several values of $\kappa_o R$ (the range of values of p_I/p_o

in the figure corresponds to sound pressures between about 110 - 170 dB (re 2×10^{-5} N/m^2)). The curves for $\kappa_o R \geq 0.05$ are essentially identical to those for a rigid perforated plate of the same thickness (which can be calculated by letting $\rho_o R/m \to 0$ in equations (3.8)). At lower frequencies, however, the elastic plate becomes progressively more transparent to the incident sound and, whereas the rigid plate damping tends to a finite limit for each value of $\kappa_o R$, the elastic plate damping ultimately decreases to zero. This is clear from Figure 5, which compares the absorption coefficients for elastic and rigid screens as a function of frequency for two values of p_I/p_o.

4. NONLINEAR DAMPING OF BENDING WAVES

4.1 Absorption by a single aperture

A flexural wave propagating over a thin, fluid loaded elastic plate of thickness h is accompanied by a traveling pressure field which takes equal and opposite values at opposite points on the surfaces of the plate. If the wave encounters a small, isolated aperture, this pressure differential causes fluid to flow through the aperture, and part of the incident energy is converted into the kinetic energy of the vorticity produced in the aperture. An approximate expression for the wave energy absorbed in this way is easily derived as follows.

Let the bending wave propagate in the x-direction and denote the displacement of the plate by

$$\zeta = \mathrm{Re}\left(Z_p e^{i(kx-\omega t)}\right), \quad k,\ \omega > 0, \tag{4.1}$$

where Z_p is constant and $kh \ll 1$ (wavelength $\gg$ h). It follows from equations (2.8) and (2.9) that the pressure jump $[p] = p(x,y,+0,t) - p(x,y,-0,t)$ is

$$[p] = -\mathrm{Re}\left(\frac{2\rho_o \omega^2 Z_p}{\sqrt{k^2-\kappa_o^2}} e^{i(kx-\omega t)}\right). \tag{4.2}$$

The bending wavenumber k is the real positive zero of the dispersion equation obtained by substituting from (4.1) and (4.2) into equation (2.7) with $\alpha = 0$ and ζ_p set equal to ζ, i.e., of

$$D(k,\omega) \equiv Bk^4 - m\omega^2 - \frac{2\rho_o \omega^2}{\sqrt{k^2-\kappa_o^2}} = 0. \tag{4.3}$$

This zero satisfies $k > \kappa_o$, and characterizes a wave that propagates subsonically relative to the fluid, and whose influence decays exponentially with distance from the plate.

Suppose the wave impinges on a small circular aperture whose center is at the origin, and whose radius R is much smaller than the bending wavelength ($kR \ll 1$). It may be assumed, without loss of generality, that Z_p is real, so that the velocity in the aperture, V_A, is determined by equation (2.4) with the

right hand side replaced by $(2\omega^2 Z_p/\sqrt{k^2-\kappa_o^2})\cos(\omega t)$. When the equation is nondimensionalized as in (3.7), we obtain

$$\frac{\ell}{R}\frac{\partial \bar{V}_A}{\partial T} + \frac{\pi}{\eta^2}\bar{V}_A|\bar{V}_A| = \frac{4\pi Z_p}{R^2\sqrt{k^2-\kappa_o^2}}\cos(2\pi T). \tag{4.4}$$

The bending wave power Π_A dissipated at the aperture is supplied to the aperture flow via the driving pressure [p], and is easily seen to be equal to $-\pi R^2\langle V_A[p]\rangle$, where the angle brackets denote a time average, i.e.,

$$\Pi_A = -\tfrac{1}{2}\omega R^2 \int V_A(t)[p(t)]dt, \tag{4.5}$$

where the integration is over the period $2\pi/\omega$ of the wave. The energy flux associated with the incident bending wave is shared between that propagated by the elastic motions in the plate and that conveyed in the evanescent motions of the fluid. The power flux Π, say, per unit length of wavefront parallel to the plate can be calculated from the formula $\Pi = (\omega|Z_p|^2/4)\partial D(k,\omega)/\partial k$, where D is the dispersion function (4.3), and the derivative is evaluated at the bending wavenumber. The ratio Π_A/Π defines the absorption cross-section of the aperture, which may be cast in the following nondimensional form,

$$\Sigma \equiv \frac{\Pi_A}{2R\Pi} = \frac{4\pi R^2\rho_o\omega^2\kappa_o\sqrt{k^2-\kappa_o^2}}{k[5k^4-4(k\kappa_o)^2-m\omega^2]}\frac{1}{M}\int_0^1 \bar{V}_A(T)\cos(2\pi T)dT. \tag{4.6}$$

where $M = \omega Z_p/c_o$ is the amplitude of the bending wave surface velocity expressed as a Mach number.

The dependence of $\Pi_A/2R\Pi$ on frequency predicted by this formula is shown in Figures 6 and 7 for different values of M respectively for the two cases (i) a steel plate in water with R/h = 3, and (ii) an aluminium plate in air with R/h = 10. In these figures the frequency is normalized by the coincidence frequency of the plate: $\omega_c = c_o^2(m/B)^{1/2}$ (above which bending waves *in vacuo* have phase velocity $\omega/k > c_o$). These results indicate that, however small be the amplitude M of the incident wave, a significant fraction of the wave energy is absorbed at sufficiently small frequencies, where the curves peak.

Equation (4.6) can be used to derive an approximate formula for the damping of bending waves on a homogeneously perforated plate. If there are N apertures per unit area of the plate, the change $\delta\Pi$ in the bending wave power over a distance δx in the direction of propagation of the wave is approximately equal to $-2NR\Pi\Sigma\delta x$, i.e.,

$$\frac{-1}{\Pi}\frac{\partial\Pi}{\partial x} = 2NR\Sigma \equiv \frac{8\alpha\kappa_o R\rho_o\omega^2\sqrt{k^2-\kappa_o^2}}{k[5k^4-4(k\kappa_o)^2-m\omega^2]}\frac{1}{M}\int_0^1 \bar{V}_A(T)\cos(2\pi T)dT. \qquad (4.7)$$

To account for damping the amplitude Z_p of the plate motion must now decrease with increasing x. If we define

$$k_I = \frac{-1}{Z_p}\frac{\partial Z_p}{\partial x} = \frac{-1}{2\Pi}\frac{\partial\Pi}{\partial x}, \qquad (4.8)$$

then $\zeta_p = \mathrm{Re}\left(Z_o e^{i(kx-\omega t)-k_I x}\right)$, i.e., $Z_p = Z_o e^{-k_I x}$, where $Z_p = Z_o$ at $x = 0$. k_I (>0) may be regarded as the imaginary component of a complex wavenumber $\kappa = k+ik_I$, where, however, k_I must itself depend on x, because of the nonlinear nature of the damping.

This formula for k_I neglects the collective influence of the apertures on the wavenumber k, i.e., it assumes that the bending wave dispersion equation is (4.3), as for an unperforated plate. Similarly, it ignores the important fact that the amplitude of the motion in the apertures will tend to be smaller than for an isolated aperture, because the pressure difference [p] must be very much smaller for the perforated plate, even if the amplitude of the plate motion is unchanged. Thus, equation (4.7) would be expected to determine an *upper bound* for the actual damping due to vorticity production.

It is convenient to express the attenuation in terms of the fractional power dissipated per wavelength ($2\pi/k$) of propagation, which is equal to $40\pi\log_{10}(e)k_I/k$ (dB) $\approx 5.46k_I/k$ (dB). Predictions of this derived from (4.7), (4.8) are illustrated in Figure 8 for a thin aluminium screen in air with 3% fractional open area and aperture radius R = 10h, when the vibration Mach number $M = 10^{-5}$, 10^{-4} and 10^{-3}. These results, and the physical constraints on the amplitudes of possible plate motions in practice, suggest that the damping is significant only at small frequencies $\omega/\omega_c \sim M$ (when the aperture

motion is nonlinear even when $M \to 0$, because the lengths of the jets become large when the period $2\pi/\omega \to \infty$).

4.2 Equations for bending waves on a perforated plate

To obtain more precise estimates of the damping, and extend these results to underwater applications where the pressure differential [p] produced by surface motion might be expected to be very much larger than in air, we now proceed to the formulate a self-consistent analytical model of flexural wave propagation over a homogeneously perforated plate. Consider motions in which the displacement ζ_P of the plate has the harmonic, traveling wave form

$$\zeta_P = \mathrm{Re}\left[Z_P e^{i(\kappa x - \omega t)}\right], \quad \omega > 0, \tag{4.9}$$

where Z_P may be taken to be a real, positive constant. The wavenumber κ must be complex, however, and for propagation in the positive x-direction we write,

$$\kappa = k + ik_I, \tag{4.10}$$

where both k and k_I must both be positive.

Expand the mean aperture displacement ζ_A in the form

$$\zeta_A = \mathrm{Re}\left[Z_A^1 e^{i(\kappa x - \omega t)} + \sum_{n\geq 2} Z_A^n e^{in(kx - \omega t)}\right], \tag{4.11}$$

where the coefficients Z_A^n $(n \geq 1)$ are generally complex quantities. The first of these, Z_A^1 is assumed to be *constant*, so that the decay of this term as the wave propagates is accounted for by the imaginary part of the wavenumber κ. This hypothesis, and the related assumption that Z_P is constant, is correct in a first approximation; it will be seen, however, that Z_A^1 and Z_P must actually vary slowly with x, but only over distances large compared to the dissipation length $1/k_I$. The higher order terms in (4.11) have real wavenumber k, and their decay is accounted for by assuming the coefficients Z_A^n $(n \geq 2)$ to be slowly varying functions of x on a scale of the bending wavelength $2\pi/k$.

The pressure fluctuations on either side of the plate satisfy the linear wave equation (2.8). The solution of this equation must have "outgoing" behavior with respect to the plate, and may be expressed in terms of ζ_P and ζ_A via the boundary conditions (2.9) where, as before, the median section of the

plate is assumed to coincide with the plane z = 0 in the undisturbed state. At distances from the plate that are large compared to the aperture spacing d, we find

$$p = -\mathrm{sgn}(z)\rho_o\omega^2 \mathrm{Re}\left\{\frac{[(1-\alpha)Z_P + \alpha Z_A^1]}{\sqrt{\kappa^2-\kappa_o^2}} e^{i(\kappa x-\omega t)-|z|\sqrt{\kappa^2-\kappa_o^2}}\right\}$$

$$- \frac{\alpha\,\mathrm{sgn}(z)\rho_o\omega^2}{\sqrt{k^2-\kappa_o^2}} \mathrm{Re}\left\{\sum_{n\geq 2} nZ_A^n e^{n(i(kx-\omega t)-|z|\sqrt{k^2-\kappa_o^2})}\right\}. \qquad (4.12)$$

The first term on the right hand side is the bending wave pressure field. The sum represents the contribution from the nonlinear components of the aperture motions. We shall argue that this latter contribution is negligible at distances much larger than d from the screen, because "waves" of wavenumbers nk and frequencies $n\omega$ ($n \geq 2$) induced by the aperture fluxes do not satisfy the dispersion equation (analogous to (4.3) and to be derived below) for flexural waves on the perforated plate, and their growth to finite amplitude is therefore opposed by the plate. Thus, the pressure jump that drives the aperture flows is taken to be

$$[p] = -2\rho_o\omega^2 \mathrm{Re}\left\{\frac{[(1-\alpha)Z_o + \alpha Z_A^1]}{\sqrt{\kappa^2-\kappa_o^2}} e^{i(\kappa x-\omega t)}\right\}. \qquad (4.13)$$

Further justification of this approximation is given in §4.4, where an alternative approach is outlined that is strictly applicable when the damping due to vorticity production is *small*.

The equation describing the unsteady motion in an aperture whose center is at (x,y) is deduced from (2.4) by replacing t by t - kx/ω, and [p] by (4.13). In nondimensional form we find

$$\frac{\ell}{R}\frac{\partial \bar{V}_A}{\partial T} + \frac{\pi}{\eta^2}\bar{V}_A|\bar{V}_A| = 4\pi \mathrm{Re}\left\{\frac{[(1-\alpha)\bar{Z}_P/R + \alpha\bar{Z}_A^1/R]e^{-2\pi iT}}{R\sqrt{\kappa^2-\kappa_o^2}}\right\}, \qquad (4.14)$$

where $T = (\omega t - kx)/2\pi$, and

$$\bar{Z}_P = Z_P e^{-ik_I x}, \quad \bar{Z}_A^1 = Z_A^1 e^{-ik_I x}. \qquad (4.15)$$

The solution of equation (4.14) depends on the complex wavenumber κ, which is the solution of the appropriate dispersion equation for the perforated plate. The latter is obtained by substituting from (4.9), (4.11) and (4.12) into the *linear*, generalized bending wave equation (2.7). When attention is confined that component of the motion of wavenumber κ and radian frequency ω the nonlinear terms from (4.11) and (4.12) may be discarded, and (2.7) yields

$$\left(1 - \frac{2\alpha\sigma}{1-\sigma}\right)B\kappa^4 - \left(1 - \frac{2\alpha R\rho_o}{(1-\alpha)m}\frac{Z_A^1}{Z_P}\right)m\omega^2 - \frac{2\rho_o\omega^2}{\sqrt{\kappa^2-\kappa_o^2}}\left(1 + \frac{\alpha}{1-\alpha}\frac{Z_A^1}{Z_P}\right) = 0. \qquad (4.16)$$

Equations (4.14) and (4.16) must solved simultaneously for $\overline{V}_A$, Z_A^1 and the wavenumber κ. The definition (4.11) supplies

$$\overline{Z}_A^1 = 2iR\int_0^1 \overline{V}(T)e^{2\pi T}\,dT. \qquad (4.17)$$

4.3 Numerical results

The nonlinear aperture equation (4.14) is solved in conjunction with equation (3.8c), which determines the variation of the length $\ell(T)$ via the empirical relation (2.6). The solution, which must be periodic with period 2π, depends on both the local amplitude $\overline{Z}_P$ of the plate motions and the wavenumber κ, given by (4.16).

The solution can be effected by the following iterative procedure. The frequency ω and magnitude $\overline{Z}_P$ of the local amplitude of the plate motion are prescribed, and equation (4.16) is first solved for κ by setting $Z_A^1/Z_P = 0$. This initial estimate for κ will be real, and corresponds to one of the two equal and opposite real roots of the dispersion equation (4.16) when $Z_A^1 = 0$; the positive root is selected when the wave is taken to propagate in the positive x-direction. The presence of the apertures will change this root, and endow it with a positive imaginary part k_I that accounts for the damping of the wave. Next, (i) equations (4.14) and (3.8c) are solved, and the result used to calculate a corrected value of $Z_A^1/Z_P \equiv \overline{Z}_A^1/\overline{Z}_P$ from (4.17); (ii) the revised value of Z_A^1/Z_P is inserted into (4.16) and the wavenumber κ is

re-calculated by iterating about its value for $Z_A^1/Z_P = 0$; steps (i) and (ii) are repeated until convergence is achieved.

If the local plate amplitude is expressed as a Mach number $M = \omega\bar{Z}_P/c_o$, this naive iteration procedure is found to converge rapidly except at very small values of M (typically less than 10^{-5}) and within an intermediate range of frequencies ω/ω_c marginally larger than M, wherein successive iterates of Z_A^1/Z_P tend to fluctuate wildly. This difficulty is avoided by using at stage (ii) of the iteration the running mean $\langle Z_A^1/Z_P \rangle$ instead of the most recently calculated approximation for Z_A^1/Z_P, where at the nth iteration

$$\langle Z_A^1/Z_P \rangle = \frac{1}{n-1} \sum_{j=1}^{n-1} (Z_A^1/Z_P)_j , \quad n > 1.$$

When n becomes large successive estimates κ_n of the wavenumber κ obtained in stage (i) are then found to converge monotonically, and a rapidly converging estimate for κ can be obtained by making use of a simple extrapolation formula of the type

$$\kappa \approx \kappa_{n-2} - (\kappa_{n-1} - \kappa) \left(\frac{\kappa_{n-1} - \kappa}{\kappa_n - \kappa} \right)^{\chi} , \qquad \chi = \ln[(n-1)/(n-2)]/\ln[n/(n-1)].$$

The fractional bending wave power dissipated per wavelength ($2\pi/k$) of propagation ($\approx 54.6k_I/k$ dB) calculated by this procedure is illustrated in Figure 9 for the aluminium plate in air considered in §4.1. A comparison of these predictions with those shown in Figure 8 (based on the absorption cross-section of an isolated aperture in an unperforated plate) reveals that the major differences occur at lower plate Mach numbers M. The scattering cross-section theory tends to overestimate the damping except at very low frequencies where the attenuation is small. Predictions of equations (4.14) - (4.17) for a perforated steel plate in water (for $\alpha = 0.05$ and $R/h = 3$) are given in Figure 10. Large fluctuations in pressure can now be caused by flexural motions of the plate because of the relatively high density of water, and the predicted attenuations are correspondingly much higher than for a screen in air.

To estimate the significance of these predictions, observe that for a plate of thickness h, the amplitude $\overline{Z}_P$ of the plate motion can be expressed in the form

$$\overline{Z}_P = \frac{Mh}{(\omega/\omega_c)(\omega_c h/c_o)}, \tag{4.18}$$

where $\omega_c h/c_o \approx 0.22$ and 0.95 respectively for an aluminium plate in air and a steel plate in water. Thus, ω/ω_c must typically be larger than M to ensure that the amplitude of the plate motion is small compared to the plate thickness. Although the latter condition is not strictly necessary for the applicability of the thin plate equation at low wavenumbers, structural motions are in practice unlikely to attain amplitudes comparable to h. Accordingly, it is only at frequencies $\omega/\omega_c \gg M$, to the right of the corresponding peaks in the Figures 9 and 10, that the present predictions are relevant. However, surface Mach numbers M are generally much smaller than discussed here, and correspondingly at the finite frequencies of interest in applications (typically $\omega/\omega_c > 10^{-4}$), it appears from these results that nonlinear damping will be negligible.

4.4 Alternative analysis applicable for small damping

The aperture equation (4.14) was derived by assuming that the dominant contribution to the local pressure jump [p] is given by the linear theory approximation (4.13), associated with the bending wave component of the pressure. This approximation accords with intuition, but its accuracy is difficult to quantify in general. An alternative formulation is possible when the damping is small, however, that fully justifies the approximation in that limit.

Let the plate and aperture displacements be taken in the form (c.f. (4.9), (4.11))

$$\zeta_P = \mathrm{Re}\left(Z_P e^{i(kx-\omega t)}\right), \quad \zeta_A = \mathrm{Re}\left(\sum_{n\geq 1} Z_A^n e^{in(kx-\omega t)}\right), \quad \omega > 0, \tag{4.19}$$

where the wavenumber k is required to be real and positive (for propagation in the positive x-direction), and where *all* of the coefficients Z_P and Z_A^n ($n \geq 1$) are assumed to be slowly varying functions of x on a scale of the flexural

wavelength $2\pi/k$. The damping of the wave is now accounted for by the decay of the coefficients Z_P and Z_A^1. As before, it may be assumed that Z_P is real.

The pressure in the fluid at distances $\gg$ d from the plate is

$$p = \frac{-\mathrm{sgn}(z)\rho_o\omega^2}{\sqrt{k^2-\kappa_o^2}}(1-\alpha)Z_P\cos(kx-\omega t)e^{-|z|\sqrt{k^2-\kappa_o^2}} + p_A, \tag{4.20}$$

where the first term on the right is the contribution from the plate motion, and p_A is the collective effect of the apertures. When the damping is small p_A may be regarded locally as a function of kx-ωt and z, in which case it satisfies the following reduced form of equation (2.8)

$$\left[\left(1 - \frac{\kappa_o^2}{k^2}\right)\frac{\partial^2}{\partial x^2} + \frac{\partial^2}{\partial z^2}\right]p_A = 0. \tag{4.21}$$

Now $\kappa_o^2/k^2 < 1$ for a subsonically propagating flexural wave, and the solution of this equation with outgoing wave behavior can therefore be expressed in terms of the limiting values as $z \to \pm 0$ of $\partial p_A/\partial z \equiv -\alpha\rho_o \partial V_A/\partial t$ by the methods of two-dimensional potential theory (Carrier, Krook & Pearson 1966). Correct to the present order of approximation we can write $\partial V_A/\partial t = -(k/\omega)\partial V_A/\partial x$, and it then follows that

$$p_A = \frac{\mathrm{sgn}(z)\alpha\rho_o\omega}{\pi\sqrt{k^2-\kappa_o^2}}\int_{-\infty}^{\infty}\frac{V_A(\tau)[\tau-(t-kx/\omega)]d\tau}{\{[\tau-(t-kx/\omega)]^2 + z^2(k^2/\omega^2-1/c_o^2)\}}. \tag{4.22}$$

The equation of motion of fluid in the aperture at (x,y) is formed by replacing t by t - kx/ω in equation (2.4), and calculating [p] from (4.20) and (4.22). In the usual nondimensional form the result is

$$\frac{\ell}{R}\frac{\partial \bar{V}_A}{\partial T} + \frac{\pi}{\eta^2}\bar{V}_A|\bar{V}_A| + \frac{4\alpha}{R\sqrt{k^2-\kappa_o^2}}\int_{-\infty}^{\infty}\frac{\bar{V}_A(T')dT'}{T'-T} = \frac{4\pi(1-\alpha)Z_P}{R^2\sqrt{k^2-\kappa_o^2}}\cos(2\pi T), \tag{4.23}$$

where $T = (\omega t - kx)/2\pi$. The principal value of the integral represents the pressure jump associated with the aperture flows.

The solution of this equation determines ζ_A from the relation $\partial\zeta_A/\partial t = V_A$, from which we find

$$Z_A^1 = 2iR\int_0^1 \bar{V}_A(T)e^{2\pi iT}\,dT. \tag{4.24}$$

Next substitute from (4.19) and (4.20) into the generalized bending wave equation (2.7). In this linear equation we are concerned solely with that component of the solution of wavenumber k and frequency ω, but with account taken of the slow variation in the amplitudes Z_p, Z_A^1 caused by damping. Hence, we can set

$$[p] = \frac{-2\rho_o\omega^2}{\sqrt{k^2-\kappa_o^2}}\,\mathrm{Re}\left\{[(1-\alpha)Z_p + \alpha Z_A^1]e^{i(kx-\omega t)}\right\}. \tag{4.25}$$

When these various substitutions are made in equation (2.7) and the separate coefficients of $\cos(2\pi T)$ and $\sin(2\pi T)$ in the resulting equation are equated to zero, we find

$$\left(1 - \frac{2\alpha\sigma}{1-\sigma}\right)Bk^4 - \left(1 - \frac{2\alpha R\rho_o}{(1-\alpha)m}\frac{Z_{Ar}^1}{Z_p}\right)m\omega^2 - \frac{2\rho_o\omega^2}{\sqrt{k^2-\kappa_o^2}}\left(1 + \frac{\alpha Z_{Ar}^1}{(1-\alpha)Z_p}\right) = 0, \tag{4.26}$$

$$\frac{-1}{Z_p}\frac{\partial Z_p}{\partial x} = \frac{2\alpha(Z_{Ai}^1/Z_p)\rho_o\omega^2\sqrt{k^2-\kappa_o^2}[1 - R\sqrt{k^2-\kappa_o^2}]}{k\left[\left(1-\frac{2\alpha\sigma}{1-\sigma}\right)(5k^2 - 4\kappa_o^2)Bk^2 - \left(1 - \frac{2\alpha R\rho_o}{(1-\alpha)m}\frac{Z_{Ar}^1}{Z_p}\right)m\omega^2\right]}, \tag{4.27}$$

where Z_{Ar}^1, Z_{Ai}^1 respectively denote the real and imaginary parts of Z_A^1. In deriving these equations derivatives of Z_p of higher order than the first have been neglected, and we have used the result $(1/Z_p)\partial Z_p/\partial x \approx (1/Z_{Ar}^1)\partial Z_{Ar}^1/\partial x$

When the ratio Z_A^1/Z_p is known, equation (4.26) becomes the dispersion equation that determines the *real* wavenumber k in terms of ω. For this value of k equation (4.27) defines an imaginary wavenumber component $k_I = -(1/Z_p)\partial Z_p/\partial x$, in terms of which the fractional wave power absorbed per wavelength is $54.6k_I/k$ dB, as before.

Equations (4.23) - (4.27) are to be solved simultaneously with equation (3.8c), and this is accomplished by the iterative procedure described in §4.3. The details are simplified by observing that, when $\bar{V}_A(T)$ has period 1, the principal value integral of (4.23) can be transformed to a regular integral

over (0,1), and (4.23) cast in the form

$$\frac{\ell}{R}\frac{\partial \bar{V}_A}{\partial T} + \frac{\pi}{\eta^2}\bar{V}_A|\bar{V}_A| + \frac{4\pi\alpha}{R\sqrt{k^2-\kappa_o^2}}\int_0^1 \frac{\{\bar{V}_A(T') - \bar{V}_A(T-[T])\}dT'}{\tan\{\pi(T'-(T-[T]))\}} = \frac{4\pi(1-\alpha)Z_P}{R^2\sqrt{k^2-\kappa_o^2}}\cos(2\pi T) \ , \tag{4.28}$$

where [T] is the integer part of T. The periodic solution of this equation is obtained by integrating from T = 0, with $\bar{V}_A(0) = 0$. During the first period $0 < T < 1$ the contribution from the integral is ignored. Integration of the equation over subsequent periodic intervals (n, n+1) is performed by evaluating the integral from the solution in (n-1,n). This procedure typically yields a closely periodic solution for $n > 6$.

The calculations have been performed for two of the cases discussed in §4.3 involving an aluminium plate in air and a steel plate in water, both for a surface Mach number $M = \omega Z_p/c_o = 10^{-4}$. The predicted attenuations are indicated by the dotted curves in Figures 9 and 10, and are seen to conform closely to the corresponding predictions based on the approximation (4.13). This agreement occurs only for the small attenuations obtaining in these cases, however. Indeed, equations (4.26) and (4.27), which determine k and $k_I \equiv -(1/Z_p)\partial Z_p/\partial x$, may also be deduced from the general dispersion equation (4.16), by expanding the solution $\kappa = k + ik_I$ in powers of Z^1_{Ai}/Z_p. The zeroth and first order approximations are respectively equivalent to equations (4.26) and (4.27). Equations (4.26) and (4.27), with terms of $O(\alpha^2)$ discarded, may also be seen to reduce to the scattering cross-section approximation (4.3), (4.7) (wherein the integral determines $Z^1_{Ai}/2R$).

5. CONCLUSION

In this paper we have investigated the influence of flow nonlinearity in the apertures of a perforated elastic screen on the attenuation of sound and of flexural vibrations. The damping is a result of the direct transfer of acoustic or vibrational energy to the kinetic energy of vorticity generated in the apertures by the incident disturbance. The sound or flexural wave produces a pressure differential across the plate, causing fluid to "jet" through the apertures. Large amplitude sound waves can experience substantial attenuations which, however, progressively diminish at lower frequencies, when an elastic plate ultimately becomes transparent to incident sound. Similarly, it is predicted that flexural waves can be significantly damped, by several dB per wavelength of propagation. Aperture nonlinearity is particularly important for low amplitude bending waves at low frequencies $\omega/\omega_c \approx M$ (M being the Mach number of the plate surface velocity), when the wave period is sufficiently long that nonlinear processes within an aperture have ample time acquire a relatively large amplitude. However, the frequencies at which this occurs are likely to be below those normally of interest in practice. At higher frequencies, and at surface wave amplitudes encountered in applications, the predicted structural damping is usually small, and it is certainly negligible compared with that which can be achieved (by the same vorticity production mechanism) when there exists a grazing mean flow past the screen or bias flow through the apertures.

REFERENCES

Barthel, F. 1958 *Frequenz* **12**, 1 - 11. Investigations on nonlinear Helmholtz resonators.

Bechert, Michel & Pfizenmaier, E. 1977 *AIAA Paper 77-1278*. Experiments on the transmission of sound through jets.

Bechert, D. W. 1979 *AIAA Paper* 79-0575. Sound absorption caused by vorticity shedding, demonstrated with a jet flow.

Cargill, A. M. 1982 *J. Sound Vib.* **83**, 339 - 354. Low frequency acoustic radiation from a jet pipe - a second order theory.

Carrier, G. F., Krook, M. & Pearson, C. E. 1966 *Functions of a complex variable*. New York: McGraw-Hill.

Cummings, A. 1984 *AIAA J.* **22**, 786 - 792. Acoustic nonlinearities and power losses at orifices.

Cummings, A. 1986 *J. Acoust. Soc. Am.* **79**, 942 - 951. Transient and multiple frequency sound transmission through perforated plates at high amplitude.

Cummings, A. & Eversman, W. 1983 *J. Sound Vib.* **91**, 503 - 518. High amplitude acoustic transmission through duct terminations: theory.

Guo, Y. P. 1991 *J. Sound Vib.* **145**, 179 - 194. Sound diffraction and dissipation at a sharp trailing edge in a supersonic flow.

Howe, M. S. 1979 *Proc. Roy. Soc. Lond.* **A366**, 205 - 233. On the theory of unsteady high Reynolds number flow through a circular aperture.

Howe, M. S. 1980a *J. Sound Vib.* **70**, 407 - 411. The dissipation of sound at an edge.

Howe, M. S. 1980b *Proc. Roy. Soc. Lond.* **A370**, 523 - 544. On the diffraction of sound by a screen with circular apertures in the presence of a low Mach number grazing flow.

Howe, M. S. 1995a *European J. Appl. Math.* (in press). The damping of flexural and acoustic waves by a bias-flow perforated elastic plate.

Howe, M. S. 1995b *J. Sound Vib.* (in press). Energy conservation and the damping of flexural waves by vorticity production.

Hughes, I. J. & Dowling, A. P. 1990 *J. Fluid Mech.* **218**, 299 - 336. The absorption of sound by perforated linings.

Ingard, U. & Ising, H. 1967 *J. Acoust. Soc. Am.* 42, 6 - 17. Acoustic nonlinearity of an orifice.

Melling, T. H. 1973 *J. Sound Vib.* 29, 1 - 65. The acoustic impedance of perforates at medium and high sound pressure levels.

Rayleigh, Lord 1945 *Theory of Sound*, Vol 2. New York: Dover.

Rienstra, S. W. 1981 *J. Fluid Mech.* 108, 443 - 460. Sound diffraction at a trailing edge.

Salikuddin, M. 1990 *J. Sound Vib.* 139, 361 - 382. Acoustic behaviour of orifice plates and perforated plates with reference to low-frequency sound absorption.

Salikuddin, M. & Brown, W. H. 1990 *J. Sound Vib.* 139, 383 - 406. Nonlinear effects in finite amplitude wave propagation through orifice plate and perforated terminations.

Sivian, J. L. 1935 *J. Acoust. Soc. Am.* 7, 94 - 101. Acoustic impedance of small orifices.

Thurston, G. B., Hargrove, L. E. & Cook, W. D. 1957 *J. Acoust. Soc. Am.* 29, 992 - 1001. Nonlinear properties of circular orifices.

Zinn, B. T. 1970 *J. Sound Vib.* 13, 347 - 356. A theoretical study of nonlinear damping by Helmholtz resonators.

PRINCIPAL SYMBOLS

B	bending stiffness of the plate
c_o	speed of sound in the fluid
$D(k,\omega)$	dispersion function (4.3)
h	plate thickness
k	real part of flexural wavenumber
k_I	imaginary part of flexural wavenumber
K_R	Rayleigh conductivity
ℓ	aperture flow length defined by (2.6)
L	effective jet length
m	$\rho_s h$, mass per unit area of the plate
M	$\omega Z_P/c_o$ or $\omega \overline{Z}_P/c_o$, Mach number of the plate displacement velocity
N	number of apertures per unit area of the plate
p	pressure
$[p]$	$p(x,y,+0)-p(x,y,-0)$
R	aperture radius
t	time
T	$\omega t/2\pi$ or $(\omega t-kx)/2\pi$
V	aggregate plate velocity, (2.10)
V_A	mean aperture velocity
V_J	jet velocity
Z_A^n	amplitude of the nth Fourier coefficient of the aperture motion
Z_P	amplitude of plate displacement

α	$N\pi R^2$, fractional open area of the plate
Δ	absorption coefficient (3.6)
η	contraction ratio of jet
ζ	$(1-\alpha)\zeta_P+\alpha\zeta_A$
ζ_A	mean displacement of fluid in an aperture
ζ_P	displacement of the plate
κ	$k+ik_I$, complex wavenumber

κ_o	ω/c_o, acoustic wavenumber
φ	velocity potential
λ_1, λ_2	end correction
ρ_o	mean fluid density
ρ_s	density of plate material
σ	Poisson's ratio of the plate material
Σ	scattering cross-section (4.6)
Π	acoustic or bending wave power
ω	radian frequency
ω_c	$c_o^2(m/B)^{1/2}$, coincidence frequency

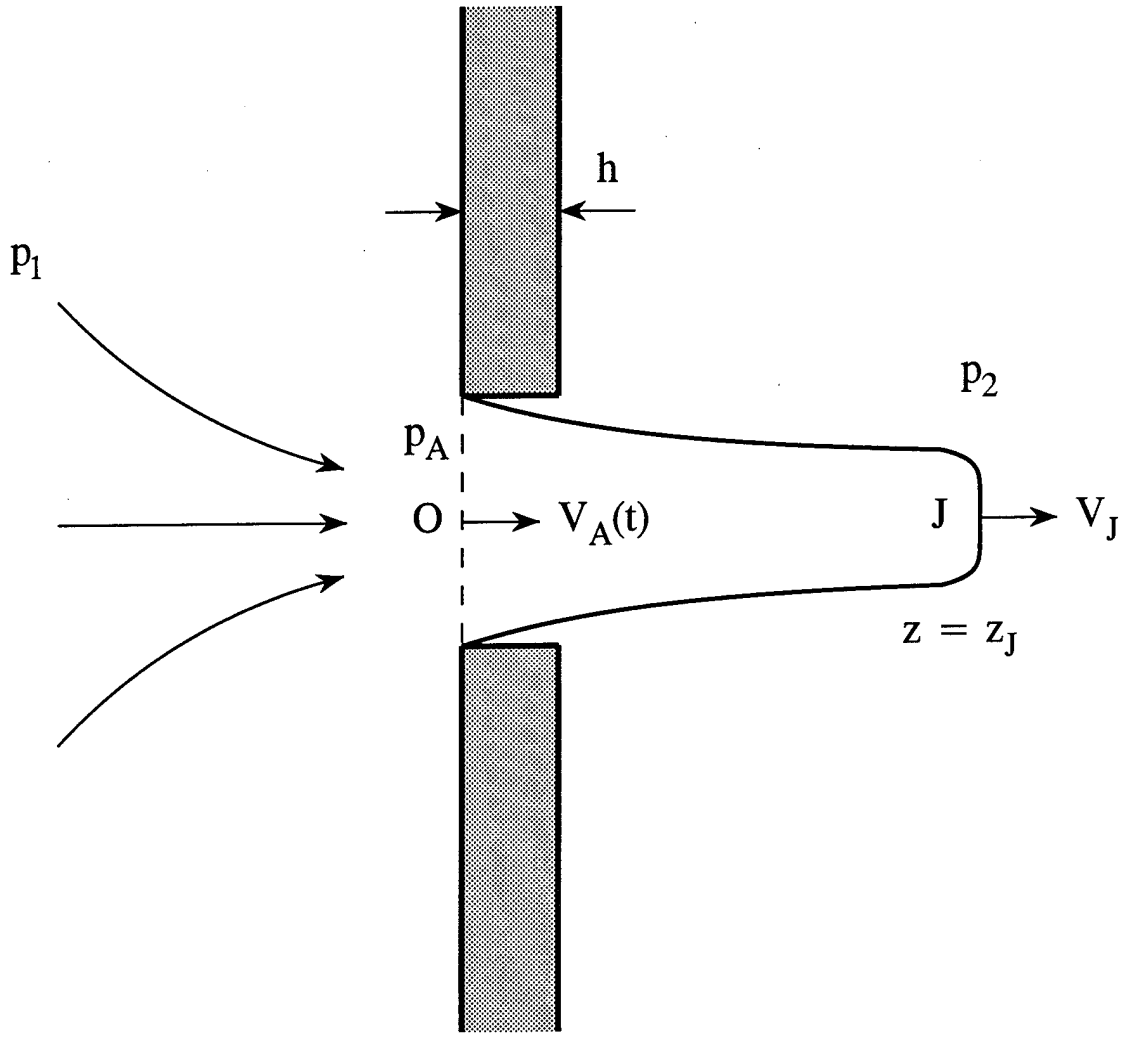

Figure 1. High Reynolds number separated flow produced by a pressure differential across a screen with an orifice.

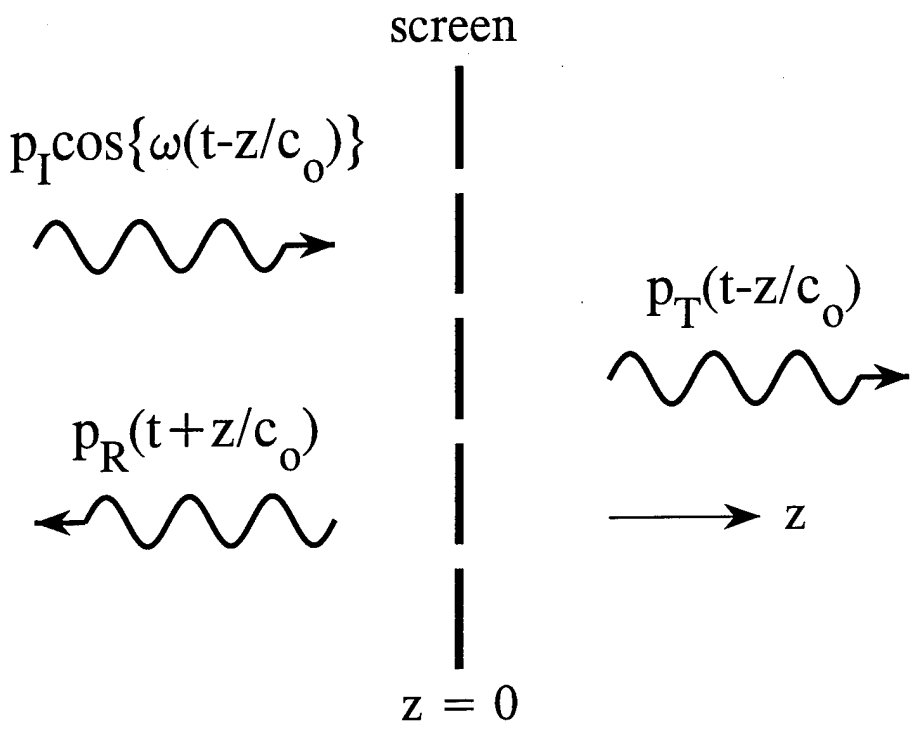

Figure 2. Interaction of a normally incident sound wave with a perforated, elastic screen.

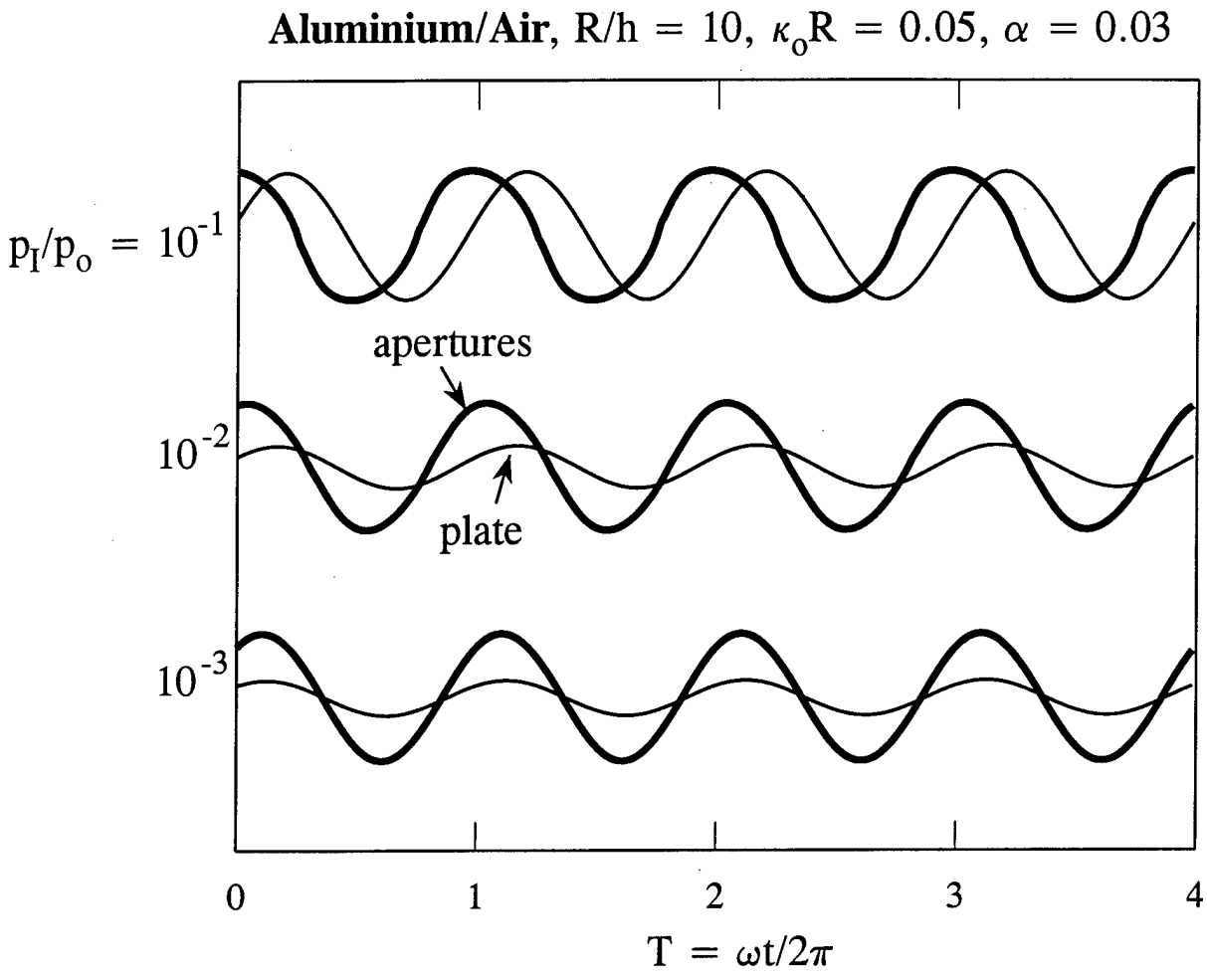

Figure 3. Relative contributions of the apertures (αV_A) and plate ($(1-\alpha)V_P$) to the effective normal velocity V of the perforated plate.

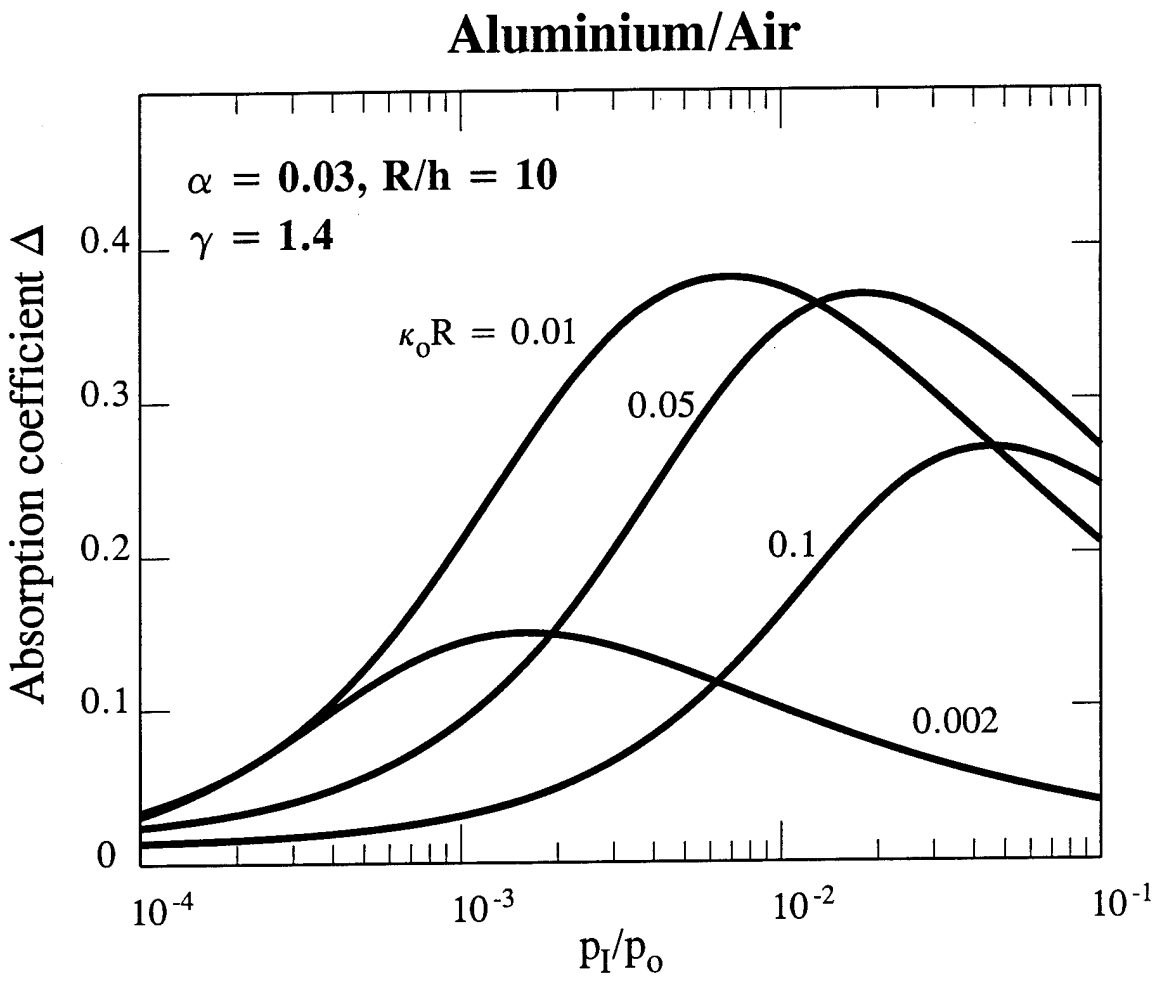

Figure 4. Absorption coefficient (3.9) for sound incident normally on an elastic perforated screen.

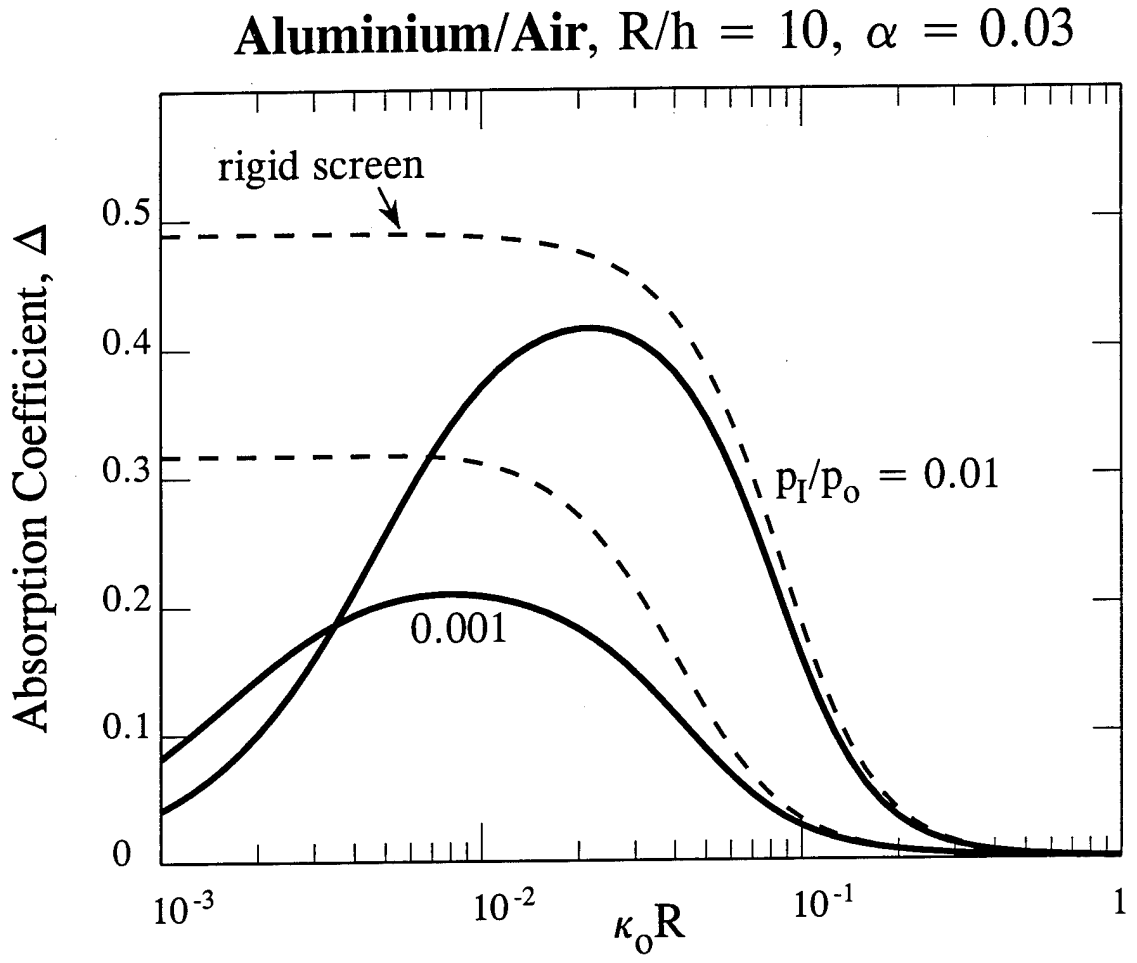

Figure 5. Comparison of the elastic screen absorption coefficient (———) with that for a rigid screen (– – – –) of the same thickness.

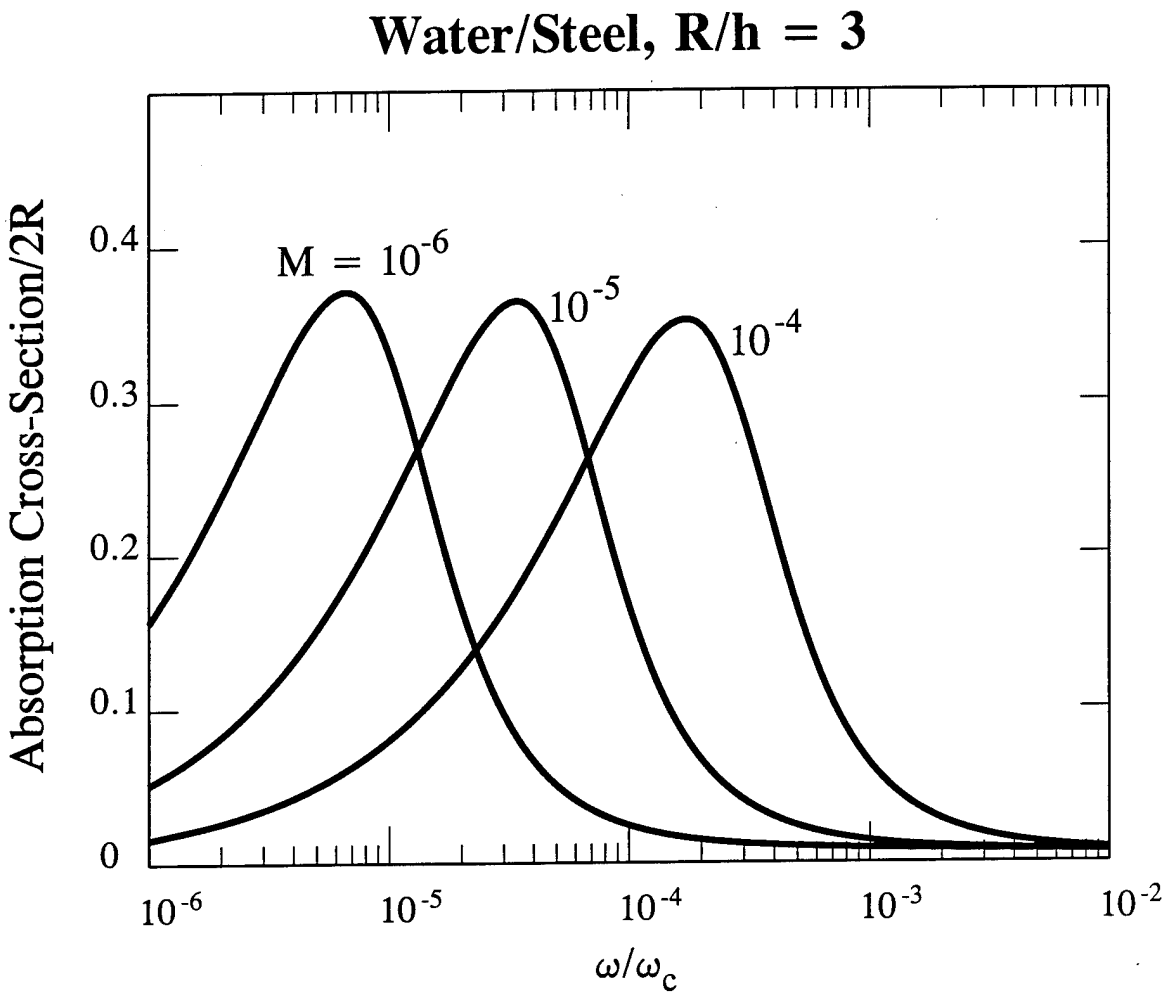

Figure 6. Absorption cross section calculated from equation (4.6) for a bending wave on a steel plate in water incident on a small circular aperture.

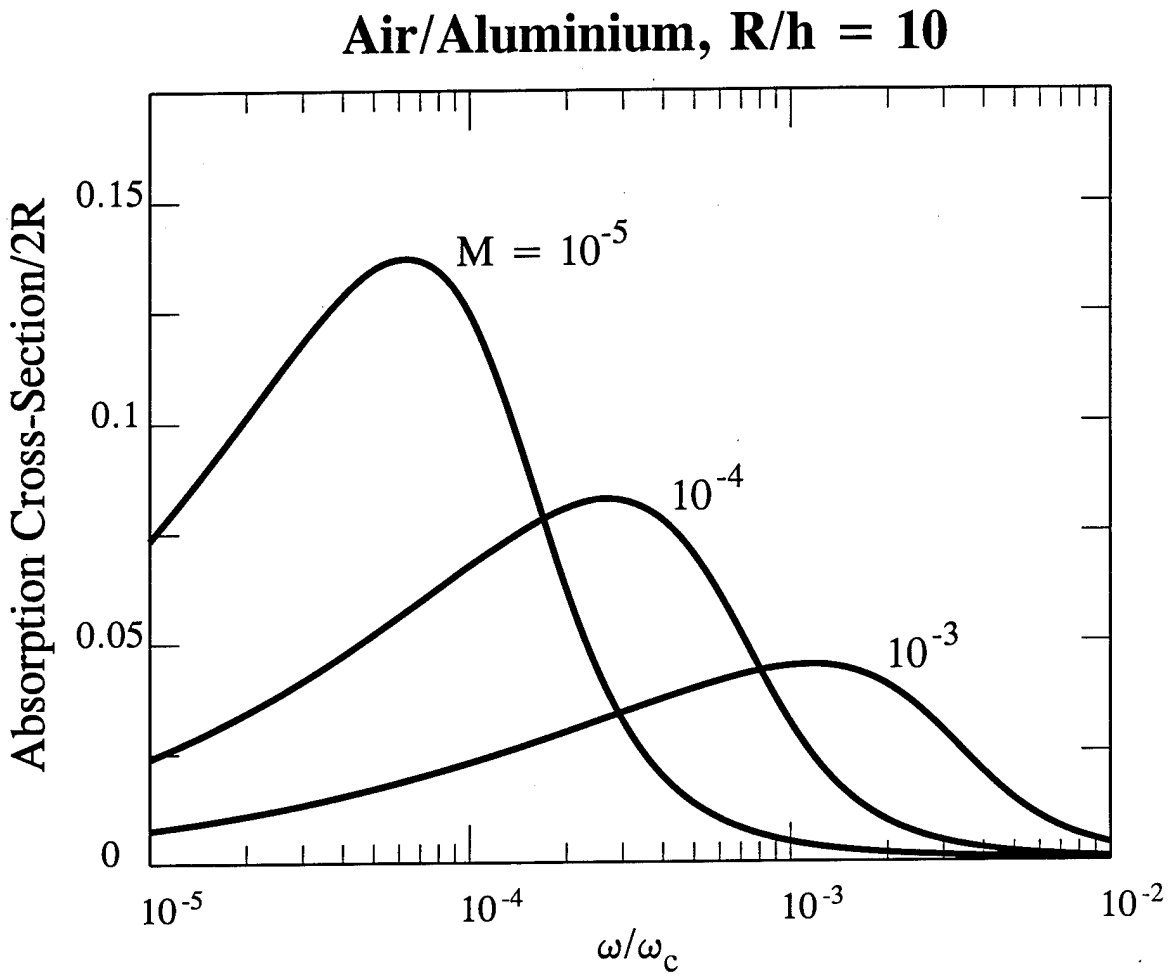

Figure 7. Absorption cross section calculated from equation (4.6) for a bending wave on an aluminium plate in air incident on a small circular aperture.

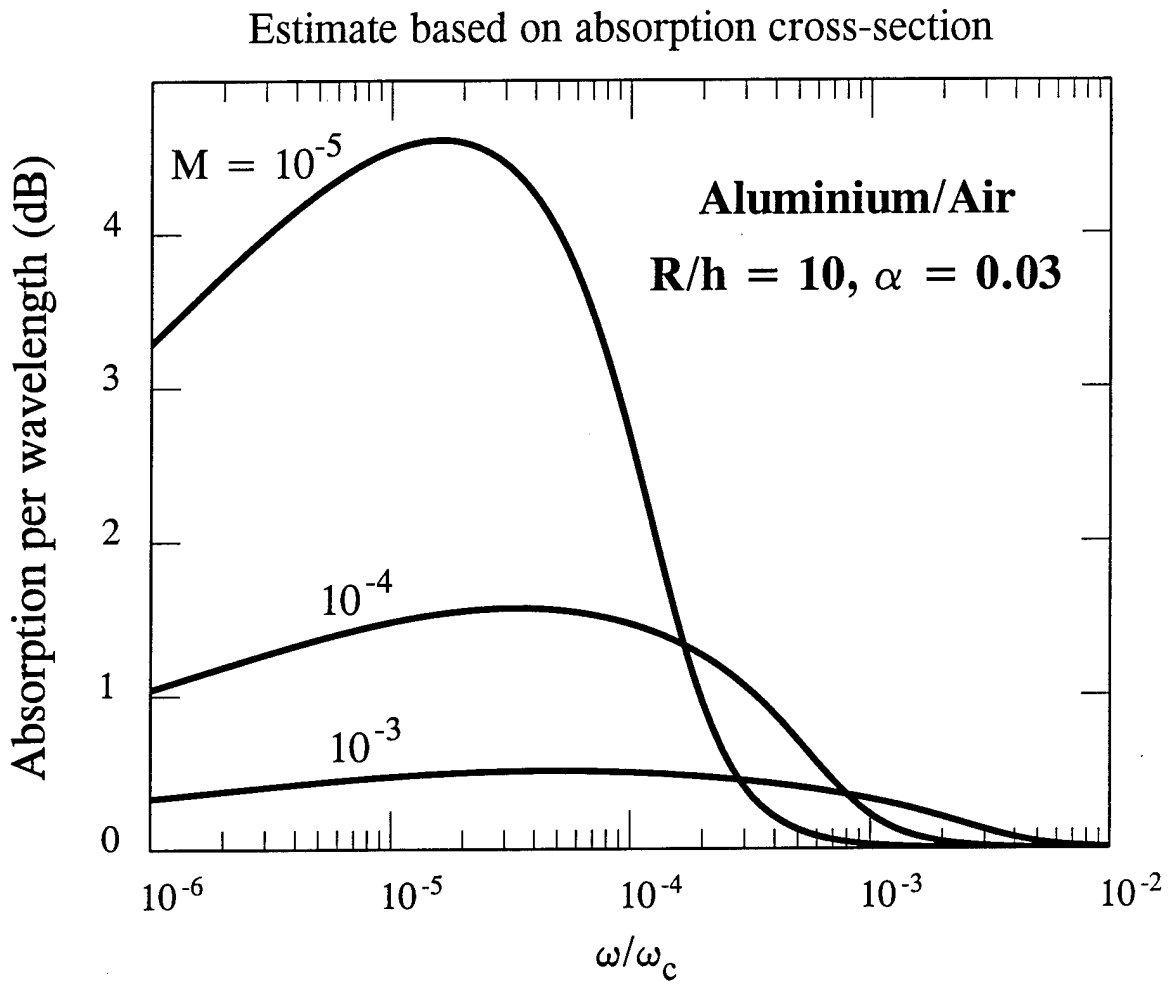

Figure 8. Estimates of the damping of bending waves on a perforated plate in air based on the absorption cross-section formulae (4.6) - (4.8).

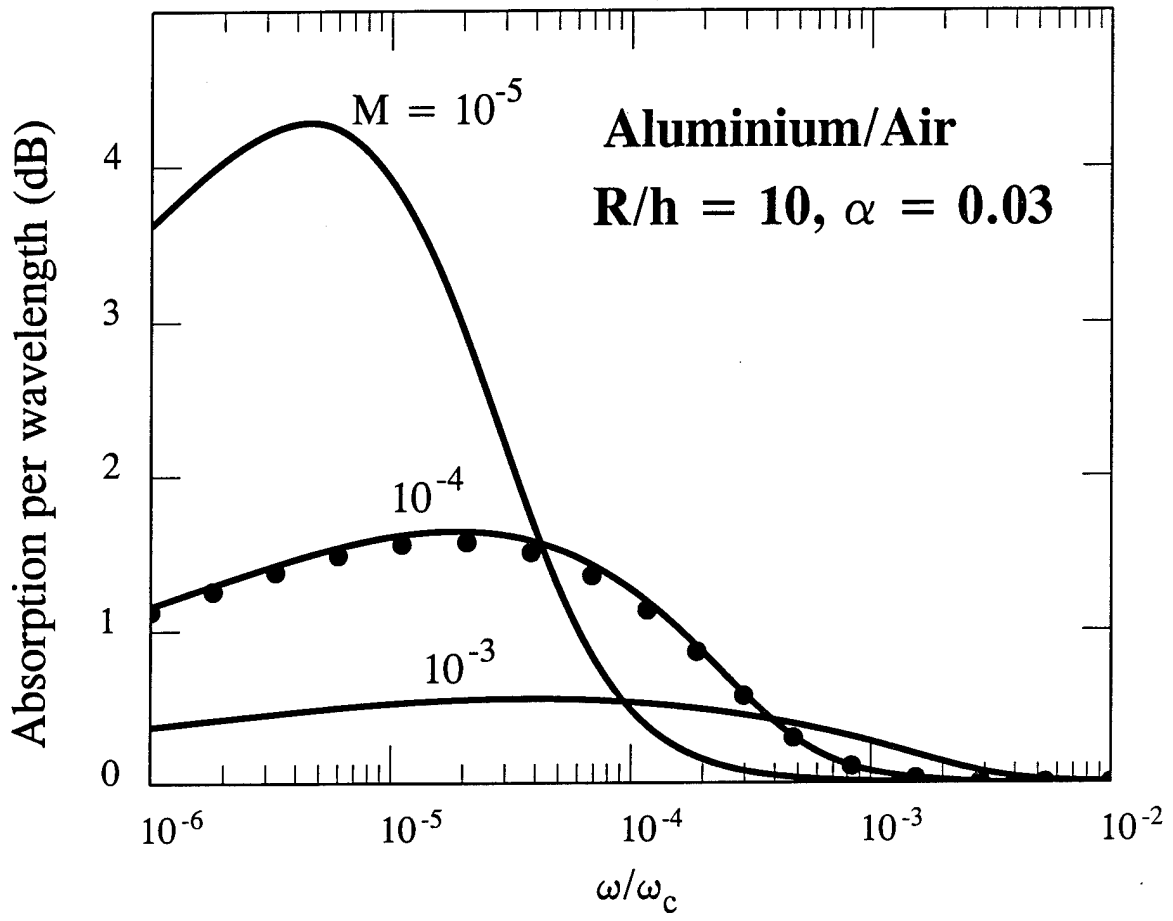

Figure 9. Damping of bending waves on a perforated aluminium plate in air for $\alpha = 0.03$ and R/h = 10: ———, predictions of equations (4.14) - (4.17); ••••, small damping approximation based on equation (4.23).

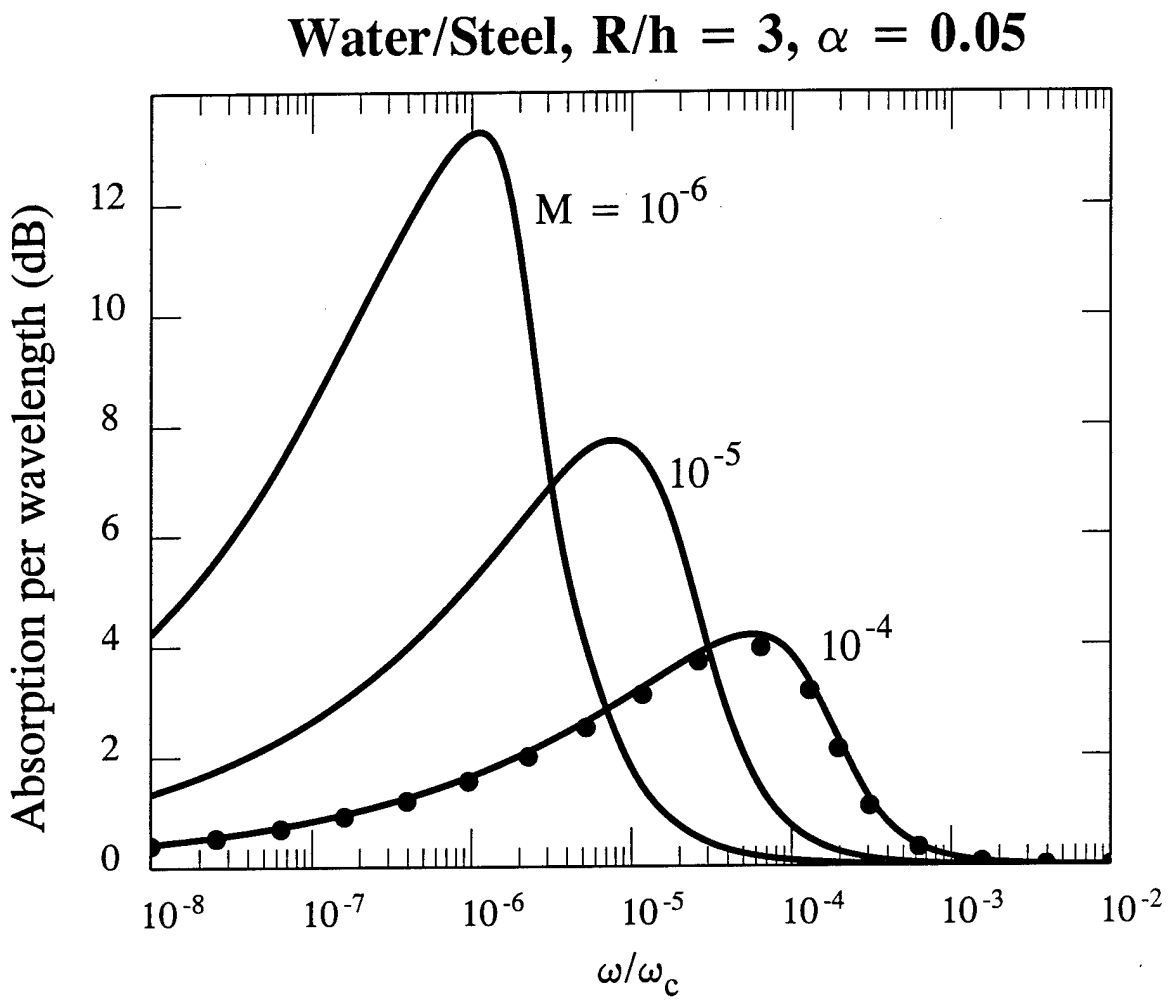

Figure 10. Damping of bending waves on a perforated steel plate in water for α = 0.05 and R/h = 3: ———, predictions of equations (4.14) - (4.17); ••••, small damping approximation based on equation (4.23).

CHAPTER 5

RECOMMENDATIONS FOR FURTHER RESEARCH

1. INTRODUCTION

The B-1B and F15 aircraft are configured with twin engine nacelles, and both have suffered premature failure of external nozzle engine flaps caused by high dynamic pressures. Model tests [1] confirm that the highest dynamic pressures occur where structural damage is observed on full scale aircraft, principally between the nozzles of the twin nacelle. Seiner *et al* [2] correlated these high pressures with jet screech tones produced by the interaction of turbulence and shock waves in the supersonic jet plumes. In particular, intense surface pressures corresponded to a dynamic coupling of the neighboring plumes, a common feature of parallel jets whose separation is less than about four or five jet diameters [3 - 5]. More recent wind tunnel tests [6, 7] have revealed that the supersonic plume resonance is actually important only at low flight Mach numbers, typically less than about 0.5. At higher flight speeds the pressures appear to be attributable to large-scale vortex structures impinging from the aircraft forebody.

In practice the dominant mechanism is determined by flight profile and aircraft configuration. The jet plume resonance can be eliminated by inserting tabs into the nozzle flow or, more effectively, by means of a small supersonic jet tube within the nozzle [7]. However, there is currently no effective means of controlling the vortex dominated pressures.

In Chapter 2 we have advanced and developed arguments to determine the damping of structural vibrations by vorticity production. The idea is that, in the presence of a mean flow a vibrating structure will generate vorticity that is subsequently convected away by the flow. Energy is required to create vorticity so that, provided the back reaction of the pressure field of the vorticity on the structure is small, structural vibrations tend to be damped. Strong back reactions are avoided if the length scale of the vorticity is small, and this can be achieved by perforating all or part of the vibrating structure, and forcing the mean flow to pass either through or over the perforates, in which case the vortex length scale is comparable to the perforation scale.

To assess the feasibility of this method for inhibiting flap vibration we have performed a series of basic, proof of principle tests using vibrating

perforated plates in the Harvard University flume. The flume has not been used for some time, and is in need of routine maintenance. In spite of this we have obtained encouraging results which are discussed below in §3. In §2 we outline an approximate theory of vibration damping based on our work described in [8, 9].

2. THEORY OF VIBRATION DAMPING

Consider a flat, rigid, rectangular airfoil of large aspect ratio and chord 2a set at zero angle of attack to a low Mach number mean flow. The flow is at speed U in the x direction of the rectangular coordinate system (x,y,z). The airfoil executes small amplitude, time harmonic motions normal to its surface (in the y direction, see Figure 1), such that its displacement at time t is $\zeta_0 \exp(-i\omega t)$, where the real parts of all complex quantities are to be taken. The rate Π_0 at which energy is supplied to the flow due to vortex shedding at the trailing edge of the airfoil is given approximately by

$$\Pi_0 = \pi\rho a U\omega^2 C_R(\omega a/U)|\zeta_0|^2 \tag{1}$$

per unit span, where ρ is the mean density of the fluid and C_R is the real part of the *Theodorsen function*

$$C(x) = iH_1^{(1)}(x)/\{H_0^{(1)}(x)+iH_1^{(1)}(x)\}. \tag{2}$$

When $\omega a/U > 1$, $C_R(x) \approx 0.5$, and

$$\Pi_0 \approx \pi\rho a U\omega^2|\zeta_0|^2/2, \quad \omega a/U > 1. \tag{3}$$

Consider next the case of an airfoil perforated with a uniform distribution of small circular apertures of radius $R \ll a$. The oscillatory motion forces fluid through the apertures and leads to the ejection of additional vorticity into the flow. Provided the aperture *Strouhal number* $\omega R/U$ is less than about 3, theoretical estimates [9, 10] indicate that energy is supplied to the fluid at a rate

$$\Pi_A' = \rho\omega\Delta|[\varphi]|^2/2, \tag{4}$$

where $[\varphi] = \varphi_+ - \varphi_-$ is the difference in the unsteady velocity potentials just above and below the aperture, and $\Delta \equiv \Delta(\omega R/U)$ is the imaginary part of the *Rayleigh conductivity* K_R of the aperture, defined by

$$K_R = 2R(\Gamma - i\Delta). \tag{5}$$

In the absence of the mean flow, K_R is real and equal to 2R (i.e., $\Gamma = 1$, $\Delta = 0$). The influence of tangential flow has been investigated in [9], with predictions for Γ and Δ shown in Figure 2. In the low frequency range $0 < \omega R/U < 3$, Δ is positive and large, and airfoil vibrations will tend to be damped at these frequencies by vorticity production in the apertures.

To estimate the damping when the distribution of apertures over the airfoil is uniform, we take the unsteady potential difference across the airfoil to be

$$[\varphi] = \beta' i\omega\zeta_1 (a^2 - x^2)^{1/2} \exp(-i\omega t), \tag{6}$$

where ζ_1 is the amplitude of the airfoil motion, β' is a constant, and the coordinate origin is at the center of the airfoil. This should be an adequate approximation for large values of $\omega a/U$, except for points very close to the trailing edge. For a rigid airfoil $\beta' = 2$, but its value is actually much smaller because of the reduction in $[\varphi]$ caused by "short circuiting" by the apertures. If there are N apertures per unit area of the airfoil, and $\alpha = N\pi R^2$ is the fractional open area, we now find by integration of (4) over the airfoil chord that the power dissipated per unit span can be cast in the form

$$\Pi_A = \alpha\beta\rho\omega^3 a^3 \Delta |\zeta_1|^2 / R, \tag{7}$$

where β is another constant.

Combining (1) and (7), for an airfoil vibrating with amplitude ζ_1, the net power dissipated per unit span by the vibrating perforated airfoil becomes

$$\Pi_1 = \rho\omega^2 aU[\pi C_R + \alpha\beta(\omega a/U)(a/R)\Delta] |\zeta_1|^2. \tag{8}$$

Suppose next that the $\Pi_1 = \Pi_0$, i.e., that the vibratory motions of the perforated airfoil at amplitude ζ_1 and the unperforated airfoil at amplitude ζ_0 are maintained by driving mechanisms delivering the same power. Then equations (1) and (8) imply that,

$$|\zeta_1/\zeta_0|^2 = \pi C_R / [\pi C_R + \alpha\beta(\omega a/U)(a/R)\Delta]. \tag{9}$$

3. PRELIMINARY DAMPING TESTS

The experiments were conducted in a low speed water flume that was capable of flow speeds up to one meter per second. Two interchangeable, rectangular steel plates were used, each of 11" span, 6" chord and 1/32" thickness. One plate was unperforated and the other was drilled with a uniform distribution of circular holes of diameter 0.25" with a fractional open area $\alpha = 0.1$. Each plate could be bolted at one end to the lower end of a wooden support, as indicated schematically in Figure 3a (where the mean flow is directed into the paper). The support could be raised or lowered to submerge the plate to a water depth of about 3 inches. The other end of the plate supported a 3" tall aluminum block, on the top of which was mounted a lead-eccentric electric motor and a polyvinylidene difluoride (PVDF) vibration sensor. The output of the PVDF was displayed on a digital oscilloscope which gave a direct reading of the voltage. Steady operation of the motor at a fixed speed caused the plate to vibrate at a known frequency, which was measured stroboscopically. The connection between the block and plate was rigid so that motion detected by the sensor also gave the amplitude of the plate motion. The arrangement was such that both the motor and vibration sensor were above the water surface.

The flow speed in the flume was adjusted to about 0.6 m/s, and was measured by observing the average travel times of several straws placed on the water surface over a distance of 2 yards. The electric motor was set to a predetermined speed, and the output (voltage) from the vibration sensor was displayed on the oscilloscope. The sensor output is proportional to the vibration amplitude ζ of the plate, and steady state amplitudes were recorded at different frequencies for both the unperforated (ζ_0) and perforated (ζ_1) plates. This permitted a comparison to be made of the vibration levels when the plates were submerged to the same depth, the motor operated at the same frequency, and when the delivered mechanical powers were the same. However, the electric motor would function in a controlled manner only for a restricted range of frequencies, and the measurements were therefore limited to the three Strouhal numbers indicated in Table 1 (which correspond to frequencies between 10 - 30 Hz). The measurements were repeated on several different occasions to guarantee the consistency of the data.

$\omega R/U$	$\lvert\zeta_0/\zeta_1\rvert^2$	$20\times\log\lvert\zeta_0/\zeta_1\rvert$ (dB)
0.35	2.4	3.8
0.5	1.23	0.9
0.95	1.86	2.7

TABLE 1: Measured Damping

The measured damping (column 3 of Table 1) corresponds to the prediction of equation (9), and is plotted as open squares in Figure 3b. To apply equation (9) to these measurements we first recognize that when $\omega R/U = O(1)$ the Strouhal number $\omega a/U$ based on the airfoil semi-chord is very large, so that Π_0 may be approximated by formula (3) (i.e., $C_R \approx 0.5$). Then (9) becomes

$$|\zeta_1/\zeta_0|^2 = 1/[1 + \delta(\omega R/U)\Delta], \tag{10}$$

where $\delta = (16/3\pi^2)\alpha\beta(a/R)^2$. A proper estimate of the coefficient β should strictly be made by solving a boundary value problem to determine the effective velocity potential of the fluid motion produced by the vibrating perforated airfoil. The solution of this problem requires the numerical integration of the equations of motion. Experience with similar problems concerned with the acoustics of perforated plates [11] indicates that β is likely to be small.

According to Figure 2 the additional damping attributable to the apertures should increase over the frequency range of the experiments. This is evidently not the case, at least for the first measurement at $\omega R/U = 0.35$, which exhibits the largest damping of nearly 4 dB. Actually, in spite of the care exercised in performing these measurements, it was not possible to obtain a definite stroboscopic reading of the drive speed for the *unperforated* plate when $\omega R/U = 0.35$: the motor was on the point of stalling, and the best that could be done was to use the speed obtained for the perforated plate (for which stalling did not occur). This presumably accounts for the anomalous result in Figure 3b at $\omega R/U = 0.35$. At the higher frequencies the constant motor speed was easily maintained, and the motor did not stall. If the measurement at $\omega R/U = 0.35$ is disregarded, the coefficient δ of equation (10)

can be adjusted to give the least squares best fit to the remaining two data points. The optimum occurs when $\delta = 0.96$, and the solid curve in Figure 3b represents the damping predicted by (10) for this value of δ. The theoretical curve peaks at $\omega R/U \approx 1.6$, where the damping rises to a maximum of about 4 dB.

4. FURTHER WORK

The possibility of achieving vibration damping of 3 dB or more can be critical for the continued safe operation of fatigue sensitive structures. Our preliminary experiments indicate that additional dampings in excess of this may be attainable by suitably perforating a vibrating control surface. The damping can be either passive, when the surface is placed in a tangential flow, or active, when fluid is forced through the apertures, or perhaps more optimally a combination of the two methods. We recommend performing two sets of experiments and concurrent analytical and numerical work. The first set of experiments should be performed in the Harvard University flume, a (largely neglected) facility that is ideal for such studies; it can be used to validate theoretical models and test new ideas suggested by the theory. A first objective should be to obtain a complete data set of results, from a carefully controlled series of tests with perforated and unperforated plates, to permit validation of the theoretical models discussed in this report.

Second, wind tunnel measurements of the type discussed above for the flume should be performed, but in a form more directly related to the nozzle flap fatigue problem (§1). One such test is illustrated schematically in Figure 4, in which the vortex wake from an upstream, spanwise oriented cylinder excites vibrations in both conventional and perforated airfoils. This configuration is an idealized analog of the excitation of an aircraft engine nozzle flap by vorticity swept over the flap from the aircraft forebody. Measurements will be made of vibration spectra for airfoils of various sections. A comparison of corresponding results obtained for the flume and wind tunnel will permit the dependence of damping on Mach number to be assessed and compared with theory. The influence of compressibility on damping will likely be important at higher Mach numbers, and this comparison will indicate when such effects need to be included in the aperture flow modeling.

Analytical work should complement and facilitate interpretation of the experiments, and permit extrapolation of measured results to full scale. This might include

- a complete analytical model of the flume experiments
- the development of a general purpose computer code for the complex Rayleigh conductivity of an aperture of arbitrary shape in a mean grazing flow.
- numerical procedures to account for the influence of finite airfoil/flap thickness, and "straking" of the flow-through cylindrical neck connecting the aperture faces.
- an investigation of the combined effects of grazing and bias flows through the apertures.

REFERENCES

1. Berndt, D. E. 1984 *Dynamic pressure fluctuations in the internozzle region of a twin-jet nacelle*, SAE Paper No. 841540.
2. Seiner, J. M., Manning, J. C., and Ponton, M. K. 1988 *AIAA J.* 26, 954-960. Dynamic pressure loads associated with twin supersonic plume resonance.
3. Wlezien, R. W. 1987 AIAA Paper No. 87-2694. *Nozzle geometry effects on supersonic jet interaction.*
4. Seiner, J. M., Manning, J. C., and Ponton, M. K. 1987 AIAA Paper No. 87-0244. *Model and full scale study of twin supersonic plume resonance.*
5. Shaw, L,, 1989 AIAA Paper No. 89-1140. *Twin jet screech suppression.*
6. Seiner, J. M., Ponton, M. K., Pendergraft, O. C., Jr., Manning, J. C., and Mason, M. L. 1990 AIAA Paper No. 90-1910. *External nozzle flap dynamic load measurements on F-15 S/MTD mode.*
7. Seiner, J. M., Manning, J. C., Capone, F. J. & Pendergraft Jr, O. C. 1992 ASME J. Eng. for Gas Turbines and Power **114**, 816 - 828. *Study of external dynamic flap loads on a 6 percent B-1B model.*

8. Howe, M. S. 1995 *Control of structural vibrations by vorticity production*, Chapter 2. Boston University, College of Engineering Rept. AM-95-004. Annual Technical Report, Grant No. F49620-94-1-0093, prepared for Air Force Office of Scientific Research.
9. Chapter 3.
10. Chapter 2.
11. Lamb, Horace 1932 *Hydrodynamics* (6th. edition). Cambridge University Press.

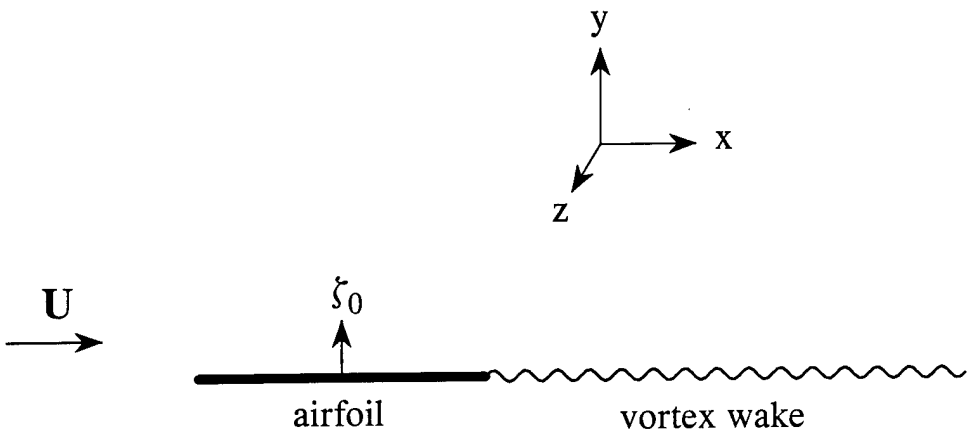

Figure 1. Airfoil vibrating in uniform mean stream.

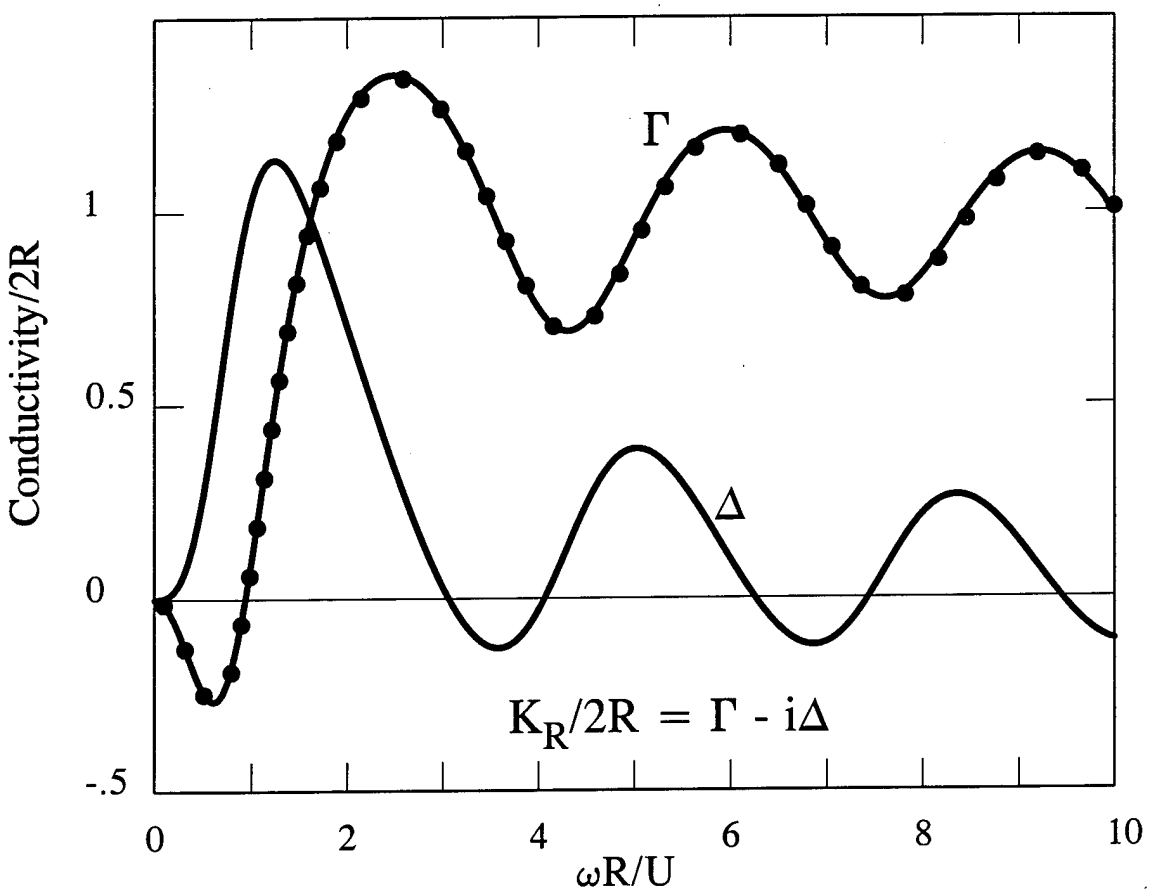

Figure 2. The Rayleigh conductivity of a circular aperture in the presence of a uniform tangential mean flow [9].

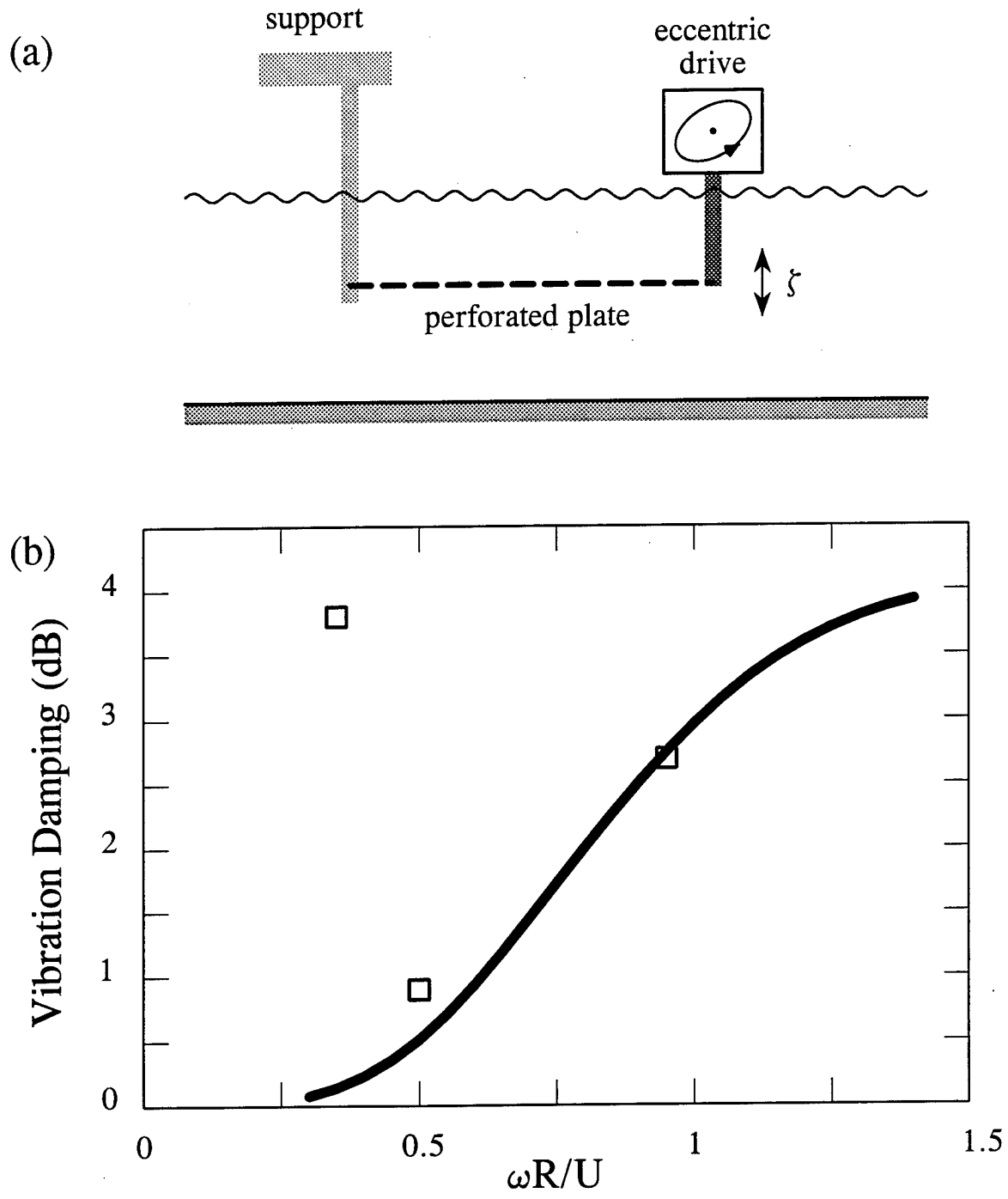

Figure 3. (a) Schematic experimental arrangement. The mean flow is into the plane of the paper.
(b) Measured damping of plate vibrations due to vorticity production in the apertures; open area = 10%, U = 0.6 m/s, R = 0.125"

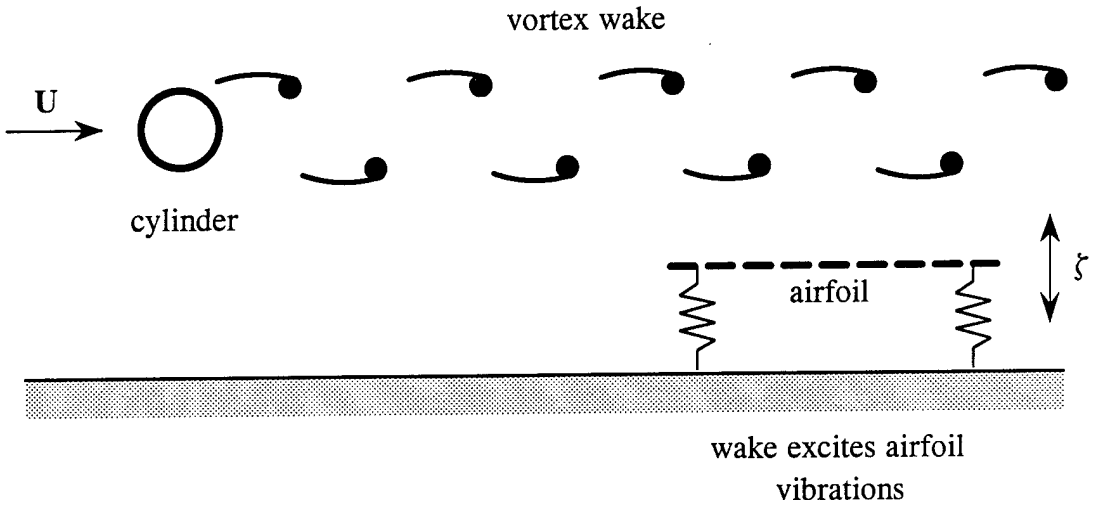

Figure 4. Vibrations induced by a vortex wake.

APPENDIX

THE DAMPING OF FLEXURAL WAVES BY VORTICITY PRODUCTION

PAPER PRESENTED AT THE 1994 WINTER ANNUAL MEETING OF THE AMERICAN SOCIETY OF MECHANICAL ENGINEERS

Report No. AM-96-006

Boston University, College of Engineering
Reprinted from DE-Vol. 75: *Active Control of Vibration and Noise*
ASME 1994

THE DAMPING OF FLEXURAL WAVES BY VORTICITY PRODUCTION

M. S. Howe
College of Engineering,
Boston University
Boston, Massachusetts

ABSTRACT

A summary review is given of theoretical predictions of the damping of sound and structural vibrations by vorticity production in the apertures of bias- and grazing-flow perforated elastic plates. Unsteady motion causes vorticity to be generated in the perforates; the vorticity and its energy are swept away by the mean flow and result in a net loss of acoustic and vibrational energy. Generalized forms of the thin plate bending wave equation are given for plates perforated with small circular apertures, and used to predict the attenuation of sound and resonant bending waves. Acoustic damping is significant when the fluid loading is small enough for the plate to be regarded as rigid. Bending waves are effectively damped only when the fluid loading is large and there is a substantial pressure drop across the plate; when this occurs the predicted attenuations are comparable with those usually achieved by the application of elastomeric damping materials.

INTRODUCTION

Aerodynamic sound is generated by turbulence and unsteady vorticity, and by their interactions with adjacent structures. Acoustic energy can also be dissipated by vorticity *production*, however, when sound impinges on a solid surface or fluid region of nonuniform mean density. For example, sound incident on the trailing edge of an airfoil in a mean flow will cause vorticity to be shed into the wake; at low Mach numbers this leads to an increase in the kinetic energy of the mean flow and wake at the expense of the sound [1, 2]. Similarly, perforated plates aligned with the mean flow through the tube banks of a heat exchanger cavity can be used to suppress cavity acoustic resonances by the production of vorticity in the perforates; the kinetic energy of the vorticity is extracted from the sound, convected away by the flow, and ultimately dissipated by viscous and thermal processes [3, 4]. The same mechanism is responsible for the greatly improved attenuation of "screech" tones in the jet pipe of a jet engine when a bias flow is maintained through the perforated heat shield normally used to protect the wall liner from contact with hot combustion products [5, 6].

The effectiveness of the acoustic attenuation in these cases is critically dependent on the presence of mean flow [7 - 10]. Analytical predictions for rigid perforated screens indicate that the attenuation is linearly proportional to the acoustic amplitude, which is in broad agreement with experiment [6 - 8, 11, 12]. In the absence of flow the attenuation is either a nonlinear function of the acoustic amplitude (and therefore weak) or is dominated by the less efficient action of viscous dissipation in the apertures.

Theoretical analyses have usually assumed the screen, plate, etc, to be *rigid*, although in practice high acoustic intensities are accompanied by structural vibrations, and a substantial part of the noise energy is contained in vibratory modes of the structure. These modes would also be expected to be damped by vorticity production, and a primary practical objective may actually be the suppression of potentially harmful structural vibrations rather than sound. The simplest model problem that exhibits structural damping by this means is that in which a *bending wave* on a thin elastic plate is reflected at a trailing edge in a parallel mean flow (see Figure 1) [13]. Incident bending wave energy is dissipated at the edge by scattering into sound, and by a transfer to the kinetic energy of the mean flow and wake. Below the coincidence frequency the efficiency with which sound is generated is usually very small, but much larger net losses are predicted owing to the generation of wake vorticity.

The predicted fractional bending wave power dissipated at the edge is plotted in Figure 2(a) for a steel plate in water for several values of the mean flow Mach number M when the edge of the plate is "free". In this figure the radian frequency ω is normalized by the coincidence frequency ω_c. For M = 0 the

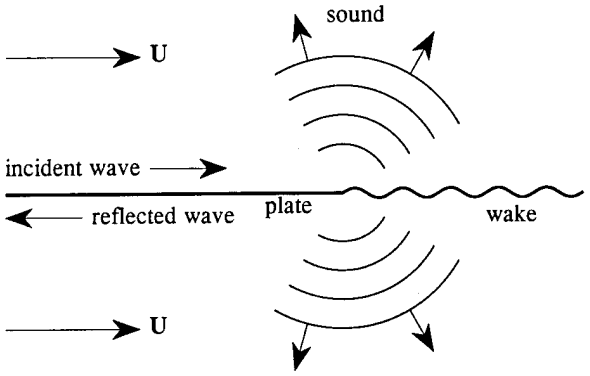

Figure 1.

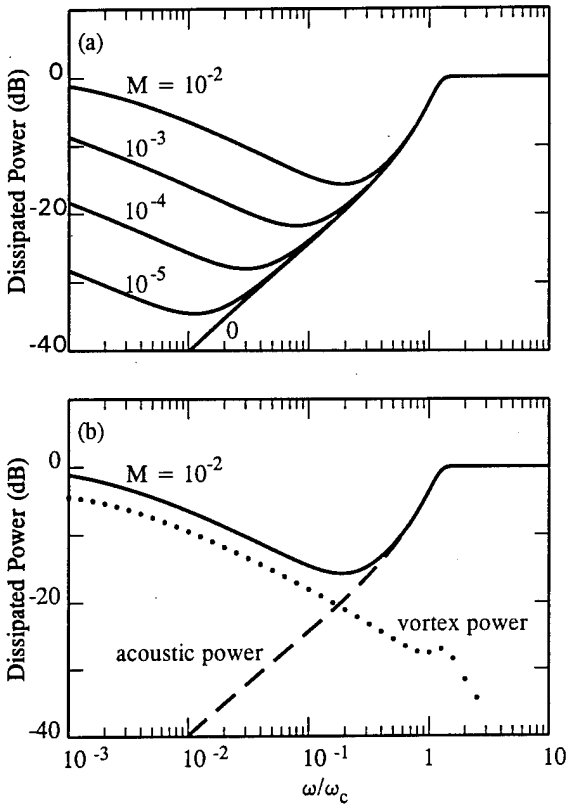

Figure 2.

dissipation can be attributed to sound radiated from the edge. When $M > 0$ there is a significant increase in power loss at low frequencies caused by a transfer of energy to the mean flow and wake, with negligible changes in the radiated sound power (at least for $M \ll 1$). This is clear from Figure 2(b), which compares the total power loss for a steel plate in water (solid curve) with the acoustic power (dashed curve) when $M = 0.01$. Inspection of Figures 2(a) and (b) confirms that the sound power is hardly influenced by the flow. At high frequencies the radiation of sound accounts for all of the dissipation; this is because, as $\omega \to \omega_c$, bending wave energy is contained principally in the evanescent motions in the fluid on either side of the plate, that propagate with negligible plate motion at a velocity which is only slightly less than the speed of sound.

The dotted curve in Figure 2(b) is the fraction of the dissipated energy which appears as kinetic energy of the vortex wake. This indicates that, over the range of frequencies within which acoustic dissipation is negligible, roughly half of the dissipated energy is used to accelerate the mean flow and half goes into the wake; this is not generally the case, but depends on the type of mechanical constraints at the edge [13].

THE BIAS-FLOW ELASTIC PLATE

Consider an elastic plate perforated with small circular apertures. Let there be N apertures per unit area each with radius R. A mean pressure differential is maintained across the plate which produces nominally steady, low Mach number, high Reynolds number jets of fluid through the apertures (Figure 3). Generalized forms of the thin plate bending wave equation have been derived in [14, 15] respectively for bias-flow and grazing-flow screens when the length scale of the motion is large compared to both the aperture radius R and the distance

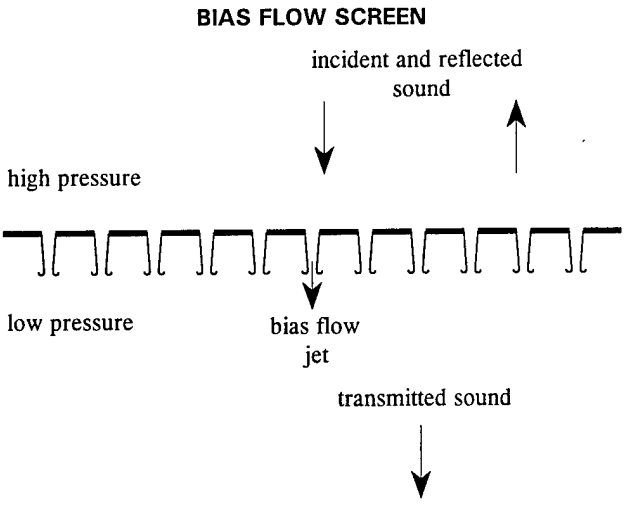

Figure 3.

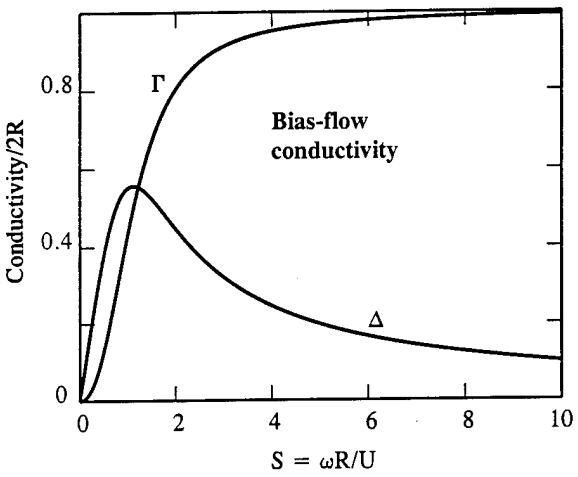

Figure 4.

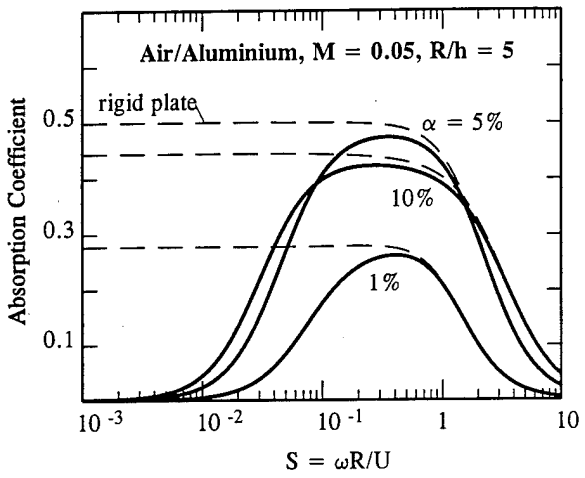

Figure 5.

between the apertures. For the bias-flow case it was shown in [14] that long wavelength, small amplitude, flexural displacements ζ (proportional to $e^{-i\omega t}$) of a plate of bending stiffness B and mass m per unit area immersed in fluid of mean density ρ, satisfy

$$\{[1-2\alpha\sigma/(1-\sigma)]B\nabla^4 - m\omega^2\}\zeta$$

$$+ \{1 + 2NRK_R[1 - (1/2R\rho\omega^2)(B\nabla^4-m\omega^2)]\}[p] = 0, \qquad (1)$$

where $\alpha = N\pi R^2$ is the fractional open area, σ is Poisson's ratio for the plate, $\nabla^4 \equiv (\partial^2/\partial x^2+\partial^2/\partial y^2)^2$ (where the z- or xy-plane coincides with the undisturbed location of the plate), and K_R is the *Rayleigh conductivity* of the apertures. [p] is the net pressure force on the plate (in the direction opposed to that of increasing ζ).

The conductivity determines the volume flux Q (in the positive ζ-direction) through an aperture as a result of a long wavelength pressure differential [p] according to the relation,

$$Q = K_R[\Phi] = K_R[p]/i\rho\omega, \qquad (2)$$

where Φ is the corresponding perturbation in velocity potential. In this limit, in which the length scale of the motion of the plate is much larger than the aperture radius R, it was argued in [14] that K_R is well approximated by its value for a *rigid* plate. K_R has the dimensions of length and is equal to 2R in a stationary ideal fluid, but becomes complex valued and frequency dependent in the presence of flow, because of the unsteady shedding of vorticity from the aperture edges.

Introducing the Strouhal number $S \equiv \omega R/U$, where U denotes the vorticity convection velocity in the bias flow jets (approximately one half of the mean jet velocity), we can write

$$K_R = 2R\{\Gamma(S) - i\Delta(S)\}, \qquad (3)$$

where Γ and Δ are real and positive (for $S > 0$). The dependence of Γ and Δ on S is shown in Figure 4 (from [14]).

Dissipation of sound

Let a plane acoustic pressure wave of the form $\exp(-i\kappa z)$ be incident *normally* on the screen from $z > 0$ (Figure 3), where $\kappa = \omega/c$ (c = speed of sound) is the acoustic wavenumber. The pressure can be taken in the form

$$p = \exp(-i\kappa z) + \Re\exp(i\kappa z), \quad z > 0,$$

$$= \Im\exp(-i\kappa z), \quad z < 0, \qquad (4)$$

where $\Re$ and $\Im$ are appropriate reflection and transmission coefficients, respectively. The displacement ζ of the screen is related to p by $\zeta = (1/\rho\omega^2)\partial p/\partial z$ $(z \to \pm 0)$. This together with equation (1) supply two equations from which $\Re$ and $\Im$ can be determined. The *absorption coefficient* $\delta = 1 - |\Re|^2 - |\Im|^2$ is equal to the fraction of the incident acoustic power dissipated at the screen. The solid curves in Figure 5 show the variation of δ with Strouhal number for sound incident on a perforated aluminium plate in air, when the bias flow convection Mach number M = 0.05 and R/h = 5, where h is the thickness of the plate. The maximum attenuation of $\delta \approx 0.5$ (3 dB) occurs at an open area ratio α = M over a range of Strouhal numbers centered on $S \approx 0.4$. At very low frequencies the impedance offered to the sound by the plate becomes negligible, the bias flow jet velocities are unmodulated by the sound, and there is no transfer of acoustic energy to hydrodynamic motions.

The corresponding predicted attenuations for a *rigid* bias-flow screen are depicted by the broken curves in Figure 5. The elastic and rigid screen predictions differ when the frequency is low enough for the screen to be regarded as acoustically transparent. The illustrated behavior is typical of cases in which the fluid loading is small (for metallic screens in air, say). For the other extreme of a steel plate in water the absorption of acoustic energy is found to be negligible at all frequencies.

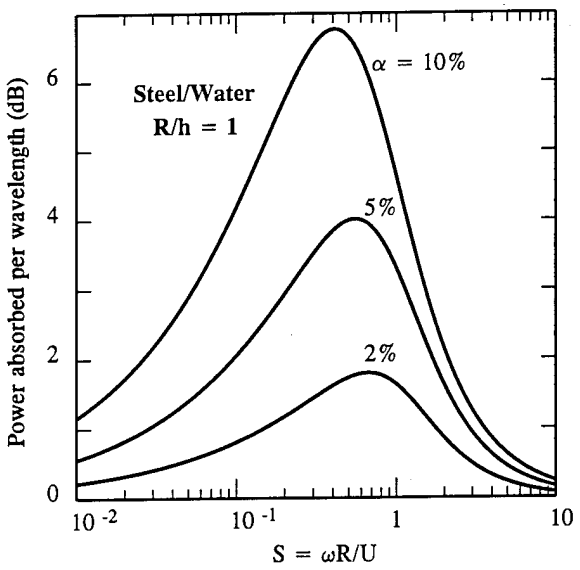

Figure 6.

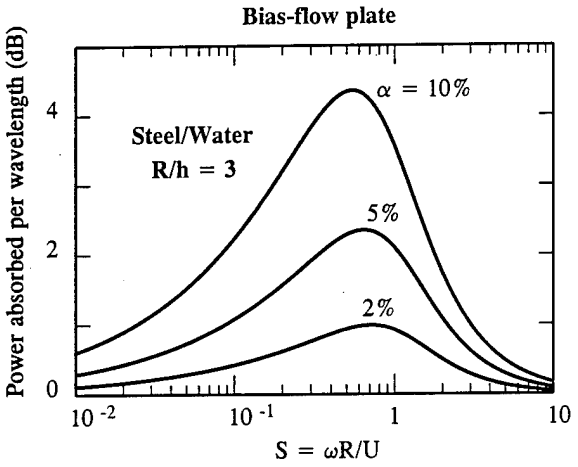

Figure 7.

Damping of bending waves

A flexural wave $\zeta = \zeta_o e^{ikx}$ with the associated pressure loading

$$[p] = -2\rho\{\omega^2/\sqrt{(k^2-\kappa^2)}\}\zeta_o e^{ikx}$$

satisfies the bias-flow bending wave equation (1) provided the bending wavenumber k is a zero of the dispersion function

$$D(k,\omega) = [1-2\alpha\sigma/(1-\sigma)]Bk^4 - m\omega^2$$

$$- \{2\rho\omega^2/\sqrt{(k^2-\kappa^2)}\}\{1 + 2NRK_R[1-(Bk^4-m\omega^2)/2R\rho\omega^2]\} \quad (5)$$

In the absence of the bias flow ($K_R \rightarrow 2R$), $D(k,\omega)$ has precisely two equal and opposite real zeros. They satisfy $|k| > \kappa$ and correspond to undamped flexural waves on the perforated plate. To the present order of approximation there is no damping due to scattering of structural energy into sound.

The absorption of bending wave energy by the bias flow jets causes the formerly real bending wavenumber k to acquire a small *positive* imaginary part that accounts for the progressive decay of the wave. The power absorbed per wavelength of propagation is plotted against the Strouhal number $S = \omega R/U$ in Figures 6 and 7 for a perforated steel plate in water and several different open area ratios α for an aperture radius R = h, 3h

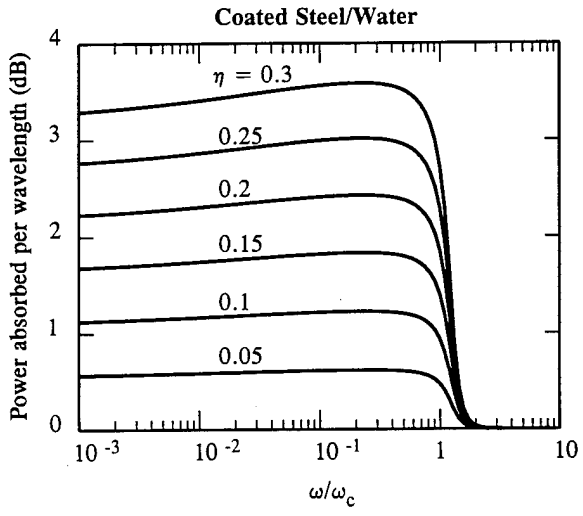

Figure 8.

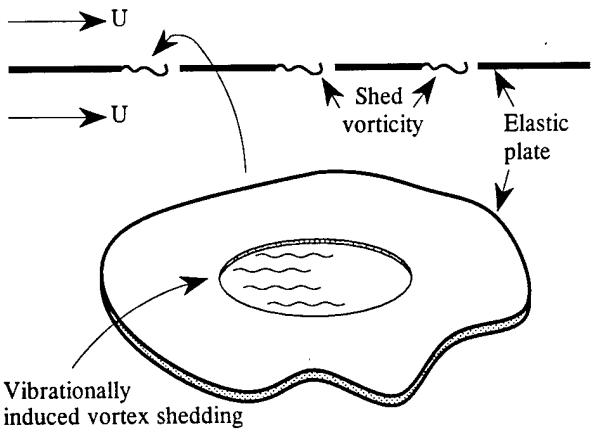

Figure 9.

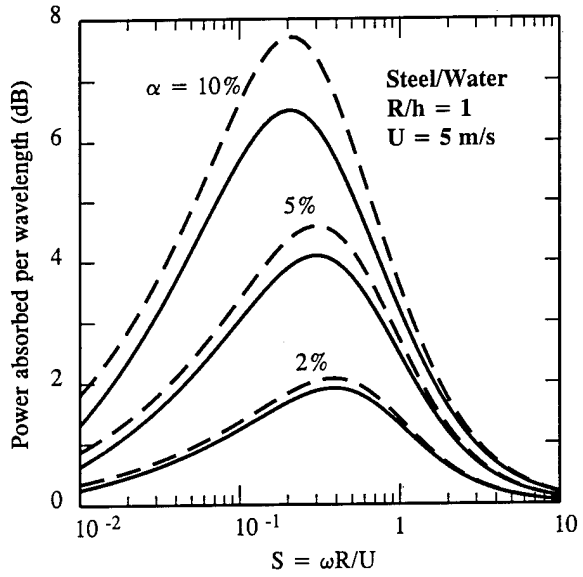

Figure 10.

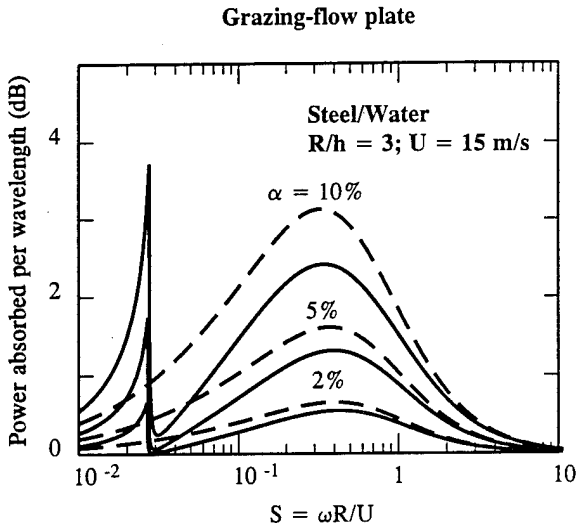

Figure 11.

respectively. The bias flow vorticity convection velocity U = 3 m/s (M ≈ 0.002). Increasing the open area ratio increases the attenuation, whereas increasing the size of the apertures reduces the maximum possible attenuation.

To assess the significance of these predictions we plot in Figure 8 the corresponding absorption of bending waves on a coated steel plate in water. For the purpose of illustration the mass of the coating is neglected, but the coating is assumed to make the effective stiffness of the plate complex, such that the bending stiffness B of the uncoated plate is replaced by $B(1 - i\eta)$, where η (> 0) is a *loss factor* whose value is determined by the properties of the coating, and is typically of the same order as shown in the figure [16]. As ω increases towards ω_c both the bending and acoustic wavelengths become comparable to the thickness of the plate and thin plate theory ceases to be strictly applicable. A comparison with figures 6 and 7 indicates that the attenuations achieved by the bias flow jets can be comparable with those predicted for the coated plate.

Much smaller attenuations are predicted for bending waves propagating on a bias flow screen in air (see [14] for details).

THE GRAZING-FLOW SCREEN

The modified bending wave equation for a perforated plate in a uniform, low Mach number tangential mean flow at speed U in the x-direction (Figure 9) is given in [15] in the form

$$\{\omega+iU\partial/\partial x\}^2\{[(1-2\alpha\sigma/(1-\sigma))B\nabla^4-m\omega^2]\zeta + (1+2NRK_R)[p]\}$$

$$- (NK_R/\rho)(B\nabla^4-m\omega^2)[p] = 0. \qquad (6)$$

The following asymptotic formulae for $K_R/2R = \Gamma - i\Delta$ are derived in [17]:

$$\Gamma \approx 2.29S^2,\ \Delta \approx 1.70S\{1 - 1.67S^2\},\ S \ll 1;$$

$$\Gamma \approx 1,\quad \Delta \approx 1/\pi S,\ S \gg 1,\quad S = \omega R/U. \qquad (7)$$

In applications to the attenuation of flexural and acoustic waves, the most significant effects occur at low Strouhal numbers $S < 1$, for which the following rational approximations are adequate for estimating dissipation rates:

$$\Gamma \approx 2.29S^2/(1 + 2.29S^2),\ \Delta \approx 1.7S/(1 + 1.67S^2). \qquad (8)$$

The variations of Γ and Δ given by these approximations are similar to those already depicted in Figure 4 for the bias-flow screen. The rational approximation for Δ is too large by a factor of 3 as $S \to \infty$, but the behavior for $S \leq 1$ should be well approximated by (8).

The flexural wave dispersion equation is now

$$[1-2\alpha\sigma/(1-\sigma)]Bk^4 - m\omega^2 - \{2\rho(\omega-Uk)^2/\sqrt{(k^2-\kappa^2)}\}$$

$$\times\{1 + 2NRK_R[1-(Bk^4-m\omega^2)/2R\rho(\omega-Uk)^2]\} = 0. \qquad (9)$$

Proceeding as for the bias-flow screen we calculate the typical attenuations illustrated in Figures 10 and 11 for a steel plate in water at different fractional open areas α and aperture radii. The results are for bending waves propagating in the direction of the mean flow (solid curves), and in the direction opposite to the mean flow (dashed curves).

Comparing these predictions with Figure 8 for a nominally homogeneous plate with one or more layers of absorptive coatings, it can be seen that the attenuations are comparable with the best obtainable by coating the plate, at least for Strouhal numbers in the interval 0.1 - 1.

CONCLUSION

The predictions presented in this paper for bias- and grazing-flow perforated elastic plates indicate that significant attenuations of sound and flexural vibrations are possible provided a sufficiently large fluctuating pressure gradient can be established across the screen to cause unsteady production of vorticity in the apertures. When the fluid loading is large (e.g., for metallic plates in water) an unrestrained elastic screen is effectively acoustically "transparent", and the damping of sound by vorticity production tends to be negligible. Large acoustic attenuations can occur for a lightly loaded plate (in air, say).

The damping of bending waves increases with the fluid loading, since the surface pressure fluctuations produced by a wave of given surface displacement tends to increase with fluid density. For bias-flow screens the damping is greatest for aperture Strouhal numbers $S = \omega R/U$ (based on the vorticity convection velocity U) between about 0.03 and 3, and the attenuation experienced by bending waves on a perforated steel plate in water can then exceed or be comparable with that for waves on a heavily coated plate. Similar results are obtained for grazing-flow screens, the maximum attenuation for waves on a perforated steel plate in water occurs for $\omega R/U$ in the range 0.1 - 1 (where U now denotes the tangential mean velocity).

ACKNOWLEDGEMENT

The work reported in this paper is sponsored by the Air Force Office of Scientific Research under grant F49620-94-1-0093 administered by Dr. Spencer T. Wu.

REFERENCES

1. Rienstra, S. W. 1981 *J. Fluid Mech.* **108**, 443 - 460. Sound diffraction at a trailing edge.
2. Howe, M. S. 1984 *IMA J. Appl. Math.* **32**, 187 - 209. On the absorption of sound by turbulence and other hydrodynamic flows.
3. Ver, I. L. 1982 *Perforated baffles prevent flow-induced acoustic resonances in heat exchangers.* Paper presented at 1982 meeting of the Federation of the Acoustical Societies of Europe; Göttingen, September 1982.
4. Ver, I. L. 1990 *Noise Control Eng. J.* **35** (Nov/Dec issue) pp. 115 - 125. Practical examples of noise and vibration control: case history of consulting projects.
5. Bloxsidge, G. J., Dowling, A. P. & Langhorne, P. J. 1988 *J. Fluid Mech.* **193**, 445 - 473. Reheat buzz: an acoustically coupled combustion instability. Part 2. Theory.
6. Hughes, I. J. & Dowling, A. P. 1990 *J. Fluid Mech.* **218**, 299 - 336. The absorption of sound by perforated linings.
7. Bechert, D., Michel, U. & Pfizenmaier, E. 1977 *AIAA Paper 77-1278.* Experiments on the transmission of sound through jets.
8. Bechert, D. W. 1979 *AIAA Paper* 79-0575. Sound absorption caused by vorticity shedding, demonstrated with a jet flow.
9. Howe, M. S. 1980 *J. Sound Vib.* **70**, 407 - 411. The dissipation of sound at an edge.
10. Howe, M. S. 1979 *Proc. Roy. Soc. Lond.* **A366**, 205 - 233. On the theory of unsteady high Reynolds number flow through a circular aperture.
11. Dowling A. P. & Hughes, I. J. 1992 *J. Sound Vib.* 156, 387 - 405. Sound absorption by a screen with a regular array of slits.
12. Cargill, A. M. 1982 *J. Fluid Mech.* **121**, 59 - 105. Low frequency sound radiation and generation due to the interaction of unsteady flow with a jet pipe.
13. Howe, M. S. 1992 *J. d'Acoustique* 5, 603 - 620. On the damping of structural vibrations by vortex shedding.
14. Howe, M. S. 1994 *European J. Appl. Math.* (in press). The damping of flexural and acoustic waves by a bias-flow perforated elastic plate.
15. Howe, M. S. 1994 Submitted to *J. Sound Vib.* Energy conservation and the damping of flexural waves by vorticity production.
16. Beranek, L. L. & Ver, I. L. 1992 *Noise and Vibration Control Engineering* New York: John Wiley.
17. Howe, M. S. 1980 *Proc. Roy. Soc. Lond.* **A370**, 523 - 544. On the diffraction of sound by a screen with circular apertures in the presence of a low Mach number grazing flow.